Permafrost modelling over different scales in arctic and high-mountain environments

Kjersti Gisnås

Faculty of Mathematics and Natural Sciences

Department of Geosciences

University of Oslo

A thesis submitted for the degree of

Philosophiae Doctor (PhD)

January 2016

Series of dissertations submitted to the
Faculty of Mathematics and Natural Sciences, University of Oslo
No. 1734

ISSN 1501-7710

Cover: Hanne Baadsgaard Utigard.
Print production: Reprosentralen, University of Oslo.

Abstract

The projected future climate changes increase the need for models that are able to predict the climate effects on the surface energy budget. With the large model developments lately, the mismatch between the scales at which atmospheric and surface variables operate on are being stressed. While atmospheric variables operate on scales of several kilometres, near-surface temperatures are highly variable, particularly in alpine areas, with significant variations on the meter scale. The snow cover has profound implications for the thermal regime of the ground, and the strong winds prevalent in high altitude and arctic environments heavily redistribute the snow cover, causing a small-scale pattern of highly variable snow depths. There is a need for quantification and new techniques to represent this small-scale variation in permafrost and land surface models.

Field observations show a variability of the mean annual ground surface temperatures within 0.5 km^2 of up to 5 °C, where spatial variation in maximum snow depth is found to be the main explaining variable. The distributions of snow in high-mountain environments are highly asymmetric, and combined with the non-linear insulating effect of snow this implies that the spatial average ground temperature in a 1 km² area cannot necessarily be determined based on the average snow cover for that area. Land surface or permafrost models employing a coarsely classified average snow depth will therefore not yield a realistic representation of ground temperatures. For arctic and high-latitude environments similar to those in Scandinavia and Svalbard, a simple representation of snow distributions clearly improves the model representation of the surface energy balance.

We employ statistically derived snow distributions within 1 km² grid cells as input to the regional permafrost model CryoGRID1, in order to represent sub-grid variability of ground temperatures. This is shown to improve the representation of both the average and the total range of ground temperatures: The model results show that we reproduce observed sub-grid ground temperature variations of up to 6 °C, with 98% of borehole observations within the modelled temperature range. Based on this more faithful representation of ground temperatures, we find the total permafrost area of mainland Norway to be nearly twice as large as what is modelled without a sub-grid approach.

As an outcome of the improvements to the regional permafrost modelling in Norway presented in this thesis, we have produced a new and improved baseline map for permafrost on the entire Scandinavian Peninsula, updating the coarsely resolved baseline map in use until today. The new map is based on an implementation of the CryoGRID1 model, with a sub-grid snow distribution routine for non-vegetated areas. The model results are qualitatively evaluated in collaboration with the national permafrost researchers with experience within the area, and against available ground thermal observations, BTS-mappings and geomorphological maps showing the location of permafrost landforms. The evaluation of the results shows that the model is capable of representing the regional patterns of permafrost very well, and it also reproduces observed ground temperatures and lower limits of permafrost at a local scale.

The statistical snow distributions derived for Norway are also implemented as tiles in a coupled atmosphere-land surface model. This increases the transition time from full snow cover to snow-free ground from a few days to more than two months at Finse, in accordance with field observations. The improved representation of the fractional snow cover reduces a cold temperature bias found in the reference simulation during the melting season, at both point scale and regional scale. As a result of the decreased albedo and increased skin temperatures during the melting season, heat and moisture fluxes are increased. These changes in energy and moisture fluxes result in increased precipitation in the mosaic approach during the melting season, which in the most affected sub-region increases the correlation between simulated and observed precipitation from 0.83 to 0.89.

The field observations and modelling efforts presented in this thesis demonstrate that land surface models and permafrost models with grid resolutions of 1 km or coarser will introduce biases in the surface energy balance if they do not adequately represent the sub-grid variation of snow. For permafrost this implies that the distribution of permafrost will be biased, but also that the response to changes in the climate forcing will be incorrect if the full range of sub-grid ground temperatures is not represented. Biased averages that do not include these small-scale effects propagate back into the coupled atmosphere models. A statistical approach as presented in this thesis is not only cost effective; it requires relatively few input parameters, all which are normally available over larger regions. This study is clear evidence that the sub-grid variability of snow depths should be accounted for in future model approaches targeting the ground thermal regime and permafrost distribution.

Acknowledgements

My greatest thanks go to my supervisors Bernd Etzelmüller, Thomas V. Schuler and Frode Stordal, as well as my colleague Sebastian Westermann. They had the main ideas behind this project, and have supported the research and provided scientific advice. Your guidance, encouragement and never-ending enthusiasm have been invaluable, and made my period as a PhD student a broadening and pleasant journey. I would also like to thank all the individuals in the CryoMet project, for valuable scientific discussions across the research fields, for great support and feedback, and not the least for nice field excursions to Iceland and Finse! This thesis would also not have been possible without the help, inspiration and support from my colleagues at the GeoHyd-section at the Department of Geosciences, UiO.

Great thanks to my PhD committee; Stephanie Werner (administrator), Prof. Vladimir Romanovsky (first opponent) and Dr. Marcia Philips (second opponent) for your valuable comments and time spent on evaluating my PhD thesis.

A large part of this thesis consists of extensive field work conducted in the mountains of southern Norway and on Svalbard. The large amount of field work would not have been possible without the help of numerous field assistants (in alphabetic order): Kjetil Aas, Bas Altena, Christopher D'Amboise, Thorben Dunse, Trond Eiken, Bernd Etzelmüller, Torborg Heid, Ketil Isaksen, Kristin Sæterdal Myhra, PiM Lefeuvre, Tobias Litherland, Simon Løvås, Maria Peter, Tomas Schellenberger, Thomas V. Schuler, Ladina Steiner, Désireé Treichler, Sebastian Westermann, Rune S. Ødegård and Torbjørn Østby. At the winter field campaigns at Finse in 2013 - 2015 the students in the courses *Snow, Snow Hydrology and Avalanches* (GEO4430) and *Atmosphere Physics* (GEF2200) provided great help, together with their teachers Thomas V. Schuler, Terje Berntsen and Frode Stordal.

A special thanks to Trond Eiken for invaluable help with planning of field work, preparation of all kind of field equipment (sometimes on very short notice), and for helping out in the field at Finse. I never feel safer and more relaxed in the field than when you are joining! The field site at Finse was established in great collaboration with Tobias Litherland, during the work for his master thesis. I really appreciated our field trips; the hard work in stormy and

cold weather and not the least the days in warm and sunny spring conditions. During the last field season at Finse I had valuable help and beautiful days in the field together with Simon Løvås. No need for a snow mobile when the Løvås-train is pulling the sled!

The field work at Juvvasshøe was done in collaboration with Ketil Isaksen (met.no). I'm really grateful for those nice days in the field (and the impressive shuffling by you and Rune!), for good scientific advices and discussions, and for always being supportive and encouraging!

Sebastian, thank you for the memorable field trips to Svalbard. I will never forget those sunny days of powder skiing around Ny-Ålesund and kayaking at flat water into Kronebreen! Also not the unforgettable after work parties on the Saturday nights at Mellageret! I'm also very grateful for your wise decisions, invaluable experience and great support when things went wrong at Finse.

Great thanks to Kolbjørn Engeland and James Stagge for help and good advices with statistics and regression analysis.

I feel very privileged for having been given the opportunity to travel abroad to inspiring field courses in Greenland, Yukon, Alaska and Svalbard, to interesting conferences, and to the Snow and Avalanche Institute (SLF) in Davos for a 3 months research visit. The stay in Davos was funded by the Kristine Bonnevie travel grant and the Industrial Liaison. Charles Fierz was a welcoming host, and I got valuable insight in physical snow modelling from working with him and Mathias Bavay, as well as the rest of the research group at SLF.

Most of the field work conducted for this thesis was funded by the CryoMet-project (project no. 214465; funded by the Norwegian Research). The work at Finse was partly funded by the hydropower companies Statkraft and ECO. The research in Ny-Ålesund was partly funded by the Arctic Field Grant (Norwegian Research Council).

Last, but not the least, I want to thank my family and friends for the support and for encouraging me to finish this work. A special thank to my boyfriend, Arne, for invaluable help with the text in the final stage of the thesis, for showing so much interest for my work, and for the great patience.

Oslo, 5 Jan 2016 Kjersti Gisnås

Acronyms and Abbreviations

1D, 2D, 3D	=	1-Dimensional, 2-Dimensional, 3-Dimensional
ALT	=	Active Layer Thickness
BTS	=	Bottom Temperature of Snow
CV	=	Coefficient of Variation
DTM	=	Digital Terrain Model
ESM	=	Earth System Model
FDD_a / TDD_a	=	Freezing / Thawing Degree Days in the air
FDD_s / TDD_s	=	Freezing / Thawing Degree Days at the ground surface
GCM	=	General Circulation Model
GCP	=	Ground Control Point
GPR	=	Ground Penetrating Radar
GPS	=	Global Positioning System
GST	=	Ground surface Temperature
IPCC	=	Intergovernmental Panel on Climate Change
k_f / k_t	=	Thermal conductivity in frozen / thawed ground
ME	=	Nash-Sutcliffe Model Efficiency Coefficient
MAAT	=	Mean Annual Air Temperature
MAGT	=	Mean Annual Ground Temperature
MAGST	=	Mean Annual Ground Surface Temperature
nF / *nT*	=	Freezing / thawing *n*-factor
RCMs	=	Regional Climate Models
RMSE	=	Root Mean Square Error
R^2	=	Coefficient of determination
SCF	=	Snow Covered Fraction
SD	=	Snow Depth
TTOP	=	Temperature at the Top Of Permafrost

Contents - PART I

1 INTRODUCTION 3

1.1 Motivation 3

1.2 Objectives 6

1.3 Outline 7

2 BACKGROUND 9

2.1 Permafrost modelling 9

2.2 The ground thermal regime 12

2.2.1 The surface offset 13

2.2.2 The thermal offset 14

2.3 Controlling factors of the surface offset 16

2.3.1 The vegetation cover 16

2.3.2 Topography and related effects of aspect and slope 17

2.3.3 The effects of a seasonal snow cover 17

2.4 Snow distribution in alpine areas 19

2.4.1 Spatial variation of snow 19

2.4.2 Snow distribution modelling 20

2.5 Permafrost monitoring and mapping 22

3 SETTING 25

3.1 The Scandinavian Peninsula 25

3.2 Field sites 27

3.2.1 Finse 27

3.2.2 Juvflye 29

3.2.3 Ny-Ålesund 30

4 DATA ACQUISITION AND METHODS 33

4.1 Field measurements 33

4.1.1 Fine-scale variability of ground temperatures 33

4.1.2 Snow surveys using Ground Penetrating Radar and differential GPS 36

4.1.3 Snow covered fraction from digital camera images and GST-loggers 39

4.1.4 Weather observations from three weather stations at Finse 41

4.2 Statistical representation of fine-scale variability of snow over regional areas 43

4.2.1 The Winstral terrain-based parameter ... *43*
4.2.2 Coefficient of variation for snow based on terrain and wind ... *43*
4.3 Regional equilibrium modelling in Norway and Scandinavia ... 46
4.3.1 Implementation of the TTOP- approach ... *46*
4.3.2 n-factor parameterization ... *46*
4.3.3 Thermal conductivities in the active layer ... *47*
4.3.4 CryoGRID1 for Norway ... *48*
4.3.5 Implementation of CryoGRID1 for Fennoscandia ... *48*
5 RESULTS ... 51
5.1 Permafrost distribution in Norway estimated by a spatial numerical model (Paper I). ... 51
5.2 Fine-scale variability of ground surface temperatures and related surface variables ... 52
5.2.1 Ground surface temperature variations ... *52*
5.2.2 Controlling factors on the surface offset ... *55*
5.3 A statistical approach to represent small-scale variability of permafrost temperatures due to snow cover (Paper II). ... 60
5.4 Spatial and temporal variability of snow distribution in a high alpine catchment ... 60
5.5 Sub-grid variation of snow in a regional permafrost model (Paper III) ... 64
5.6 Snow covered fraction derived from repeated digital camera images and ground surface temperature loggers ... 66
5.7 A tiling approach to represent sub-grid snow variability in coupled land-surface – atmosphere models (Paper IV). ... 69
5.8 A new permafrost map for the Scandinavian Peninsula (Paper V). ... 70
6 GENERAL DISCUSSION ... 71
6.1 Statistical representation of fine-scale snow variation ... 72
6.2 The effect of a sub-grid representation of snow in regional permafrost models and land-surface schemes ... 73
6.3 A new baseline map for permafrost in Scandinavia ... 74
6.4 Bridging terrestrial and atmosphere models ... 75
6.5 Outlook ... 76
7 CONCLUSIONS ... 77
8 REFERENCES ... 79
9 OTHER PUBLICATIONS DURING THE PHD PERIOD ... 91
9.1 Scientific publications ... 91
9.2 Conference publications ... 92
A APPENDIX ... 93

PART II – Journal Publications

This thesis is based on five papers which are referred to by roman numerals. The papers are ordered according to thematic considerations.

Paper I:

Gisnås, K., B. Etzelmuller, H. Farbrot, T. V. Schuler, and S. Westermann. 2013. CryoGRID 1.0: Permafrost distribution in Norway estimated by a spatial numerical model. *Permafrost and Periglacial Processes*. doi: 10.1002/ppp.1765, 2013

Paper II:

Gisnås, K., Westermann, S., Schuler, T. V., Litherland, T., Isaksen, K., Boike, J., and Etzelmüller, B.: A statistical approach to represent small-scale variability of permafrost temperatures due to snow cover. *The Cryosphere*, 8, 2063-2074, doi: 10.5194/tc-8-2063-2014, 2014.

Paper III:

Gisnås K, S. Westermann, T.V. Schuler, K. Melvold and B. Etzelmüller. Small-scale variation of snow in a regional permafrost model. *The Cryosphere Discuss.*, 9, 6661-6696, doi: 10.5194/tcd-9-6661-2015, 2015.

Paper IV:

Aas, K.S., K. Gisnås, S. Westermann, T. Berntsen. A tiling approach to represent sub-grid snow variability in coupled land-surface – atmosphere models. Submitted to *Journal of Hydrometeorology,* January 2016.

Paper V:

Gisnås K., B. Etzelmüller, C. Lussana, J. Hjort, A.B.K. Sannel, K. Isaksen, S. Westermann, P. Kuhry, H.H. Christiansen, A. Frampton, A. Frampton and J. Åkerman: A new permafrost map for the Scandinavian Peninsula. Submitted to *Permafrost and Periglacial Processes,* February 2016**.**

PART I

1 Introduction

1.1 Motivation

Permafrost is one of the key elements of the global cryosphere and the periglacial environments, occupying approximately a quarter of the landmass of the Northern Hemisphere (Figure 1) (Zhang et al., 2000). Permafrost is defined as ground remaining at or below 0 °C for at least two consecutive years (French, 2007). The *active layer* is defined as the upper part of the ground experiencing seasonal thawing and freezing. Both the spatial extent of permafrost and the thickness of the active layer are thus solely defined by the thermal regime. Consequently, both are highly sensitive to changes in the surface energy budget. Because of the dampening of temperature amplitudes with depth, permafrost gives a filtered signal of the long-term changes in ground surface temperatures, and is therefore a useful climate indicator. It is also a controlling factor of the landscape evolution in both arctic and alpine regions on different spatial and temporal scales (Etzelmüller et al., 2003).

A large number of studies have shown evidence of substantial global warming over the last decades, with the most pronounced increase in the high-latitude regions of the northern hemisphere. Here, temperatures have risen 0.6 °C per decade over the last 30 years (IPCC, 2013). This has greatly affected the terrestrial cryosphere. Evidence of increasing ground temperatures is reported from many regions, including the Nordic area (Isaksen et al., 2001; Harris et al., 2003; Isaksen et al., 2008a; Christiansen et al., 2010).

Figure 1: Distribution of permafrost in the Northern Hemisphere according to (Brown et al., 1997) with distribution of TSP borehole observations as a part of the GTN-P network indicated with red and green dots.

General Circulation Models (GCMs) predict an accelerated warming trend towards the end of the 21st century, most likely with a global surface temperature increase exceeding 1.5°C relative to 1986-2005 (IPCC, 2014). This will lead to increases in permafrost temperatures, deepening of active layers, and complete degradation of permafrost will occur in some regions. By the end of the 21st century the near-surface permafrost extent is projected to decrease by between 37% (RCP2.6) and 81% along the *Representative Concentration Pathways* (RCP) 2.6 and 8.5 (IPCC, 2013). This may trigger climate feedback effects from local to global scale, and will highly affect ecosystems, infrastructure and communities in the

Arctic. Large amounts of greenhouse gasses (CO_2, CH_4, N_2O) are prospected to be released into the atmosphere from thawing of organic-rich permafrost (Schuur et al., 2008; Elberling et al., 2010). Current permafrost areas are projected to become a net emitter of carbon over the 21st century (IPCC, 2014), causing them to act as a positive feedback mechanism on the climate system. These processes are poorly represented in the GCMs (IPCC, 2013), and considerable effort is currently being made to better represent permafrost and its possible feedback mechanisms in future models.

In mountain permafrost areas, studies indicate a temperature dependent stability in steep slopes and vertical rock faces (Gruber and Haeberli, 2007; Krautblatter et al., 2013). A high number of rock slides originating from rock walls with permafrost have been observed in the Alps during the last decades, with increasing intensity in warmer periods (Gruber et al., 2004a; Noetzli et al., 2006). However, mountain permafrost change as a trigger mechanism for rock instability is not yet fully understood.

Great advances have been made during the last decades towards better monitoring of ground temperatures and summer thaw in permafrost areas, with data collected in a Global Terrestrial Network for Permafrost (GTN-P, Figure 1). Because permafrost is an "invisible" phenomenon, spatial models of ground temperatures are required to be able to quantify the current distribution of permafrost on a global scale. Such models are crucial to be able to project the response of ground temperatures to a warming climate with the potential related feedbacks. Earth System Models (ESMs) operate on grids with a resolution of 50 to 300 km, which is far too coarse to adequately represent topography and land surface processes. Downscaling is therefore necessary to do any detailed impact assessment. Regional Climate models operate on finer spatial resolutions of down to 4 km, which improves the representation of atmosphere variables (e.g. Stendel et al., 2007). However, because of the extreme heterogeneity of the land surface compared to atmosphere variables, the energy exchange at the surface is still not sufficiently resolved at this resolution. This is particularly true for arctic and high alpine environments, where the topography and surface properties vary on the meter scale.

The high computational cost of increasing the spatial resolution in existing land surface models necessitates evaluation of alternative techniques to represent the fine-scale variability at the land surface. Sufficient knowledge of each parameter's contribution to the spatial variability of energy exchange between the ground allows for application of a statistical

representation of the crucial parameters in order to reproduce most of the observed variation. However, implementation of a statistical downscaling scheme in regional land surface models requires knowledge of the spatial behaviour of the selected parameters down to a fine scale over large areas. It is therefore a need for both detailed investigations of fine-scale processes, as well as acquisition of large spatially distributed datasets that allows for understanding of the regional behaviour.

The seasonal snow cover exerts a major influence on the thermal regime of both the terrestrial cryosphere and glaciated areas, mainly because it acts as a very effective insulator during the cold season. The insulating effect of snow increases non-linearly with depth, and combined with the asymmetric distribution of snow normally found in mountain areas, large biases are potentially introduced in models by the averaging effect of coarsely resolved snow data. The high albedo of a snow covered surface compared to bare ground significantly influences the local surface energy balance. The timing of the onset and offset of the snow cover is therefore important both for weather forecasting and climate models. Snow cover is also a crucial part of the hydrological regime, particularly in Norway. 40 % of the Norwegian land area is situated above 600 m a.s.l. as large plateaus and u-shaped valleys, storing major parts of the runoff as seasonal snow (Erlandsen et al., 1997). In mountain regions snowmelt contributes with as much as 85 % of the annual runoff (Dingman, 2002). A precise representation of the distribution and properties of the seasonal snow cover in Norwegian mountain regions is therefore valuable not only for land surface modelling and weather forecasting, but also for flood forecasting and run-off prognoses in the hydro power industry, as well as snow avalanche forecasting (Kronholm et al., 2010).

1.2 Objectives

There is a large scale gap between the coarsely-resolved ESMs used to predict future climate changes and the finely-resolved land surface schemes required to evaluate both glacier mass balance, snow distribution and ground thermal conditions. In order to provide sound predictions of how the terrestrial cryosphere will respond to future climate changes, we need up- and downscaling procedures for surface processes. The NFR-funded CryoMet project addresses this problem, focusing on how snow processes influence the surface energy balance. As part of the CryoMet project, this thesis seeks to contribute to the downscaling

procedures of snow in mountain environments. The objectives are summarized by the following main goals:

1) Quantify the variability of ground temperatures within an area corresponding to a typical grid-cell used in regional permafrost models and land surface schemes, as well as develop a better understanding of which surface parameters are the primary contributors to this variability.
2) Develop downscaling schemes for representation of snow distribution in non-vegetated high-mountain areas of Norway.
3) Evaluate the effect of an integrated sub-grid distribution of snow in numerical permafrost models and land surface schemes.
4) Provide a new permafrost map for Finland, Sweden and Norway.

The goals are achieved through detailed field studies of critical parameters governing the atmosphere-ground interactions at three different high-alpine sites in Norway. These field observations are combined with reanalysis of a large set of available ground temperature data and snow depth surveys. Together, this forms the basis for detailed analysis, statistical downscaling, calibration of parameters and model evaluation.

1.3 Outline

This thesis is composed of two parts. PART 1 provides an overview of the presented research and yet unpublished results. A general background on the ground thermal regime and its controlling factors is given in *Chapter 2*, together with an overview of snow and permafrost monitoring and modelling. The geological and climatological settings of the study area and field sites are presented in *Chapter 3*. *Chapter 4* provides a main overview of the methodologies applied in the research of the thesis, with detailed descriptions of the field and modelling approaches. Short summaries of each of the publications forming the basis of thesis are given in *Chapter 5*, together with unpublished additional material related to each of the publications. An overall discussion of the results and implications for the scientific community is provided in *Chapter 6*. Conclusions and outlook are presented in *Chapter 7* and *Chapter 8*, respectively. A list of related journal and conference publications published during the PhD work, but not included in the thesis, is given in *Chapter 10*.

PART II consists of the five scientific papers forming the basis of this thesis. Papers I and II are peer-reviewed and published, Paper III is at the time of writing published as a discussion paper, while Paper IV and Paper V is submitted and in review. All papers are published or submitted to internationally recognized scientific journals.

2 Background

2.1 Permafrost modelling

The two main categories of mountain permafrost distribution models today are regionally calibrated empirical-statistical models and physically based process-oriented models (Riseborough et al., 2008; Harris et al., 2009). Empirical-statistical permafrost models relate documented permafrost occurrences to topo-climatic factors, such as elevation, slope and aspect, mean annual air temperature (*MAAT)* and solar radiation (Hoelzle, 1996; Etzelmüller et al., 2001; Wright et al., 2003; Heggem et al., 2005). These models have been criticized for being grey boxes with topo-climatic factors selected according to their relative influence on the total energy balance exchange (Harris et al., 2009). They also assume a steady-state condition and neglect effects of a three dimensional topography on heat fluxes in the ground. However, such models are easily applied, require only limited input parameters, and are relatively reliable if they are well calibrated locally or regionally. Process-based models give a more detailed and physical reconstruction of the energy fluxes between the atmosphere and the permafrost, treating all the factors of the surface energy budget explicitly. They therefore require large amounts of precise input data. They are particularly well suited for sensitivity studies with respect to interactions and feedbacks involved under climate-change scenarios (Harris et al., 2009).

Process-based permafrost models can be categorized based on temporal, spatial and thermal criteria (Riseborough et al., 2008). Spatially, ground temperatures can be modelled in one dimension at a single point location, in two dimensions over transects, or geographically over

a larger area. The spatial resolution should vary with the scale of implementation, from continental to regional or local scale. The relative importance of climate, topography and ground conditions varies respectively (Harris et al., 2009). Spatial resolution should match the scale of variation in the area of implementation. Mountain permafrost is characterized by large variability and it has therefore been questioned whether a regional model can reproduce a permafrost distribution in mountainous areas (Harris et al., 2001b; Riseborough et al., 2008; Harris et al., 2009).

Temporally, models can either define a steady-state permafrost condition (equilibrium models), or a transient evolution from an initial state to a current or future state (transient models). Simple thermal models can calculate the presence or absence of permafrost, active layer depth or annual averages of temperatures at the ground surface or top of the permafrost. These models are frequently based on empirical-statistical relations using transfer functions between air and ground temperatures. Numerical models may define longer term progression of a deep-ground temperature profile (transient modelling), and are more complex representations of the ground thermal regime (Riseborough et al., 2008).

The last climate reports by IPCC have highlighted the impact of increasing ground temperatures caused by the coming century climate changes predicted by the GCMs. This has led to an increased focus on transient permafrost modelling, which has so far taken two main directions: (1) the so called *post-processing method* (Sazonova and Romanovsky, 2003; Nicolsky et al., 2007; Zhang et al., 2008) with a one-way coupling between the GCM and the permafrost model, and (2) a two-way coupled scheme where the permafrost model is integrated in the GCM, or in ESMs.

In the post-processing approach, national, regional and global permafrost models of different levels of sophistication are forced with output from GCMs. The main problem with the post-processing approach is that the feedback from the ground is not coupled back into the GCM. In addition, the coarse resolution of the GCMs does not represent the permafrost processes satisfactorily. This is improved by using downscaled regional climate models (RCMs) with higher resolutions, to force the permafrost model. The post-processing approach is often used to run equilibrium models, and the transient evolution of steady-state conditions can be reproduced. However, the model will not give any information about when the steady-state situation will occur because of the significant time lag between air temperatures and ground

temperatures. Even with these limitations, studies show satisfactory results using relatively simple equilibrium models (Sushama et al., 2006; Riseborough, 2007).

The ESMs typically comprise fully coupled atmosphere, ocean, land, sea ice and often biogeochemical components. Examples of ESMs with integrated permafrost models are the Community Land Model (CLM; Lawrence et al., 2011) and the Organizing Carbon and Hydrology in Dynamic Ecosystems (ORCHIDEE; Koven et al., 2011). The more sophisticated fully coupled ESMs give a more direct modelling of the permafrost dynamics. However, it has been problematic to obtain good results with this method, due to shallow soil columns, absence of an organic layer on the surface, errors in the climate model (e.g. Lawrence and Slater, 2005). In addition, as with the post-processing approach, the coarse resolution does not represent the permafrost processes satisfactorily.

Since the Fourth Assessment Report, major efforts have been directed towards improving the representation of permafrost in such models. The fifth phase of the Coupled Model Intercomparison Project (CMIP5) compares and evaluates the performance of the permafrost models in a range of these ESMs against observations and theoretical expectations (Taylor et al., 2011). In this way the predicted fate of permafrost under scenarios with temperature increase is evaluated. The intercomparison of permafrost models has identified large variations in modelled mean soil temperatures (Koven et al., 2012). The disagreements can be traced to the representation of the surface offset, and in particular its mediation by snow in winter. There is also a wide variety in the amount of dampening of the mean and the amplitude of soil temperatures with depth. These are partly related to differences in the modelled soil physical properties and the coupling between soil temperature and hydrology, particularly for organic layers. Some models represent the organic content as a mixture of organic and mineral properties, instead of as separate units through the soil column (Koven et al., 2012).

2.2 The ground thermal regime

The ground thermal regime is determined by the surface energy balance as an upper boundary condition, the geothermal heat flux as the lower boundary condition, and the thermal properties of the ground Figure 2. While the temporal variability of the geothermal heat flux is normally disregarded, the surface energy balance varies over different time scales corresponding to the annual and the daily cycles of solar radiation. The surface energy balance as a sum of sensible, latent and ground net heat fluxes (Figure 2) can be formulated as (e.g. Hartman, 1994):

$$\frac{\partial Q}{\partial t} = SW_{net} + LW_{net} - SH - LH - GH - G_{melt} \quad (1)$$

where Q denotes the energy balance of the uppermost surface layer. SW_{net} and LW_{net} are the net short and long wave radiation fluxes, SH and LH are the sensible and latent heat fluxes, GH is the energy exchange between the surface and the underlying ground, and G_{melt} is the melting of snow/ice in the uppermost surface layer.

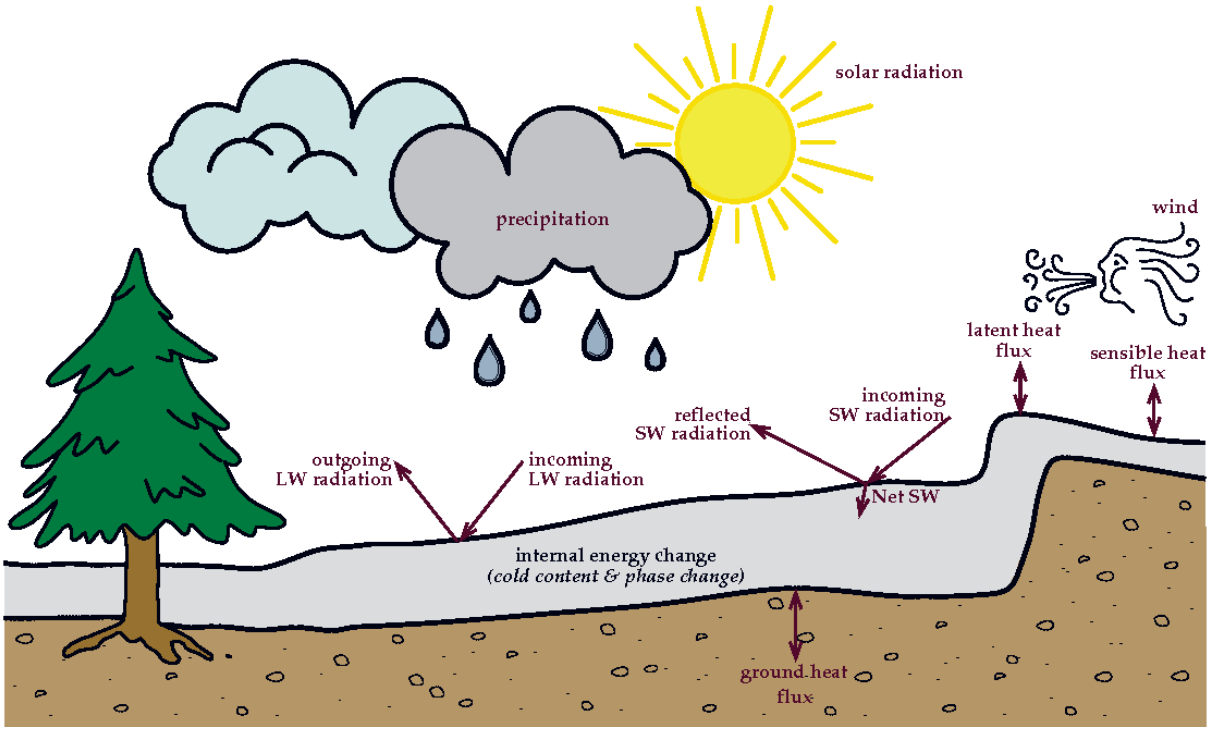

Figure 2: The main components contributing to the surface energy balance. The figure is taken from the description of the Snowpack model (e.g. Bartelt and Lehning, 2002) on the web site https://models.slf.ch/docserver/snowpack/html/general.html.

The amount of heat transported in or out of the ground is governed by the surface energy budget and the thermal properties of the ground material. The properties include the *thermal conductivity k* (W m^{-1} K^{-1}) determining the rate of heat transfer, and the *volumetric heat capacity C* (J m^{-3} K^{-1}) controlling the magnitude of temperature change introduced by the heat transfer (Williams and Smith, 1989). The heat transfer equation under transient conditions forms the basis for all geothermal models, and can be expressed through the general one-dimensional diffusion equation for heat in the form:

$$C_{eff}\frac{\partial T}{\partial t} = \frac{\partial}{\partial z}\left(k\frac{\partial T}{\partial z}\right) \quad (2)$$

The material is a porous media of different components such as organic matter, minerals and water, all having different values for *k* and *C*. When water contained in the material undergoes freezing and thawing, release and absorption of latent heat of fusion is the dominant factor in the heat flow (Williams and Smith, 1989). This is normally accounted for by subsuming its effect in the volumetric effective heat capacity parameter C_{eff} *(Riseborough et al., 2008)*:

$$C_{eff} = \sum x_i \rho_i c_i + L(\partial\theta_u/\partial T) \quad (3)$$

where θ_u is the volumetric unfrozen water content of the subsurface material, T is the temperature of the ground (°*C*) and *L* is the volumetric latent heat of fusion (J m^{-3}). The volumetric heat capacity is summed over each component of the ground, *i* (ice, solid earth material, water, etc.). *x* is the volume fraction of the component, ρ the density (kg m^{-3}) and *c* the specific heat capacity (J kg^{-1}).

2.2.1 The surface offset

Solar radiation is the main controlling factor of ground temperatures and permafrost distribution on a regional scale (e.g. Hoelzle, 1996; Etzelmüller et al., 2001; Gruber et al., 2004a; Etzelmüller et al., 2007). However, the surface energy balance, reflected in the ground surface temperatures (GSTs), is not only controlled by the local climate: it is also modified by a range of site-specific topoclimatic variables such as vegetation, snow cover, soil moisture and topography. These variables serve as a buffer layer resulting in an offset between air temperatures and GSTs, called the *surface offset*. The combination of several variables, some being inter-correlated and some having high spatial heterogeneity, makes physical model representation of all parameters in the surface offset a highly challenging task. The controlling factors of the surface offset constitute a key topic of this thesis, discussed in detail in Section 2.3.

For model purposes, where a detailed representation as described above is not possible due to computational restrictions or lack of detailed input data, empirical-based transfer functions (*n*-factors) are used to link the temperatures at the ground surface to the air temperature. *n*-factors are computed as ratios of annual accumulated freezing and thawing degree days between the ground surface (DD_S) and the air (DD_A):

$$nF = \frac{FDD_S}{FDD_A},\ nT = \frac{TDD_S}{TDD_A} \quad (4)$$

Freezing (*FDD*) and thawing (*TDD*) degree day indexes are integrated negative or positive daily temperatures, respectively (Klene et al., 2001):

$$DD = \int_0^{t_s}(|T - T_F|)dt \quad (5)$$

T_F is the freezing temperature of water (0°C), T is the daily mean temperature in the air or at the ground surface, t_s is the duration of the thawing/freezing season. *n*-factors were originally used for engineering purposes (Lunardini, 1978), but have also shown to be applicable in modelling natural environments (Jorgenson and Kreig, 1988; Taylor, 1995; Klene et al., 2001; Juliussen and Humlum, 2007).

A relation for the mean annual ground surface temperature (*MAGST*) can be derived from degree days in the air together with *n*-factors:

$$MAGST = \frac{TDD_A \times nT - FDD_A \times nF}{P} \quad (6)$$

where P is one year in days (365 days).

2.2.2 The thermal offset

The moving freezing front during winter season and thawing front during summer season are governed by the annual cycle in the surface energy budget. The ground down to maximum thaw depth, corresponding to the ground undergoing annual phase change in permafrost areas, is termed the active layer. *The thermal offset* ΔT is defined as the difference between *TTOP* and *MAGST,* where *TTOP* is defined as the mean annual temperature at the top of the permafrost or the bottom of the seasonal freezing layer (Goodrich, 1978; Burn and Smith, 1988; Smith and Riseborough, 1996). Thermal conductivity of ice is approximately four times higher than water, and the thermal offset therefore highly depends on the moisture content of the subsurface materials. When water is present in the ground, the heat transfer out of frozen

ground in winter will exceed the heat transfer into the ground through the thawed active layer in summer. This implies progressively lower mean annual temperatures down towards the bottom of the active layer, and makes it possible to maintain permafrost also when the mean annual ground surface temperature is above 0 °C.

The most common analytical equation for the moving phase change boundary in permafrost models is the Stefan approximation, widely used in field based studies of thaw depth (e.g. Nelson et al., 1997; Shiklomanov and Nelson, 2003; Heggem et al., 2006). The primary assumption of this approximation is that sensible heat is ignored, and all heat flow is used to exchange heat at the freezing or thawing front. When ignoring transient effects, the step change in temperature, i.e. $|T - T_F|t$ can be replaced by annual accumulated freezing or thawing degree days (see Eq. 5), and the Stefan solution can be written as:

$$Z = \sqrt{\left[\frac{2k}{\theta_w L}\right]\left[DD_{gs}\right]} \tag{7}$$

where Z is the depth of the thawing or freezing front and θ_w is the water content of the ground. DD_{gs} is degree days at the ground surface, which is often used instead of a step change in temperature when the formula is applied for field use (Lunardini, 1981).

In general, permafrost will exist when seasonal thaw does not thaw all of the frozen ground. Therefore, to determine the occurrence of permafrost from freezing and thawing indexes at the ground surface alone, a simplified version of Stefan solution is employed (Carlson, 1952):

$$k_f \times FDD_s > k_t \times TDD_s \tag{8}$$

where k_f and k_t are thermal conductivities of the ground in frozen and thawed state, respectively.

Assuming a steady state situation over the one-dimensional heat diffusion equation Romanovsky and Osterkamp (1995) derived an analytical expression for the thermal offset based on a transformation of the Stefan thawing problem for the active layer and on the definition of thermal offset.:

$$\Delta T = \begin{cases} \frac{TDD_s}{P}\left(\frac{k_t}{k_f}-1\right) & if\ k_f FDD_s \geq k_t TDD_s \\ \frac{FDD_s}{P}\left(1-\frac{k_t}{k_f}\right) & if\ k_f FDD_s < k_t TDD_s \end{cases} \tag{9}$$

This equation was previously stated by Kudryavtsev (1981), but without any derivation. By rearranging this formula and including *n*-factors for the surface offset, we get a solution for the mean annual temperature at the seasonal maximum depth of the freezing or thawing front. This solution is referred to as the TTOP-approach (Smith and Riseborough, 1996):

$$TTOP = \begin{cases} \frac{(TDD_a \times nT \times r_k - FDD_a \times nF)}{P} \text{ for } k_t TDD_s \leq k_f FDD_s \\ \frac{\left(TDD_a \times nT - \frac{1}{r_k} \times FDD_a \times nF\right)}{P} \text{ for } k_t TDD_s \geq k_f FDD_s \end{cases} \quad (10)$$

where

$$r_k = \frac{k_t}{k_f} \quad (11)$$

2.3 Controlling factors of the surface offset

The large fine-scale variability in GST at the meter scale is a result of the high complexity in the buffer layer. The complexity of the buffer layer stems from (1) a high degree of spatial heterogeneity in several of the influencing variables, (2) a set of different effects from each variable, and (3) interaction between the variables.

2.3.1 The vegetation cover

The influence of vegetation on the ground temperatures is complex and related to several different processes. Trees affect the soil moisture and organic content, shade the ground from direct solar radiation, intercept snow, and act as snow fences accumulating wind blown snow. Depending on the forest species and canopy density, in combination with the amount of potential incoming solar radiation, the vegetation may decrease or increase the ground temperatures. Permafrost areas in the Swiss Alps and in Scandinavia are generally restricted to non-forested areas (Hoelzle, 1996; Isaksen et al., 2008a; Harris et al., 2009; Farbrot et al., 2013), mainly because of the cooler summer seasons and high redistribution of snow. Consequently, the shading effect is less important, while accumulation of wind drifted snow in the vegetation insulates the ground. In Scandinavia, vegetation near the permafrost zone consists mainly of shrubs and mountain birch. This low vegetation acts as a very effective snow fence that can be buried entirely by snow during winter, additionally increasing the surface albedo. In more continental permafrost areas, such as in the Yukon Territory, Alaska (Dingman and Koutz, 1974) and Mongolia (Heggem et al., 2006), permafrost may occur

below tree stands, even when permafrost is not present in the surrounding terrain. This is attributed to the effect of trees shading the ground from the very high amount of solar radiation during summer season in more continental climates. The vegetation in these more low-land permafrost areas is dominated by larger tree species such as black and white spruce.

2.3.2 Topography and related effects of aspect and slope

On the macro-scale, topography influences the atmospheric conditions such as air temperatures and precipitation patterns, and therefore also the amount of precipitation falling as snow. The main effect of the local topography is the influence on the amount of potential incoming solar radiation in a single point location, related to the aspect and shading from surrounding topography. Indirectly, topography influences the drainage patterns and therefore the soil moisture, the distribution of vegetation, as well as the local variation in wind speed. The latter controls the erosion and accumulation related to wind drifting of snow. The variation in solar radiation is particularly important in mid-latitudes where the total amount of solar radiation is high. Topographic features such as mountain peaks and rock walls, three-dimensional by nature, introduce three-dimensional thermal effects in the ground (Gruber et al., 2004b; Noetzli et al., 2007).

2.3.3 The effects of a seasonal snow cover

The seasonal snow cover is a decisive factor controlling the ground thermal regime and the surface energy budget, in particular in cold regions with a sparse vegetation cover (e.g. Goodrich, 1982; Isaksen et al., 2001; Zhang et al., 2001; Ishikawa, 2003; Luetschg et al., 2004; Luetschg et al., 2008). Its most important property impacting the ground temperatures is its seasonality. In addition, its influence on ground temperatures is related to the combination of four main physical properties of snow: (1) the high surface albedo, (2) the high emissivity, (3) the low thermal conductivity, and (4) the latent heat of fusion.

(1) The high surface albedo leads to a reduction in absorbed solar radiation, which again may cause a lowering of the temperature at the surface. In arctic regions where the incoming solar radiation during the snow covered season is low, this effect is less pronounced, but still observable. At more southerly latitudes the small scale pattern of snow during melt-season highly influences the near surface temperatures.
(2) Emissivity of snow varies from 0.96 to 0.99 and it therefore acts nearly as a "blackbody" in thermal infrared wavelengths. This gives a possible increase in the efficiency in the longwave radiation exchange, which may decrease the ground surface

temperatures. However, it should be noted that in some cases the emissivity of the ground surface without a snow cover is almost as high, or even higher, as for snow.

(3) Dry snow mainly consists of air and ice crystals, resulting in an extremely low thermal conductivity ranging from close to 0.0 W m^{-1} K^{-1} for fresh to about 0.5 W m^{-1} K^{-1} for very dense ripened snow (Figure 3, Sturm et al. (1997)). The low thermal conductivity makes the seasonal snow cover an effective insulator, and a sufficiently thick snow cover depending on the climate and snow properties, typically around 50 - 80 cm in Norway and the Swiss Alps, nearly disconnects the ground surface temperatures from the cold air temperatures (Haeberli, 1973). This results in higher GSTs close to 0°C. The insulating effect of snow makes snow the dominating parameter modifying the energy exchange to the ground in high-mountain and arctic environments where the vegetation cover is sparse (e.g. Smith, 1975; Goodrich, 1982; Zhang, 2005; Farbrot et al., 2011; Morse et al., 2012). The snow cover therefore often determines the boundary between continuous and discontinuous permafrost in these environments (Smith and Riseborough, 2002).

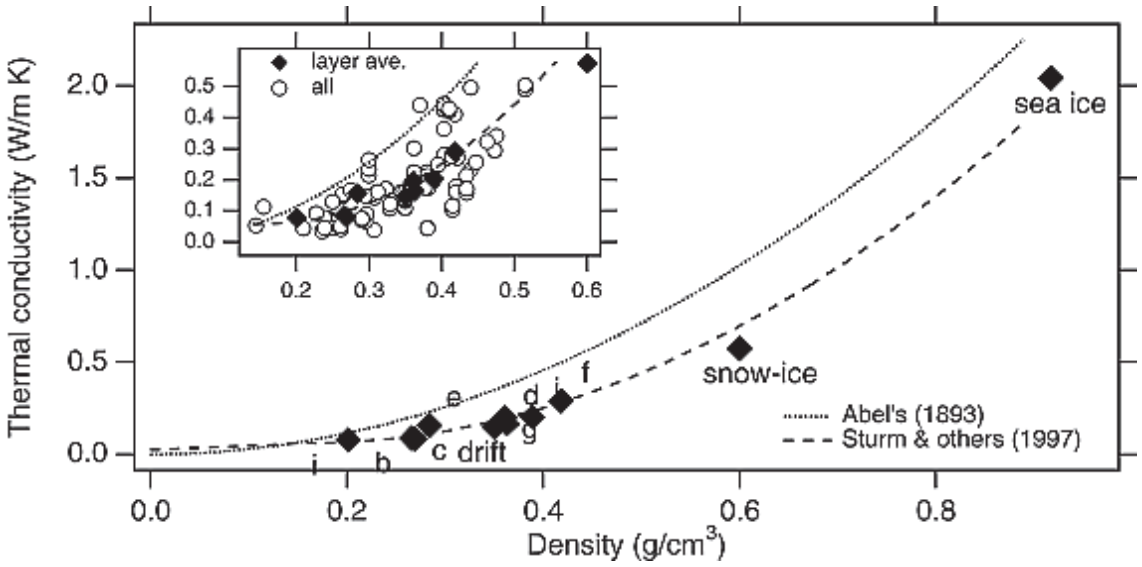

Figure 3: Relation between thermal conductivity and density of snow (from Sturm et al., 1997).

(4) The energy required to melt ice, the latent heat of fusion, is 334 J g^{-1}. For snow and ice rich materials the energy required to thaw the material is by far larger than the energy required to increase or decrease its temperature. Snow melt is therefore an energy sink, and keeps the ground surface at 0 °C until the snow is entirely melted, even though the air temperatures are well above 0 °C. In areas with a thick snow cover and high air

temperatures during melt-season, this has a significant effect on the soil temperatures. (Harris et al., 2009). If the snow cover is highly redistributed with large variation in snow depths, the latent heat of fusion effect introduces large spatial variations in GST during the melt-season.

The timing of the onset and offset of the snow cover influences its effect of temperature increase or decrease on the ground (Zhang, 2005; Luetschg et al., 2008). An early establishment of snow in the fall relative to when air temperatures are falling below 0 °C yields an insulating effect on the ground. Contrary, a late offset in spring results in a decrease in ground temperatures. However, a thin snow cover with high albedo during fall is likely to have a cooling contribution since the insulating effect is less than the reduction in absorbed energy due to reflection. A thick snow cover has a great impact on soil temperatures, as it insulates from the cold air temperatures. This effect increases with colder winter environments. However, a thicker snow cover will also imply a longer duration of snow covered season, sometimes into late spring and summer. If the snow cover lasts long enough, the albedo and latent heat effects exceed the isolating effect during winter, and the total effect of the thick snow cover will be a cooling of the ground (Zhang, 2005).

2.4 Snow distribution in alpine areas

2.4.1 Spatial variation of snow

The spatial variation of snow depths is a result of several mechanisms operating on different scales in different environments. At large scales of hundred meters to several kilometers orographic effects on the precipitating clouds result in large variations in precipitation and snow depth (e.g. Førland et al., 1997; Anders et al., 2007; Schuler et al., 2008; Jarosch et al., 2012; Mott et al., 2014). Depending on the storm type and the size and shape of the surface topography, precipitation amounts can be enhanced either on the windward side, the leeward side or at the ridge top (Houze, 2012; Mott et al., 2014). At more local scales (< 1 km) the variation in snow cover thickness is mainly driven by the local wind field, influence by local topography and vegetation.

At high altitudes and in arctic areas, strong winds in combination with open terrain heavily redistributes the snow, yielding significant variability in snow depth over distances from tens of centimetres to hundreds of meters (Sturm et al., 1995; Bruland et al., 2001; Liston et al.,

2007). Here, high elevations and exposed terrain, often in combination with a relatively long season of drier snow conditions, lead to a high frequency of blowing snow and accumulation in lee of terrain features, topographic depressions and vegetation (Pomeroy and Gray, 1995; Liston and Sturm, 1998). Secondly, drifting snow leads to significant sublimation of wind-borne particles and locally loss of snow of up to 10 % (Liston and Sturm, 1998; Liston and Sturm, 2004; Groot Zwaaftink et al., 2011; Bernhardt et al., 2012). However, averaged over the catchment scale the loss is probably only a 2-3 % (Groot Zwaaftink et al., 2011; Bernhardt et al., 2012).

The impact of vegetation on snow depth variability in vegetated regions is important where the snow depths are less than the vegetation height. Here, snow distribution mechanisms operate on the scale from tens to hundreds of meters (Liston, 2004). In these areas canopy-intercepted snow leads to mass loss by sublimation, but also tree wells around the tree trunk, with radiuses up to 5 meters (Sturm, 1992). These accumulation variations depend on leaf area, canopy density, and forest species (e.g. Moeser et al., 2015).

During melt season spatially variable factors controlling the surface energy budget can lead to spatially variable melt rates and a further change in the variability of snow depths (Liston, 1999; Mott et al., 2011; Egli et al., 2012). The governing factor is the incoming solar radiation, spatially variable with aspect and shading from surrounding topography and vegetation. This effect is particularly important for high-mountain areas at more southerly latitudes. Additionally, vegetation and surrounding topography contribute by emitting long wave radiation (e.g. Pomeroy et al., 2003; Pomeroy et al., 2009), and local advection can produce enhanced snow melt at the edges of snow patches (Liston, 1995).

2.4.2 Snow distribution modelling

To model the local wind drifting of snow, models with different levels of physical sophistication, number of input parameters, and computational cost can be applied. The models can be classified into 1D point models, 2D, and fully spatial distributed 3D models. Temporally, models can be classified in models simulating individual storm-events and models simulating the entire snow season. For the purpose of an improved representation of the surface-energy balance, a snow simulation for the entire snow season is normally required.

During the past decades there has been a great advance in the development of snow distribution models that physically describe saltation and suspension as the main mechanisms for moving snow (e.g. Pomeroy et al., 1998; Essery et al., 1999; Liston et al., 2007; Lehning

and Fierz, 2008). The models vary in complexity; however, the development tends to go towards more realistic representations of the physical processes. The earlier models tried to capture the first-order physics, while still being able to simulate spatial snow distribution over the entire snow season (Pomeroy et al., 1997; Liston and Sturm, 1998; Essery et al., 1999; Jaedicke et al., 2000; Durand et al., 2005). To manage this, the complexity of the snow transport was partly reduced to empirical and analytical relationships between topographical parameters, wind speed and transport rates. Winstral and Marks (2002) and Winstral et al. (2002) developed terrain-based parameters to characterize the effects of wind on snow redistribution in complex terrain, without any physical representation of the snow pack. All these models are able to simulate observed snow cover patterns, but the magnitude is often deficient (Liston and Hiemstra, 2008). This might be due to shortcomings in the model physics, errors in the meteorological forcing data due to e.g. mismatch in resolution, near surface wind fields (Bernhardt et al., 2009) or gauge undercatch in windy environments (Liston and Sturm, 2004), or also errors in the boundary conditions due to relatively low-resolution topography and vegetation data (Liston and Sturm, 1998; Liston et al., 2007).

Lately, more complex models have been developed to solve 3D wind-fields by applying atmospheric models over high-resolution grids (Gauer, 2001; Liston et al., 2007; Lehning and Fierz, 2008; Bernhardt et al., 2009; Mott and Lehning, 2010). The scales required for representing the driving mechanisms of snow transport are debated, but in complex terrain, such as in alpine mountain areas, it is suggested that the small scale redistribution by saltation and suspension are not captured even by horizontal resolutions as fine as 25 m (Lehning and Fierz, 2008; Raderschall et al., 2008). High spatial resolution in combination with a complex 3D-representation of the physical processes ultimately results in considerable computational cost for simulations over even small sub-catchment areas. The increased model complexity therefore results in temporal and spatial restrictions. The size of the area of interest, the time span of simulations required for the purpose, the availability of input parameters, as well as the spatial resolution and quality of surface characteristics must be considered to select an appropriate model.

2.5 Permafrost monitoring and mapping

Monitoring of thermal profiles of ground temperatures in permafrost is a sensitive method for detecting long-term changes in the surface energy balance over annual to century time scales. The low conductivity in the ground filters the high frequency climate signals in the atmosphere, and preserves only the long term signals. Long term observations of the thermal regime in boreholes are therefore necessary to understand the changes on the ground regime in a warming climate, and to validate models. The second important variable to monitor in order to analyze changes in permafrost is the active layer thickness. Changes in the active layer thickness could be expected as a response to changes in the surface climate, particularly in summer. It may have significant temporal and spatial effects on the carbon balance of the tundra (Romanovsky and Osterkamp, 1995; Schuur et al., 2008), terrain stability and thus also human infrastructure in cold regions (Nelson et al., 2002), and natural hazards and landscape processes in general (Harris et al., 2001a).

The Global Terrestrial Network for Permafrost **(**GTN-P**)** was developed in the 1990s, and is the primary international program concerned with monitoring permafrost parameters (Burgess et al., 2000). It was established with the aim of obtaining a comprehensive view of the spatial structure, trends and variability of changes in the active layer thickness and permafrost temperature. Two global monitoring programs are established to coordinate observations of these two key variables: the Thermal State of Permafrost (TSP) and the Circumpolar-Active-Layer-Monitoring (CALM) program. CALM was initiated already in 1991 (Nelson et al., 2004). It was among the international permafrost community's first large-scale efforts to construct a coordinated monitoring program capable of producing data sets suitable for evaluating the effects of climate change. The goal of the program is to measure inter-annual to -decadal variations in the active layer thickness, near-surface temperature and surface movement over local to global geographic scales using standardized protocols. During the International Polar Year (2007-09) major steps in monitoring of ground temperatures were taken through the TSP program (Romanovsky et al., 2010b). New networks of boreholes instrumented with data loggers were established world wide, such as in the Nordic countries (Christiansen et al., 2010), Canada and Alaska (Smith et al., 2010), central Asia (Zhao et al., 2010), Russia (Romanovsky et al., 2010a), and in Antarctica (Vieira et al., 2010).

In Scandinavia, occurrences of permafrost in mountains were described already in the beginning of the 20th Century (Reusch, 1902). However, the research on frozen ground was

restricted to mires and palsas up to the late 1980s. During the 1960s and 1970s there were several studies on landform features as indicators for permafrost, including ice cored moraines (Østrem, 1964), rock glaciers, and non-sorted polygons (Rapp and Annersten, 1970; Rapp and Clark, 1971; Rapp, 1982). Still, the majority of the studies were restricted to palsas both in Norway (Sollid and Sørbel, 1974; Åhman, 1977; Sollid and Sørbel, 1998), Sweden (Rapp, 1982) and Finland (Seppälä, 1986; Seppälä, 1997). A new detailed inventory of rock glaciers and ice cored moraines from field observations, previous maps and aerial images was published in 2010 by Lilleøren and Etzelmüller (2011).

Already in the 1950s, frozen ground was found at a depth of 70 meters in a well drilled in bedrock in northern Sweden (Ekman, 1957). Observations of frozen bedrock were in the same period reported from construction work in northern Finland and Sweden (Ekman, 1957; Åhman, 1977). However, widespread research and mapping of mountain permafrost did not occur until the 1980s, when geophysical methods were introduced in permafrost research. Extensive permafrost was measured down to 50-100 m depths in bedrock in northern Sweden and Finland (King, 1982; King and Seppälä, 1987). Mountain permafrost limits based on geophysical, seismic and geothermal investigations, together with large surveys of the *basal temperature of snow* (BTS), were drawn for northern Sweden (King, 1982), southern and northern Norway (King, 1983), as well as for Finnish Lappland (King and Seppälä, 1987). These findings were supported by soil temperature measurements (Jeckel, 1988). The large collection of field investigations spread all over the Scandinavian Peninsula formed the basis of the first mapping of high mountain areas as sporadic, discontinuous and continuous permafrost zones (King and Åkerman, 1993).

During the period 1997-2000 the EU-initiated project PACE (Permafrost and Climate in Europe) established several deep boreholes and measurement sites for near-surface energy exchange monitoring. The aim was to improve mapping and modelling of permafrost in European high-mountain areas. Three deep boreholes (>100 m) were drilled in the Nordic area at Janssonhaugen (Svalbard), Tarfalaryggen (Sweden) and Juvvasshøe (Norway) (Isaksen et al., 2001). These boreholes provided valuable insight in the thermal regime of high mountains, and found lower ground temperatures and deeper permafrost in the high mountain areas than earlier expected. As part of the TSP program several new boreholes were established in bedrock in the mountain areas of northern Norway in 2005-2008 (Sollid et al., 2003; Isaksen et al., 2008b). The NFR (Norwegian Research Council) funded CRYOLINK project established a monitoring network for mountain permafrost and seasonal frost in

southern Norway in 2008 (Farbrot et al., 2011). In total, more than 25 boreholes were drilled during these campaigns, covering areas from the maritime west coast to more eastern inland areas. In parallel with the development of the Nordic borehole networks, a Swiss Permafrost Monitoring Network (PERMOS) were established in the year 2000. Today the PERMOS network includes 14 temperature sites where near-surface temperatures, borehole temperatures, and ERT are measured, and 14 Kinematics Sites, where terrestrial surveys and photogrammetric analyses are performed and/or air photos are taken regularly.

In addition to the borehole campaigns, large efforts have been made to map lower limits of permafrost through BTS-surveys, ground surface temperature measurements and DC resistivity tomography data (Ødegård et al., 1992; Ødegård et al., 1996; Isaksen et al., 2002; Heggem et al., 2003; Hauck et al., 2004; Heggem et al., 2005; Farbrot et al., 2008; Isaksen et al., 2008a; Juliussen and Humlum, 2008; Ødegaard et al., 2008).

Empirical-statistical models for permafrost have been implemented for central eastern Norway (Heggem et al., 2005; Juliussen and Humlum, 2007), southern Norway (Etzelmüller et al., 1998) and the Nordic countries (Etzelmüller et al., 2008). Despite the large monitoring efforts during the last decades, the *Circum-Arctic permafrost and ground ice map* (Brown et al., 1997) still represents the state of the art of permafrost mapping of the Nordic (Figure 1).

3 Setting

3.1 The Scandinavian Peninsula

Norway, Sweden and northern Finland form the Scandinavian Peninsula. The geology of the peninsula consists of a stable large crust of very old metamorphic rock (c. 2500-3100 Ma old). The Scandinavian Caledonides, also called the Scandes, stretches through most of Norway and adjacent parts of Sweden, forming the highest mountains of Scandinavia with peaks up to 2469 m a.s.l. (Galdhøpiggen, Norway). The mountain chain formed during the Caledonian orogeny c. 400 Ma ago when slices of older basement were thrust several 100 km eastwards over the edge of the Fennoscandian Shield. During the opening of the Atlantic Ocean in Tertiary, the margin of Scandinavia was tilted, with highest land heave in the west (see summary by Gabrielsen et al. (2010)).

The present topography of Scandinavia is a result of subsequent modulation by multiple glaciations the last 3 Ma, while the sediment cover over the bedrock is mostly related to the last one or two major glaciations. Pre-existing mountain river systems in the west were linearly carved by the glaciers, producing the present fjord landscape. Remains of paleic surfaces were preserved both between the fjord systems and towards the east, indicating cold-based and non-erosive conditions during at least the latter glaciations. In some areas, local glaciations have dominated over longer time periods, leaving alpine relief forms.

The sediment cover in Scandinavia is governed by the architecture and deglaciation pattern of the Pleistocene ice sheets. Only c. 43 % of the land area is today covered by till. These

deposits are unevenly distributed, with increasing coverage and thickness of tills towards the east. In high mountain areas, bedrock and only thin covers of till or regolith dominate, while valleys are often filled with glaciofluvial and fluvial sediments. Over certain elevation limits, depending on latitude and distance from coast, mountain slopes and plateaus are covered by coarse block fields. These block fields can be several meters thick, with coarse boulders overlying finer sediments. During the Holocene, a climate shift from the warm climate under the Holocene Optimum (5–9 ky BP) towards cooler and wetter conditions in the second half of Holocene favoured the accumulation of organic material in wetlands. This material covers wide areas in central and especially northern Scandinavia. Both the block fields and the organic material play crucial roles for the thermal regime and distribution of permafrost in the area.

The present climate of the Scandinavian Peninsula is highly variable; with *MAAT* ranging from below -5 °C in the highest parts of the Scandes (> 2000 m) up to 9 °C along the coast. In the northernmost areas *MAATs* are often below 0 °C almost all the way down to sea level. The Scandes represents a significant orographic barrier for the prevailing westerly winds from the Atlantic Ocean, creating a strong east-west gradient in the annual precipitation pattern. The west coast features a maritime and wet climate with sites of annual precipitation amounts higher than 3000 mm, while the driest areas to the east of the mountains receive less than 300 mm during a year. This gradient is also present in the maximum snow depths, ranging up to 6 meters in the mountains west of the water divide, while normally up to only 2 meters to the east. More than 40 % of the landmass in Norway is large plateaus and u-shaped valleys located above 600 m a.s.l., storing major parts of the potential run-off as seasonal snow. As much as 25 % of the area is located above the alpine treeline at elevations higher than 1000 m a.s.l. These areas are highly exposed to strong westerly winds from the Atlantic Ocean, resulting in a heavy redistribution of the snow cover.

The majority of the permafrost in both Norway and Sweden is found in mountainous settings. However, in the northern parts of Scandinavia, much of the permafrost is located in mires, often producing palsa landforms signifying sporadic permafrost distribution. These are widespread north of approximately 68 °N both in Norway, Finland and Sweden, and are found at elevations from sea level and up to 1000 meters a.sl, but normally just above the local treeline. Single palsas are also found at Dovrefjell and in Femundsmarka in southern Norway. These are located above 1000 m a.s.l. (Sollid and Sørbel, 1998), but most of them have shown clear signs of degradation during the last decade (Hofgaard and Wilmann, 2011).

The southernmost observation of permafrost in Scandinavia is reported from Gaustatoppen in southern Norway (59.9 °N), with frozen bedrock down to 1500 m a.s.l. (Etzelmüller et al., 2003). In central southern Norway lower limits of permafrost are found to decrease from 1650 m a.s.l. in western Jotunheimen (Etzelmüller et al., 2003) to 1450 m a.s.l. in the eastern parts and at Dovrefjell (Isaksen et al., 2002; Farbrot et al., 2011). At entirely snow free sites local permafrost occurrences are found down to 1350 m a.s.l. at Dovrefjell (Sollid et al., 2003). The easternmost parts of southern Norway feature a more continental climate, resulting in lower limits of permafrost (LLP) down to 1000 m a.s.l. (Heggem et al., 2005). In northern Norway, there is a similar gradient of decreasing LLP with the increasingly continental climate further from the coast. In coastal areas permafrost exists above c. 1250 m a.s.l., while in Kilpisjärvi and Abisko, located on the more eastern side of the Scandes, permafrost exists down to c. 800 – 850 m a.s.l. (Ridefelt et al., 2008). In inner parts of Finnmark permafrost is widespread down 400 m a.s.l. (Farbrot et al., 2013).

3.2 Field sites

The main study sites are located along a latitudinal transect from southern Norway to Svalbard; Finse (60.2°N), Juvflye (61.3°N), and Ny-Ålesund (78.6°N). The locations represent different permafrost environments ranging from sporadic to continuous permafrost coverage, from very high and wind exposed mountain permafrost to low maritime arctic permafrost, and from highly rugged to slightly undulating high Arctic landscape.

3.2.1 Finse

Finse (1222 m asl) is located in the upper part of a valley at the northern margin of the Hardangervidda mountain plateau. The valley bottom lies at an altitude of 1200m a.s.l., and consists of the Precambrian basement rock, which was eroded down to a peneplain at the end of the Precambrian times. From above 1350 meters a.s.l. the basements rocks are overlain by phyllite originating from Cambrium-Silur. The bedrock is also partly covered by weathering materials and block fields Figure 4. The surrounding mountains, with Hallingskarvet to the north and Hardangerjökulen plateau glacier (ca. 73km^2; Andreassen and Winsvold (2012)) in the south, reach altitudes above 1800 m a.s.l. Located within the highest mountain area between Oslo and Bergen, Finse is climatically situated in the transition zone between the maritime western coast and the more continental eastern parts of southern Norway. It belongs to the low alpine zone, and is about 250 meters above tree line. Summer temperatures

normally reach above 20 °C, while in winter temperatures can be below -30 °C. The *MAAT* for 1960-1990 was -2.2 °C, with average annual precipitation of 990 mm for the same period. More than half of the precipitation usually comes as snow, with snow accumulation normally starting in late October, and lasting until June. Prevailing wind direction is from the west, and due to strong winds during winter season, there is a high spatial variability of snow depths. The general lower limit of permafrost in this area is estimated to 1550 m a.s.l. (Etzelmüller et al., 2003). However, DC-resistivity soundings at 1450 m a.s.l. (Etzelmüller et al., 1998) and observations of cold ice (<0 °C) at the glacier front of Midtdalsbreen (1400 m a.s.l.) indicate permafrost at snow-free sites a lower elevations (Lilleøren et al., 2013).

The 1x1 km field site (subset in upper right corner in Figure 4) is located just to the west of Vesle Hansbunut, 3.5 km southeast of Finse railway station. The field area lies around 100 m higher than the valley bottom, and features a rough and undulating topography. The vegetation cover is sparse, and the surface is dominated by coarse moraine deposits, block fields and bedrock. Due to the elevated location in the valley and the surface material, the water content in the ground is relatively low.

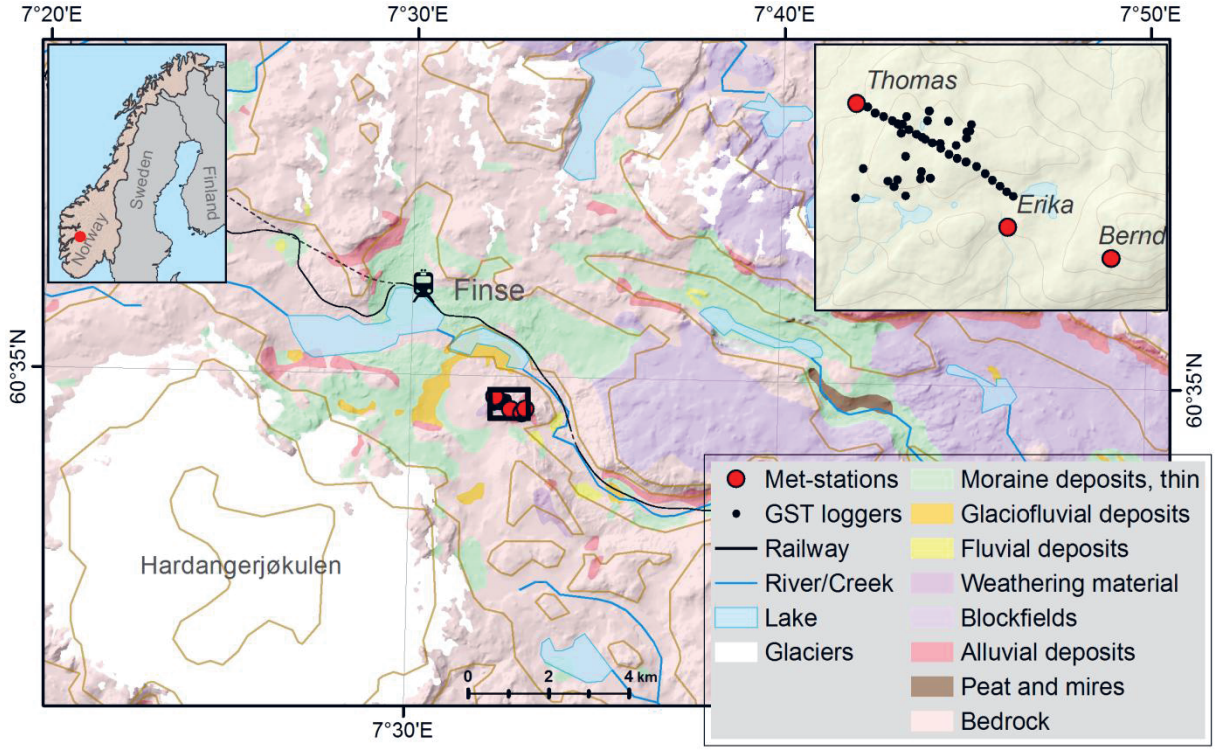

Figure 4: Map of the Finse field site, marked with the black rectangle, located 1.5 km southeast of the Finse train station. The three weather stations are marked with red dots, and the GST-loggers with black dots. The snow surveys are conducted along transects of the grids indicated in the subset (upper right corner).

3.2.2 Juvflye

Juvflye (1400-1850 m a.s.l.) is a 4 km^2 mountain plateau in Jotunheimen, surrounding the west and northwestern side of Galdhøpiggen (Figure 5). The mountain massif consists of gabbro and gneisses from the Caledonian nappe, partly with thick moraine deposits covering the bedrock. The terrain is open with sparse vegetation, mainly consisting of lichens and mosses.

The area is on the divide between eastern and western climates, and featuring very strong winds, on average exceeding 10 m/s in the snow accumulation season. The *MAAT* for the normal period is -2.8 °C, with annual precipitation amounts around 1000 mm. The precipitation normally falls as snow from October, and melt in most of the area in early July. The top of the plateau is within the continuous permafrost zone, and a 129 m deep borehole at Juvvasshøe (1850 m a.s.l.) indicates 300 m deep permafrost (Isaksen et al., 2001). Based on BTS-surveys, DC-resistivity measurements and boreholes, the lower limit of permafrost is estimated to be around 1460 m a.s.l. in the area (Isaksen et al., 2002; Farbrot et al., 2011). The ALT at the top plateau is from 1 to 1.5 meters, while the thickness increases up to 8 meters at 1460 m a.s.l.

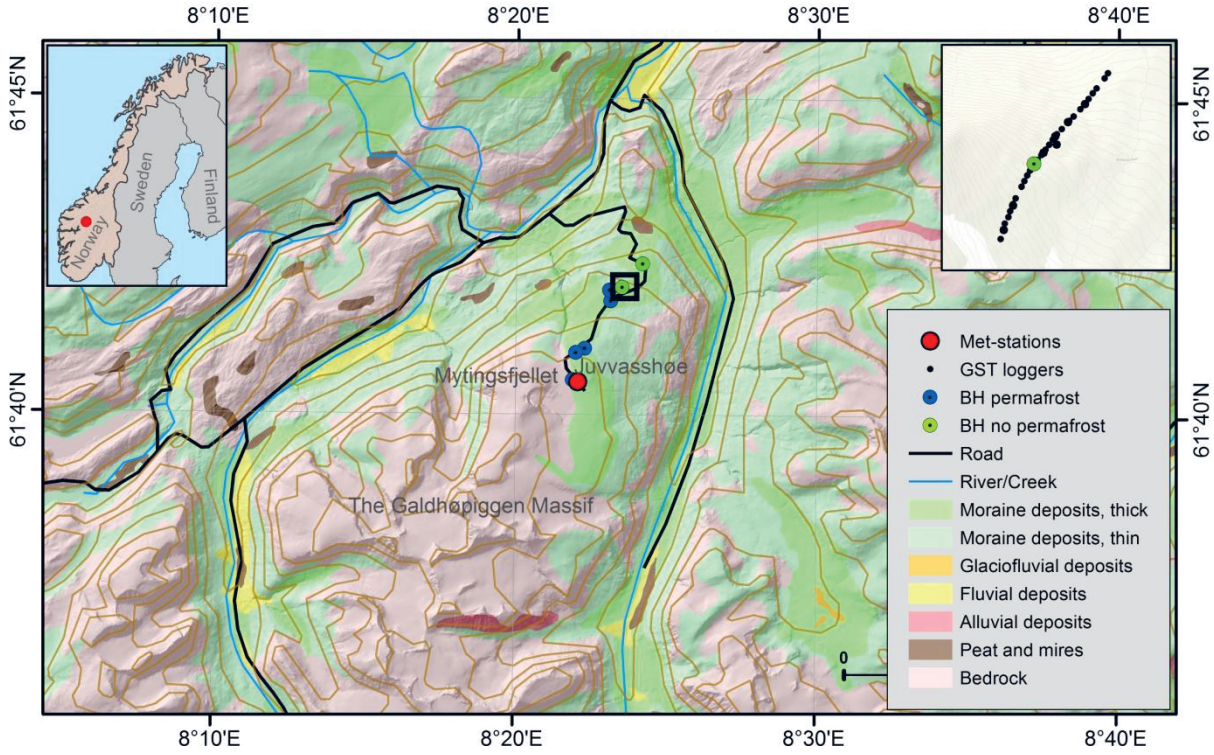

Figure 5: The Galdhøpiggen massif with the Juvvasshøe field area marked with a black rectangle. Boreholes with permafrost and seasonal frost are indicated with blue and green dots, respectively.

The field site (1374-1497 m a.s.l.) is located in a 15° steep slope facing northwest, 400 m below Juvvasshøe (upper right in Figure 5). The location is chosen to cross the lower limit of permafrost, and coincides with an already established transect of 150 points having 14 years of recorded BTS, maximum snow depths and DC resistivity profiles (Isaksen et al., 2011).

3.2.3 Ny-Ålesund

Ny-Ålesund (20 m a.s.l.) is located at the Brøgger peninsula at the west coast of Spitsbergen, Svalbard, featuring a maritime climate with cool summers and relatively mild winters. The Ny-Ålesund field site is located 2 km southwest of Ny-Ålesund, half way between the fjord and the terminus of the nearest glacier, Brøggerbreen (Figure 6).

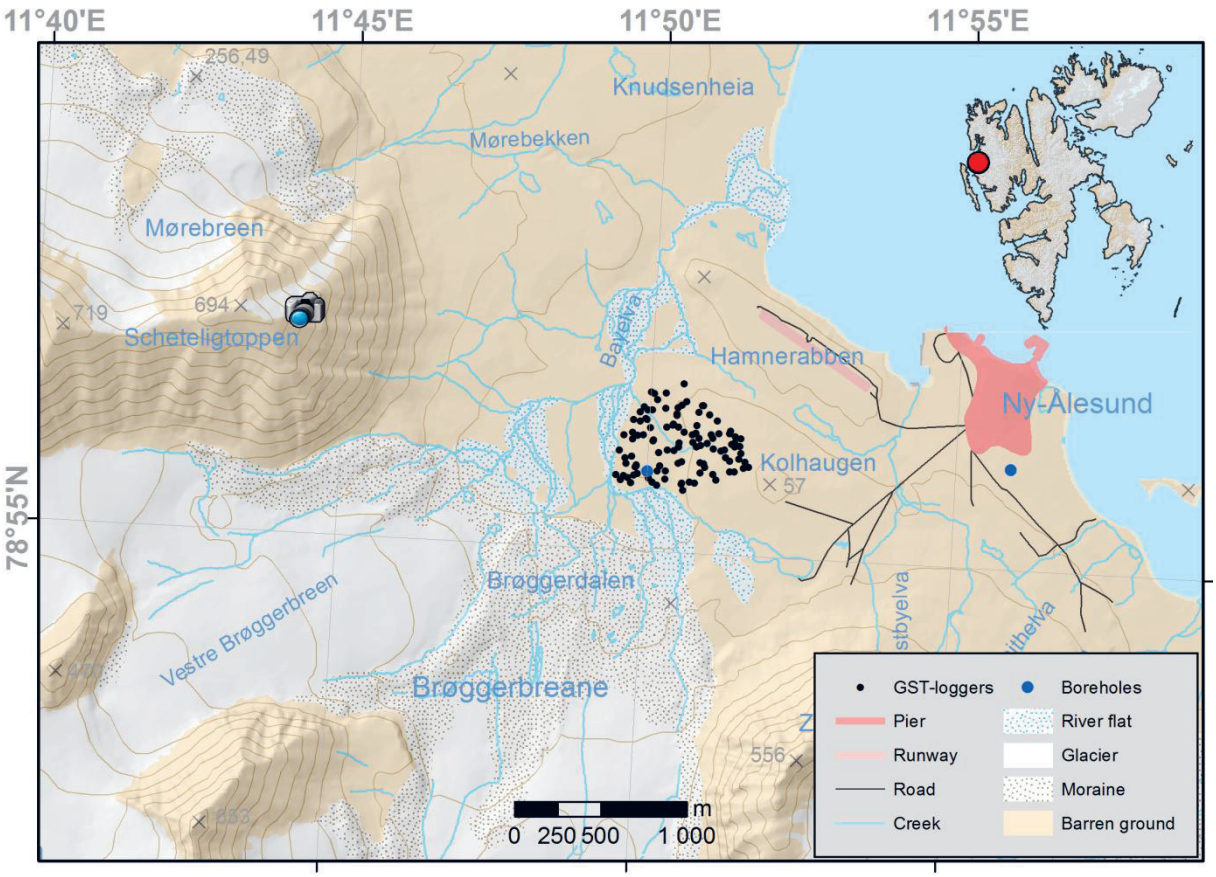

Figure 6: Ny-Ålesund field area. The location of the automatic digital camera is indicated with a camera symbol. The location of the field site corresponds to the location of GST-loggers.

The topography is gentle and ranges from 10 to 40 m a.s.l. *MAAT* for the period 1961-1990 is -6 °C, and mean annual precipitation is around 500 mm. The precipitation is falling mostly as snow between September and May. The snow normally last until late June, resulting in length of snow seasons from 215 to 315 days (Winther et al., 2002). The average snow depth in the terrain is around 60 cm, with variations from 0 to 300 cm due to wind drift (Bruland et al., 2001). Wind speeds are generally relatively gentle with prevailing wind direction from the southeast along Kongsfjorden. The area is within the continuous permafrost zone. The active layer in a borehole located near the village is 1.8 meters, and ground temperatures at a depth of 9 meters is -2.3 °C (Christiansen et al., 2010). The field site in Ny-Ålesund is located in near Bayelva river (indicated with the black dots), and is later referred to as "Bayelva" field site. A full surface energy balance station operated by the Alfred Wegner Institute (AWI) is located in the field area.

4 Data acquisition and methods

4.1 Field measurements

4.1.1 Fine-scale variability of ground temperatures

Arrays of 33 to 105 loggers were distributed to capture the sub-grid variation of GST within 1x1 km areas at each of the three field sites. In Ny-Ålesund the loggers were randomly distributed over a 500x500m area (Figure 6). The loggers at Juvvasshøe were installed with 20 m spacing over a 500 m long transect going down slope (Figure 5). At Finse 26 loggers where randomly distributed in a 500x500 m area, while 20 were installed with 20 m spacing over a 500 m transect going east – west (Figure 4). The loggers were installed approximately two cm below the ground surface to avoid direct sunlight during the snow free season (examples in Figure 7).

Two types of temperature loggers where used to measure ground surface temperatures; *HOBO Water Temperature Pro v2 Data Logger* (U22-001), having a measurement accuracy of ±0.21 °C, and *iButton* temperature data loggers (DS1920) from Maxim Integrated measuring with a temperature resolution of 0.0625 °C and an accuracy of ±0.5 °C. The waterproof HOBO loggers where used for the 24 randomly distributed logger sites at Finse,

and a 4 particularly wet sites in Ny-Ålesund. iButtons were used for the remaining ground surface measurements sites. To avoid animals disturbing the loggers, they were only marked with a small wooden stick (Figure 7, c and d). In Ny-Ålesund rocks were placed in a triangle around the logger site (Figure 7, b). Photos taken of all logger sites in addition to GPS coordinates simplified the revisit of the logger sites. High precision differential GPS with 10 cm accuracy was used to record the locations at Juvvasshøe and Finse (Fig. 8 and Fig. 9), while a hand held GPS with 2 to 5 meter accuracy was used in Ny-Ålesund.

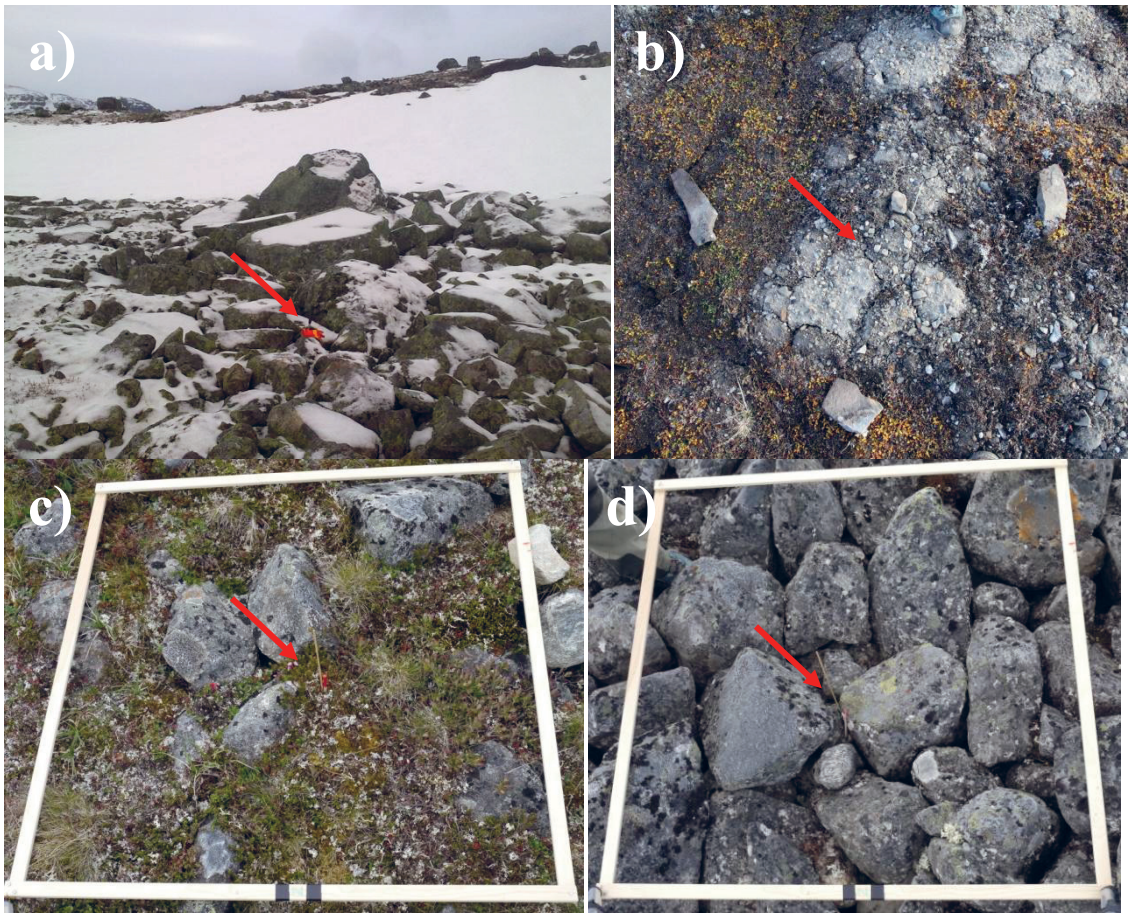

Figure 7: Example of GST-logger locations at Finse (a), Ny-Ålesund (b) and at Juvvasshøe (c and d).

Measurement periods and total number of loggers are summarized in Table 1. The loss of data loggers each season ranged from 3 % in Ny-Ålesund, up to as much as 30 % at Juvvasshøe. 14 % of the data loss resulted from loggers that were not found, while 86 % was caused by defect data loggers. The defect data loggers were exclusively *iButtons*, experiencing water infiltration into the logger when freezing in. To protect the *iButtons* from water damage they were either packed in zip-lock plastic bags wrapped in tape, or sealed with shrink tube. The loggers in Juvvasshøe were neither sealed nor packed in plastic bags, resulting in a high

percentage of defect loggers. In Ny-Ålesund most of the loggers were sealed with shrink tube, and only loggers at drier sites were wrapped in plastic. This turned out to dramatically reduce the damage. None of the *iButtons* in shrink tubes failed, and it is therefore suggested to use this for all loggers in the future.

Data is collected over the period 17.11.2011 – 21.09.2015 with slightly varying measurement periods at the three sites (see Table 1). Mean annual averages are derived for hydrological years. However, due to depleted batteries and memory restrictions, some of the loggers lack data for the end of the observation period. These periods are always in the end of summer season when all loggers are snow free and the spatial variation is low. Daily temperature data is here interpolated based on the daily temperature ratio between the logger and the mean value of all the loggers during snow free seasons. To obtain data for full hydrological years, air temperatures were used as substitutes where ground temperatures were missing.

Table 1: Overview of the collection of ground surface temperature (GST) data at Finse, Juvvasshøe and Ny-Ålesund.

Site	Measurement period	No. loggers	No. dead loggers	Temporal resolution
Ny-Ålesund	15.08.2012 – 12.09.2013	105	3	iButtons: 4 hours
	12.09.2013 – 09.09.2014	104	9	
Juvvasshøe	27.07.2012 – 14.07.2013	33	9	iButtons: 4 hours
	14.07.2013 – 08.06.2014	33	10	
Finse	17.11.2011 – 21.09.2012	24	0	Hobo: 2 hours
	21.09.2012 – 30.09.2013	46	5	Hobo + iButtons
	30.09.2013 – 30.09.2014	46	4	Hobo + iButtons
	30.09.2014 – 21.09.2015	46	4	Hobo + iButtons

Snow depths were measured manually with a probe at the approximate time of snow maximum at each data logger (Fig. 9). Several surface parameters, including maximum snow depth (*SD*), surface cover, relative wetness, potential incoming solar radiation (*IR*), aspect, slope, and curvature, are described for each data logger site. Surface cover is classified in the following four classes: organic material, moraine material, block field and bedrock. Relative wetness is qualitatively classified in wet, medium and dry at one time during the summer. The timing was chosen to not follow directly after a rain event. *IR*, aspect, slope and curvature are

derived from digital terrain models (DTMs) with horizontal resolutions of 4 meter at Finse and 10 meter at Juvvasshøe and in Ny-Ålesund. *IR* was calculated for 1st July using an integrated ArcGIS 10 tool, which is based on methods from the hemispherical view shed algorithm developed by Fu and Rich (2002) and Rich et al. (1994).

Figure 8: Set up of the base station for the differential GPS used for snow surveys at Juvvasshøe. The mountain Mytingsfjellet, with the Kjelen cirque and the Juvfonna ice patch are seen in the background. Photo: Ketil Isaksen.

4.1.2 Snow surveys using Ground Penetrating Radar and differential GPS

Snow surveys using *ground penetrating radar* (GPR) were carried out at snow maximum at the three field sites over several seasons; Finse (2012-2014), Juvvasshøe (2009, 2012-2013) and Ny-Ålesund (2013). This method was preferred over terrestrial laser scanning because of the flat undulating terrain, making it difficult to get an overview of the entire field area. This method is also relatively inexpensive.

The surveys were conducted by pulling a GPR behind a snowmobile along transect in a predefined grid (Fig. 8). The GPR directs high frequent electromagnetic (EM) pulses into the ground, and arrival times of reflected pulses from the subsurface are recorded. Knowing the

velocity of the EM signal in the observed medium between the antenna and the reflecting surface (the wave speed; m ns^{-1}), the two-way travel time (ns) can be converted into distance (m). The very large contrast in EM properties of the snow and the underlying material makes the ground surface a strong reflector. The GPR is therefore an effective and widely used method of determining the bottom of the snow layer (Winther et al., 1998; Bruland et al., 2001; Bruland et al., 2004; Marchand and Killingtveit, 2005).

Figure 9: GPR snow survey with the Radar antenna on a sled behind the snowmobile (background), and annual repeated snow survey with differential GPS (foreground). Photo: Ketil Isaksen.

A GPR system (RAMAC, Malå GeoScience) with a shielded antenna measuring at the frequency of 800 MHz was used to obtain the best resolution of snow depths, assuming snow depths from 0 to 10 meters. A GPS-receiver simultaneously recorded the position together with the GPR. The snowmobile was driven at speeds between 5 and 10 m/s, and radar traces were acquired at time intervals of 0.25 s. Filtering of the GPR-data along with extraction of the ground surface reflection was performed using the *Reflex* software. Bulk snow density of the snow pack was measured at several sites in the area of each GPR survey. The snow packs were at sub-zero temperatures at all surveys. The permittivity and thus the wave speed of the radar signal in dry snow was derived from bulk snow density by an empirical relation (Kovacs

et al., 1995). Manual probe measurements taken along the radar tracks served as validation data for the processed radar data.

The snow surveys in Ny-Ålesund and Finse are sampled along predefined grids of 1x1 km, with 250 m grid spacing. Additionally, a smaller grid of 250 x 250 m with grid spacing 50 m was sampled at the centre of the grid at Finse (Figure 4). Because of the steep topography at Juvvasshøe, the tracks were sampled along the terrain gradient instead of a grid. The snow surveys cover from 11 to 28 km, and consist of 8000 to 60 000 processed data points (Appendix A1). For further studies, these are averaged for each 1 m^2 and 10 m^2. Grid cells containing less than three samples were excluded.

Errors in the determination of snow depths mainly arise from lateral variability of snow densities, inaccuracy in the extraction of the surface reflection, and modification of the snow pack in the path behind the snowmobile. The largest variability of snow densities was found at Finse, with densities of 334 ± 40 kg m^{-3}, giving wave speeds of 234 ± 6 m μs^{-1} and an uncertainty of ± 2 cm for snow depths of 1 m. These errors are however minor compared to those possibly introduced by inaccurate extraction of surface reflections, introducing errors of 10-15 cm. The snowmobile will also modify the snow pack with approximately 3 to 20 cm, depending on the snow density and driving speed.

In the GPR data at Juvflye and Finse snow depths below 10 cm are most likely underrepresented. The main reasons are (1) lower accuracy of the extraction of radar reflections for shallow snow packs because of very noisy signal caused by strong vibrations in the GPR antenna, and (2) underrepresentation of bare blown areas because of snowmobile driving restrictions over bare ground. The underrepresentation is likely to be largest at Juvflye, where large entirely bare blown areas are not covered by the GPR. Additionally, because of the steep terrain, the snowmobile had to be driven at a higher speed, introducing more noise in the data. The gentle topography in Ny-Ålesund facilitated slow driving over a regular grid, resulting in little noise and a good representation of the area.

During the winter season 2015, differential GPS was used to measure snow depths along the tracks in the predefined grids, instead of a GPR. A GPS antenna was mounted on a sled pulled by skiers, logging precise (x,y,z)-position at time intervals of 1 s, resulting in an average sample spacing of 1 meter. Simultaneously a GPS-antenna at a survey control station point in the centre of the field area recorded satellite data used for post-processing of the GPS coordinates. This allowed for calculation of high-accuracy positions of ± 5 cm. Snow depths

were derived from the difference between observed elevation at the top of the snow pack and a high resolution (ground resolution of 50 cm) DTM. The DTM was derived using stereo photogrammetry from a drone flight 22nd Sept 2015. From an average height of 120 m, the drone recorded 800 images with an average ground resolution of 4 cm. 9 ground control points and four 1 km transects were measured with differential GPS the same day as the drone campaign, and served as validation data. The root mean square error (*RMSE*) between the DTM and the validation points were below 10 cm.

4.1.3 Snow covered fraction from digital camera images and GST-loggers

Over repeated seasons, an automated digital camera was installed at Scheteligfjellet (78 55.5''N, 11 44.3''E) at an altitude of 566 m a.s.l., pointing down to the Bayelva basin to monitor the snow melt in the study area (Figure 10). At the end of the snow accumulation season the camera was mounted on a small tripod in some protruding bedrock, and then removed in the end of summer. Powered by a solar panel, it has operated with varying success during the melting seasons of 2012 – 2014. 30 distributed ground control points (GCPs) were collected to orthorectify and georeference the camera images (Figure 11, upper).

Figure 10: Camera location at Scheteligfjellet, with view over the settlement of Ny-Ålesund and the field area in Bayelva.

Images were orthorectified iteratively in MATLAB using the same relation between image pixels and the corresponding GCPs for repeated images. Shifts in the camera position during the operational season were marginal in 2012, but a slight shift occurred at June 6th 2013. Two sets of image pixels were therefore used for the 2012 data series. The projection parameters for the orthorectification are derived from an iterated best fit, where only the position of the camera and the GCPs with corresponding image pixel coordinates are known. The fitted projection parameters include rotation vector (x,y,z), focal length of the camera, principal point location, distortion coefficients (radial and tangential) and the skew coefficient between x and y pixel. The projection was computed using the Camera Calibration Toolbox for MATLAB (Bouguet, 2013).

A method to automatically classify snow covered pixels was derived in MATLAB. Only images with good visibility were used, being approximately one per day during the melt season. Because of different light in the images, the threshold of the pixel intensities in the red, green and blue (R,G,B) bands separating snow from barren ground is not constant between images. K-means clustering is therefore used to derive two clusters from the data arrays of the RGB bands in every image. The cluster with the higher centre intensity is snow, while the lower is barren ground. In order to always obtain large contrast in the image, a black border was kept around the image. This kept the cluster centre of the barren ground class low enough to avoid inclusion of snow in shadowed areas. In images with very little snow and large contrasts in the colours of the ground surface, typically at the end of the melt season, both clusters happen to centre in barren ground intensities. To avoid misclassification, a threshold was set if the maximum blue band intensity for the two cluster centres was below 210, and the difference between them was less than 80. In these cases a threshold of 600 for the sum of R, G and B intensities was applied. The results were visually controlled after classification. The snow covered fraction (SCF) for the study area in Bayelva during melt season was computed as fraction of pixels classified as snow covered within the study area, masked out from the images (Figure 11, blue line in the lower image).

The presence of a snow cover at each of the ground GST-loggers was determined based on the dampening of observed diurnal temperature variation at the ground surface compared to in the air. This method is previously used to determine the height of the snow cover from vertical arrays of temperature loggers (Lewkowicz, 2008; Hipp, 2012). Snow cover was determined as present if all of the following three conditions were met:

1. Average daily GST below 0.5°C
2. The normalized difference index for variation in air temperatures and GST > 0.4°C

The SCF for each day was simply determined as the fraction of GST-loggers classified as snow covered. The resulting SCF-curve derived from the GST-loggers is very similar to the SCF-curve derived from the digital camera images, even though the SCF-curve from GST-loggers does not manage to reproduce snow falls in late melt season. The representativeness of the SCF-curve is highly depending on the density and representativeness of loggers.

4.1.4 Weather observations from three weather stations at Finse

A crucial part in snow drift modelling is the interpolation of wind speed and direction, as well as calculations of snow surface threshold friction velocity. Three HOBO weather stations were installed in the field area at Finse in the beginning of the observation period in 2011 to measure the effect of the local topography in exposed and sheltered locations. The two westernmost stations (*Thomas* and *Erika*) are HOBO micro stations measuring air temperature, humidity, wind speed, gust, and wind direction. These are located at the upwind (*Thomas*) and at the lee (*Erika*) side of the hill in the field area with respect to the dominant westerly to north westerly wind direction (Figure 4). The third station (*Bernd*) is located 30 meters down from the summit of Vetle Hansbununten at a location exposed at all dominant wind directions, and serves as a reference station of the main wind directions in the valley. The station measures incoming and outgoing short wave radiation in addition to the parameters at the two other stations. All stations perform measurements every 4 minutes, while they log the average of observations with 1 hour temporal intervals.

Ground surface temperature loggers and vertical arrays of *iButtons* temperature loggers were also installed at the stations. The vertical temperature arrays were used to derive daily snow depths, based on the dampening of observed diurnal temperature variation at each of the temperature loggers compared to in the air. The two stations on each side of the hill are normally buried by snow, even with a station height of 3.5 meters (*Thomas*) and 4 meters (*Erika*). The ground surface below the reference station is normally bare blown during the entire winter, and the snow depth is therefore not measured here.

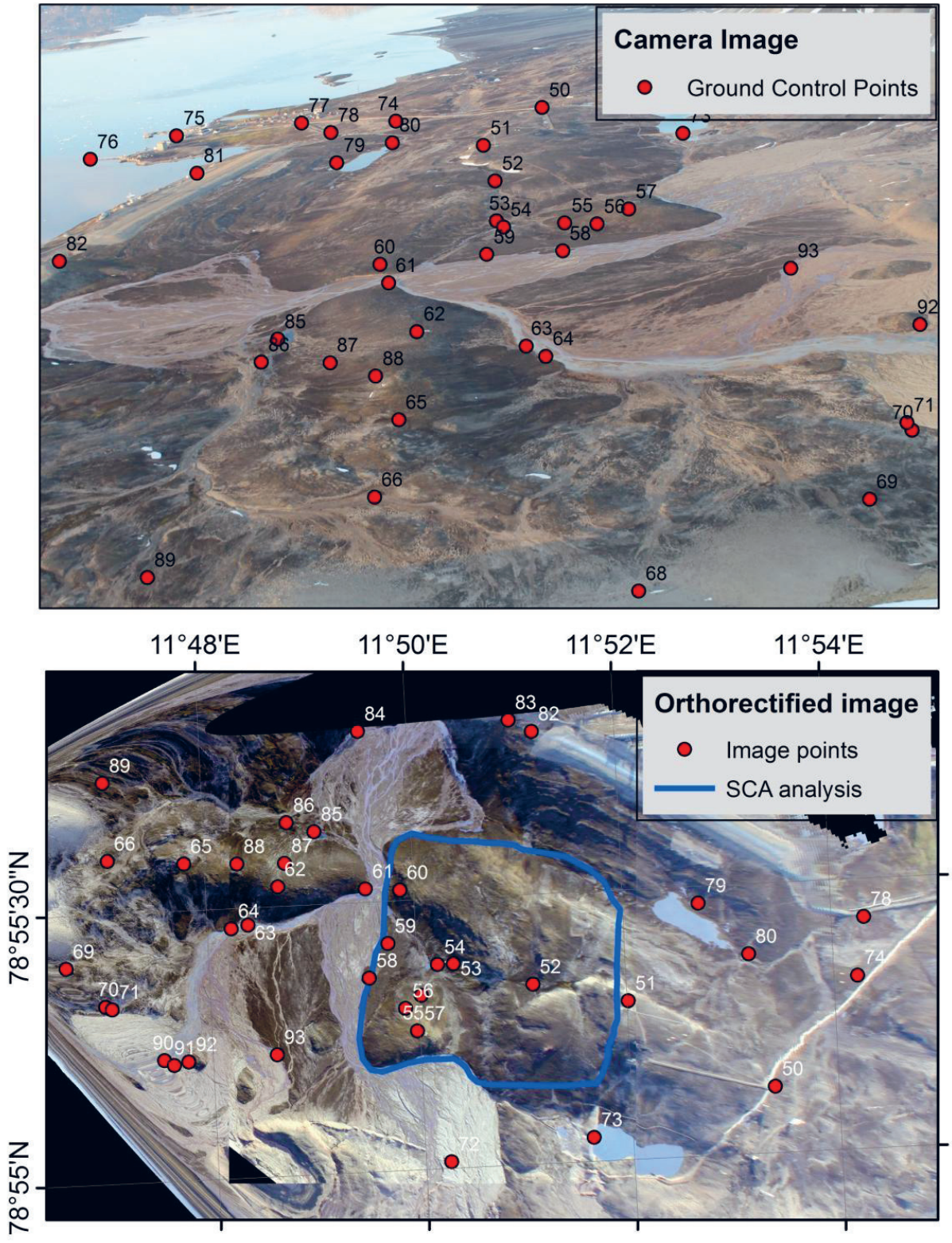

Figure 11: Example of digital camera image used for classification of snow covered area with distribution of ground control points (upper). An example of an orthorectified image with corresponding image control points is shown in the lower image. The area used for the snow covered area analysis is indicated with the blue line.

4.2 Statistical representation of fine-scale variability of snow over regional areas

4.2.1 The Winstral terrain-based parameter

The *terrain-based parameter* (Winstral et al., 2002; Winstral and Marks, 2002) quantifies a grid cell's extent of shelter or exposure (*Sx*) by determining the slope between the source cell and the cell of greatest upward slope in terrain upwind from the source cell. The upwind terrain is defined as a sector towards the prevailing wind direction *d* constrained by the maximum search distance (*dmax* = 100 m) and the search window (*A*) with a chosen width of 30°. The cell of the maximum upward slope is identified for each directional vector, and each of the vectors are separated by *inc* = 5°. *Sx* for the given source cell is finally calculated as the average of the maximum upward slope gradient of all seven directional vectors, giving the degree of exposure or shelter in the range -1 to 1, where negative values indicate exposure.

$$Sx_{d,A,dmax}(x_i y_i) = max\left[\tan\left(\frac{Z(x_v,y_v)-Z(x_i,y_i)}{[(x_v-x_i)^2+(y_v-y_i)^2\,]^{0.5}}\right)\right] \quad (12)$$

where (x_i, y_i) are the coordinates of the cell of interest, and (x_v, y_v) are the set of all cell coordinates located along the search vector defined by (x_i, y_i), *d* (the prevailing wind direction), A (azimuth of the search direction) and *dmax* (maximum search distance).

4.2.2 Coefficient of variation for snow based on terrain and wind

To estimate a realistic degree of exposure based on the observed wind pattern at a local site, *Sx* was computed on a 10 meter resolution DTM for each of the eight prevailing wind directions *d* = [0°, 45°, 90°, 135°, 180°, 225°, 270°, 315°]. The resulting 8 maps of *Sx* were weighted based on the wind fraction (wf_d). The wind fraction (wf_d) is a weighting factor to account for different exposure due to variations in wind direction over one season, and is calculated as the fraction of wind observations from a window ±22.5° around a given wind direction *d* over the accumulation season. The accumulation season is here chosen as January to March, where wind speeds below a threshold of 7 m/s are excluded, as an average limit for wind speeds resulting in major wind drifting of dry snow (Li and Pomeroy, 1997; Lehning and Fierz, 2008).

A combination of the *Sx* parameter and regression analysis is used to produce a model for the coefficient of variation of maximum snow depths (CV_{sd}) within 1 x 1 km (Figure 12). The coefficient of variation of exposure degrees (CV_{Sx}) within each 1x1 km grid cell is computed

by aggregating the *Sx* map from 10 meter to 1 km resolution by applying the following formula:

$$CV_{Sx} = \text{std}(e^{Sx})/\text{mean}(e^{Sx}) \quad (13)$$

Sx values below the 2.5th and above 97.5th percentiles of the *Sx* distributions are excluded, giving $Sx \approx [-0.2, 0.2]$. Multiple regressions with $CV_{Sx,}$ elevation above treeline (z) and maximum snow depth (μ) as predictors were performed to obtain the best model for CV_{sd}. Ideally, wind speeds should be included as predictor, but because available wind data does not reproduce the local variations in wind speeds over land sufficiently, elevation was used.

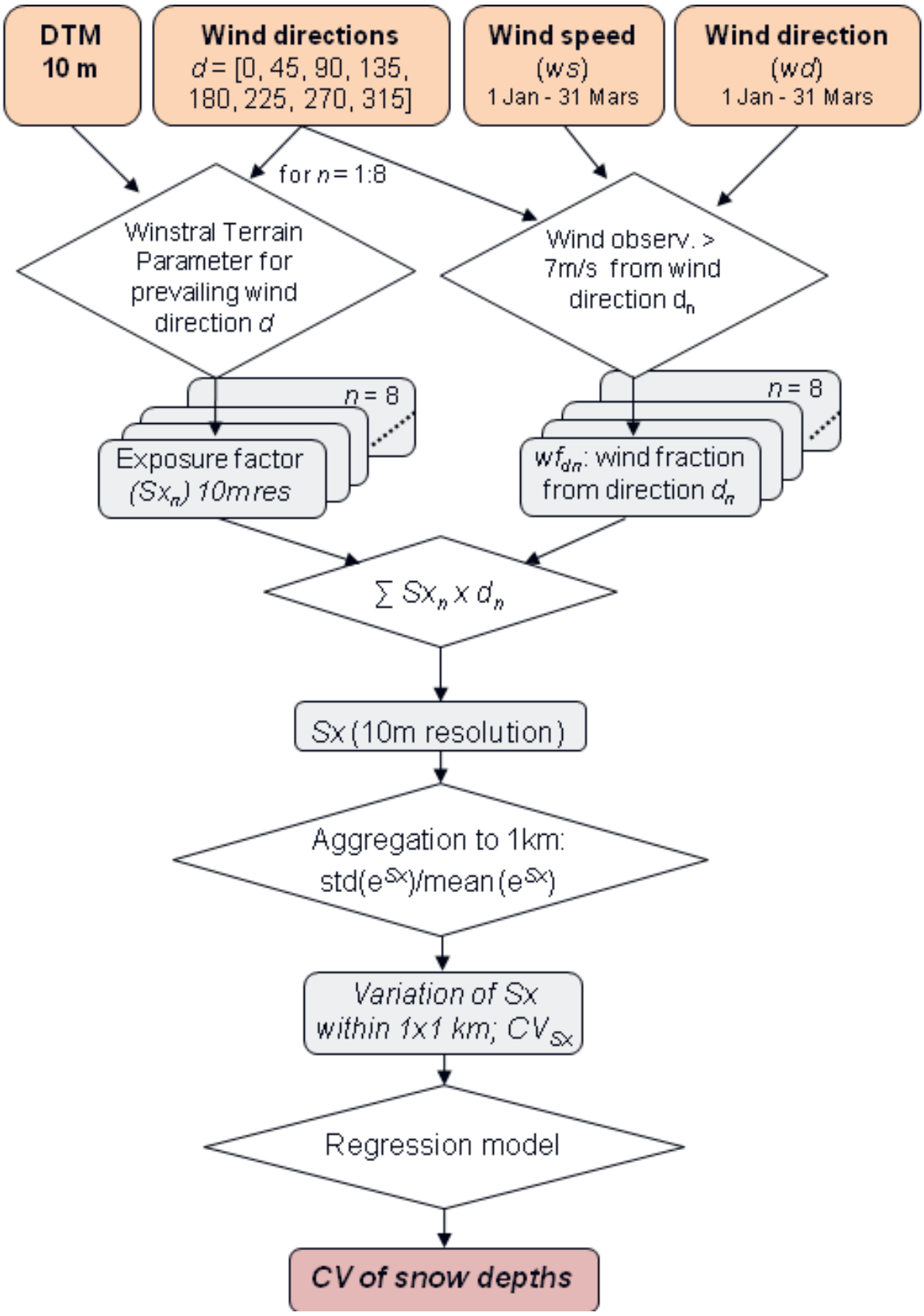

Figure 12: Schematic overview of the statistical snow distribution model.

4.3 Regional equilibrium modelling in Norway and Scandinavia

4.3.1 Implementation of the TTOP- approach

Many different attempts with varying degrees of sophistication have been made to model the climate – permafrost relationship. The TTOP-model (Smith and Riseborough, 1996) is an equilibrium model of the climate-permafrost relationship treating the atmosphere-ground temperature regime as a three layer system, consisting of (1) air temperature, (2) ground surface temperature and (3) temperature at the top of permafrost/base of seasonally frozen ground (*TTOP*). The model was first designed and implemented on continental scale to evaluate the conditions controlling the limits and continuity of the permafrost in the Canadian Arctic (Smith and Riseborough, 2002). Later it has been implemented at regional scale (1 km^2) in several areas (e.g. Wright et al., 2003; Juliussen and Humlum, 2007; Lewkowicz et al., 2012; Gisnås et al., 2013; Westermann et al., 2015b), and show good agreement with available information on permafrost distribution.

4.3.2 *n*-factor parameterization

Empirical-based transfer functions (*n*-factors) are used to link the temperatures at the ground surface to the air temperature. *n*-factors are computed as ratios of annual accumulated freezing and thawing degree days between the ground surface and the air (see Sect. 2.2.1 for details).

The impact of vegetation on the summer surface offset is parameterized by empirical *nT*-factors. The factor is also indirectly related the snow cover by accounting for the shorter season of thawing degree days at the ground surface in areas with a thick snow cover. *nT* normally varies between 0.8 and 1.2 depending on the type of surface cover and subsurface material properties (Jorgenson and Kreig, 1988; Taylor, 1995; Klene et al., 2001; Karunaratne and Burn, 2004). Observed *nT* in Norwegian mountain areas are close to unity, mainly because they are exposed to much wind during summer season. The surface boundary layer is therefore well mixed, resulting in small differences between air and ground surface temperatures. This is not valid for steep rock walls, where the effect of solar radiation dominates.

nF parameterizes the winter surface offset, and is related to the insulating effect and thereby the thickness of the snow cover. The connection between air and ground surface temperatures is highly variable during the winter season, and *nF* ranges from as low as 0.15 up to unity

depending on the thickness, density and thermal conductivity of the snow cover (Jorgenson and Kreig, 1988; Taylor, 1995; Klene et al., 2001; Karunaratne and Burn, 2004). In addition, *nF*-factors vary with the water content in the active layer because of the release of latent heat during freezing.

n-factors are specified for the following four land cover classes; (1) forest, (2) shrubs, (3) open non-vegetated areas (4) mires and (5) blockfields. Large ensembles of field observations are used to parameterize *n*-factors for each of the classes. The parameterization of *n*-factors in open areas is based on data from 17 stations measuring daily air- and ground temperatures and daily snow depth (Farbrot et al., 2011), and the arrays of GST-loggers at Finse and Juvvasshøe. For this land cover class the *n*-factors are related to maximum snow depth. The parameterization of the remaining surface classes is based on data from more than 300 ground surface temperature data loggers distributed all over Norway. These are connected to gridded air temperature data. For the forest and shrub classes the fine-scale variation of ground temperatures is less heterogeneous than in high mountain environments, and this method is therefore valid. Site specific temperature measurements in forests, shrubs and mire areas in Norway are sparse and air/ground temperature studies carried out in Canada (Taylor, 1995; Karunaratne and Burn, 2004) and Alaska (Jorgenson and Kreig, 1988; Klene et al., 2001) are therefore used as supplements to determine *n*-factors for these surface cover classes.

4.3.3 Thermal conductivities in the active layer

The thermal conductivity ratios (r_k) are parameterized from a combination of petrophysical data provided by the Geological Survey of Norway (Olesen et al., 2010), sediment property data provided by University of Alaska, Fairbanks *(GIPL)*, and from the literature (Williams and Smith, 1989). Bulk thermal conductivity (k) can be calculated in different ways, but is here calculated as the geometric mean of k in each soil constituent (i) raised to the power of the respective volume fraction (x), where n is the number of soil constituents:

$$k = \prod_{i=1}^{n} k_i^{x_i} \tag{14}$$

The geometric mean has no physical basis, but is widely used to calculate thermal conductivity for mixed soils, and is considered valid for saturated soils (Johansen, 1975). Subsurface material properties influencing the r_k-factor are also examined in Riseborough (2004), both with empirical and theoretical thermal conductivity models. The study concluded that the geometric mean gives the overall best estimate of bulk conductivity in mixtures with a

wide range of porosities; however, the uncertainty in conductivity estimates of unsaturated soils is greater at lower soil moisture contents. The TTOP-model assumes a constant r_k, and does not include the effect of unfrozen water. Mineral soils range in r_k from 0.6 to 0.9, depending on the water content. The greatest range in r_k values is found in organic soils varying from 0.3 in saturated soils to near 1.0 for dry organic soil (Smith and Riseborough, 2002). r_k for bedrock is close to 1.0, and therefore bedrock has negligible thermal offset. The parameterization used in this thesis is presented in Paper I.

4.3.4 CryoGRID1 for Norway

CryoGRID1 is an implementation of the TTOP-model for Norway at a grid resolution of 1km^2. The model is forced with operationally gridded daily air temperature (Tveito and Førland, 1999; Mohr and Tveito, 2008) and snow depth data (Saloranta, 2012) from the period 1957-2014 provided by the Norwegian Meteorological Institute and the Norwegian Water and Energy Directorate (www.senorge.no), hereafter *SeNorge*. 24-hour mean temperatures at a height of 2 meters and accumulated precipitation are de-trended and interpolated. Snow data is produced from gridded air temperatures and precipitation data applying a simple snow model accounting for accumulation, compaction and melt.

The *n*-factors for the five land cover classes are assigned to the corresponding classes in the Norwegian CORINE Land Cover (CLC) map. CLC is a seamless European land cover vector database, initiated by the European Environment Agency (EEA), where changes in land cover and use are mapped from satellite images. The Norwegian Forest and Landscape Institute are responsible for the production of the Norwegian part of the map, and deviates from the EEA standards by also including existing data sources such as the AR5- and N50-maps for land cover. Three versions are released over the respective time series; 1990-2000 in CLC2000 (Heggem and Strand, 2010). The parameterization of r_k for each soil class is assigned to the sediment maps provided by the Geological Survey of Norway (Thoresen, 1991). As a supplement to the sediment and vegetation maps, a blockfield map for Norway classified from Landsat satellite images is used (Gisnås, 2011).

4.3.5 Implementation of CryoGRID1 for Fennoscandia

A TTOP-implementation for the Nordic countries; Finland, Sweden and Norway, is made on the basis of CryoGRID1. A Nordic Gridded Climate Data set (NGCD), produced by met.no, is used as forcing data. The dataset is based on stations observations from all three countries, and is available for the period 1981-2010. Snow depth data is produced by the same *SeNorge*

snow model v.1.1.1. *n*-factors are assigned to CLC2012 (Aune-Lundberg and Strand, 2010). The *n*-factor parameterization for open non-vegetated areas is kept as in CryoGRID1, while for the other land surface classes it is adjusted slightly based on additional datasets from Sweden and Finland. Sediment and bedrock data is provided by the Geological Survey of Finland, the Geological Survey of Sweden and the Geological Survey of Norway. All three datasets are unified into one classification, following the one for r_k in CryoGRID1. The parameterization of r_k is kept as in CryoGRID1, except for mires where additional data are used from Abisko in Sweden (Sannel et al., 2015).

5 Results

The main results of the thesis are provided in this chapter. Brief summaries of the main results from the publications are given, together with additional unpublished material related to the publications.

5.1 Permafrost distribution in Norway estimated by a spatial numerical model (Paper I).

In this paper we present the CryoGRID1-model for permafrost, an implementation of the TTOP-model (Smith and Riseborough, 1996), employed over the entire Norwegian mainland at 1x1 km resolution. The model accounts for the spatial distribution of air temperatures, maximum snow depth, vegetation and thermal properties of the ground material. Field measurements of the surface offset in relation to different surface characteristics are used for parameterization, and large datasets on ground properties are collected to derive ground thermal conductivities. These datasets have served as a basis for several later model attempts for permafrost in Norway.

The model manages to reproduce the large scale patterns of permafrost in Norway, observed lower limits of permafrost and the east-west gradient in lower limit of permafrost. The results show good agreement with ground and ground surface temperatures, as well as BTS-surveys and regional inventories of rock glaciers and palsas. According to the model, 6.1-6.4 % of the Norwegian mainland is underlain by permafrost in an equilibrium situation with the 1981-

2010 climate. One of the main issues with the model is representation of snow in mountain areas. The model results are too warm compared to borehole observations. This is mainly because of too much snow in the model run compared to the bare blown situations at the borehole sites. The bare blown situation at the exposed borehole sites is representative for large parts of the mountain areas in Scandinavia, which are often exposed to strong winds and undergo heavy redistribution of snow. Snow depths above an elevation of 1000 m a.s.l. were therefore reduced with 30%.

5.2 Fine-scale variability of ground surface temperatures and related surface variables

In this section we present the entire data series (2011-2015 at Finse and 2012- 2014 at Juvvasshøe and Ny-Ålesund) from the arrays of GST-loggers distributed within footprints of 0.5 km^2 at the three field sites (Figure 4 - Figure 6). The effect of the surface variables described in Sect. 4.1.1, are quantified using stepwise regression analysis for the measured summer and winter surface offsets at the logger sites.

5.2.1 Ground surface temperature variations

Variations in *MAGST* of up to 5 °C were observed within the footprints, with similar variations observed at the low relief site in Ny-Ålesund as in the high-alpine sites at Finse and Juvvasshøe (Table 2). Even with the minor snow depth variations measured in Ny-Ålesund, reflected in the low coefficient of variation (*CV*), there are large variations in *MAGST*. The spatial variation is mainly introduced during the snow covered season, lasting from December to March/April (Figure 13). In early spring, when the snow pack is ripened, the variation is lower, while large variations are observed during the time of melt-out (June/July). The variation in monthly GST is very low during the snow free season.

The annual pattern of spatial variation is similar over the four years of observations at Finse (Figure 14). The variation in monthly mean temperatures during the snow free season is in the order of 2 °C or less, with larger variation from December to March. During January and February the spatial variation is in the order of 4-5 °C for all years, with the largest variation in 2012/2013 (Figure 15). This year was, with respect to both air and ground surface temperatures, colder than the other years of observations at all field sites. Consequently, the variation in the insulating effect of the snow cover increases, and the variations in GST were

larger than the other years. In the following hydrological year (2013/2014), none of the loggers at Juvvasshøe and Finse featured *MAGST* below 0 °C (Table 2). Large inter-annual variations are observed in the duration and timing of the melt season (Figure 14), occurring during June and July in 2012 and 2015, June in 2013 and 2014. This corresponds to the timing of when the fraction of snow covered loggers decrease from approximately 0.5 to 0.2. However, even with the long and late timing of the snow melt at Finse in 2012 and 2015 the spatial variation in *MAGST* these years is lower than what is observed in 2012/2013 with a comparably short snow melt.

Table 2: *MAAT* and average *MAGST* are calculated among all loggers at each of the field areas. Snow depths are measured manually with a probe at the logger sites at the time of maximum snow depth. Coefficients of variation (*CV*) are calculated for each of the manual snow depth surveys.

	Year	***MAAT***	***MAGST***				**Snow depth**	
		Mean	*Mean*	*Minimum*	*Maximum*	*% < 0°C*	*Mean*	*CV*
Finse	11/12	-0.7	1.0	-0.4	2.5	12 %	1.2	0.9
	12/13	-2.2	0.8	-1.9	2.7	30 %	1.2	1.0
	13/14	0.17	2.0	0.5	3.6	0 %	1.3	0.9
	14/15	-0.17	1.1	-0.1	2.5	8 %	1.3	0.9
Juvvasshøe	12/13	-2.8	-0.3	-1.5	1.2	76 %	0.6	1.1
	13/14	-0.9	1.2	0.3	2.2	0 %	0.9	0.9
Ny-Ålesund	12/13	-4.1	-2.0	-5.1	-0.1	100 %	0.7	0.5
	13/14	-3.5	-0.2	-3.3	0.9	47 %	1.4	0.2

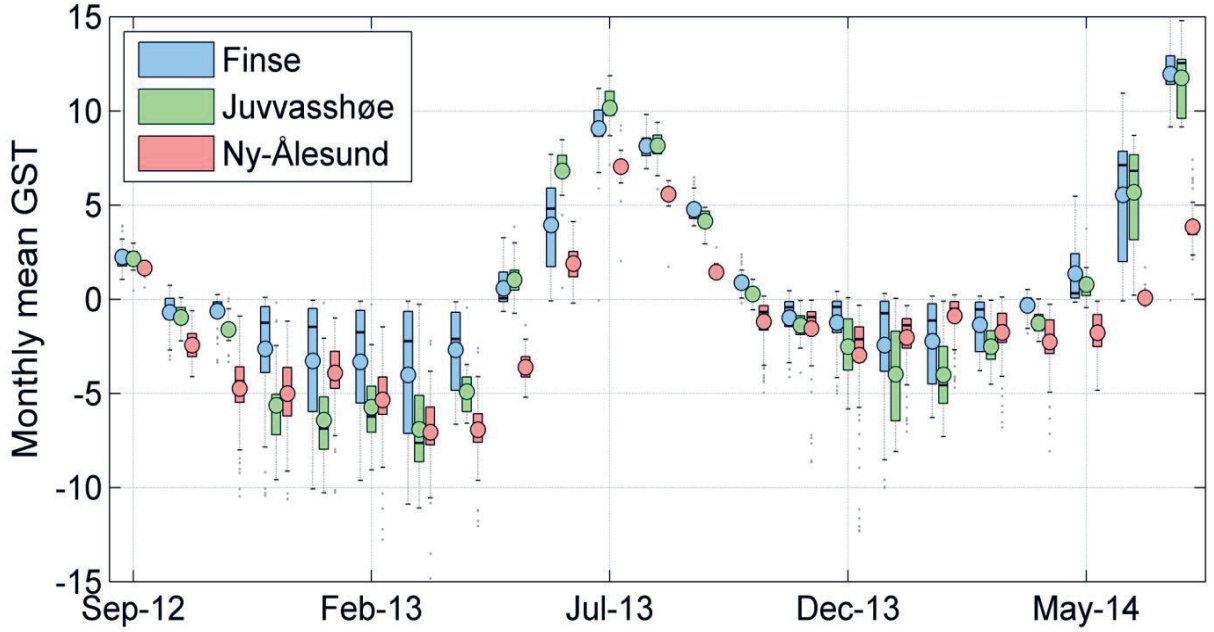

Figure 13: Spatial variation in monthly mean ground surface temperatures (GSTs) at the three field sites.

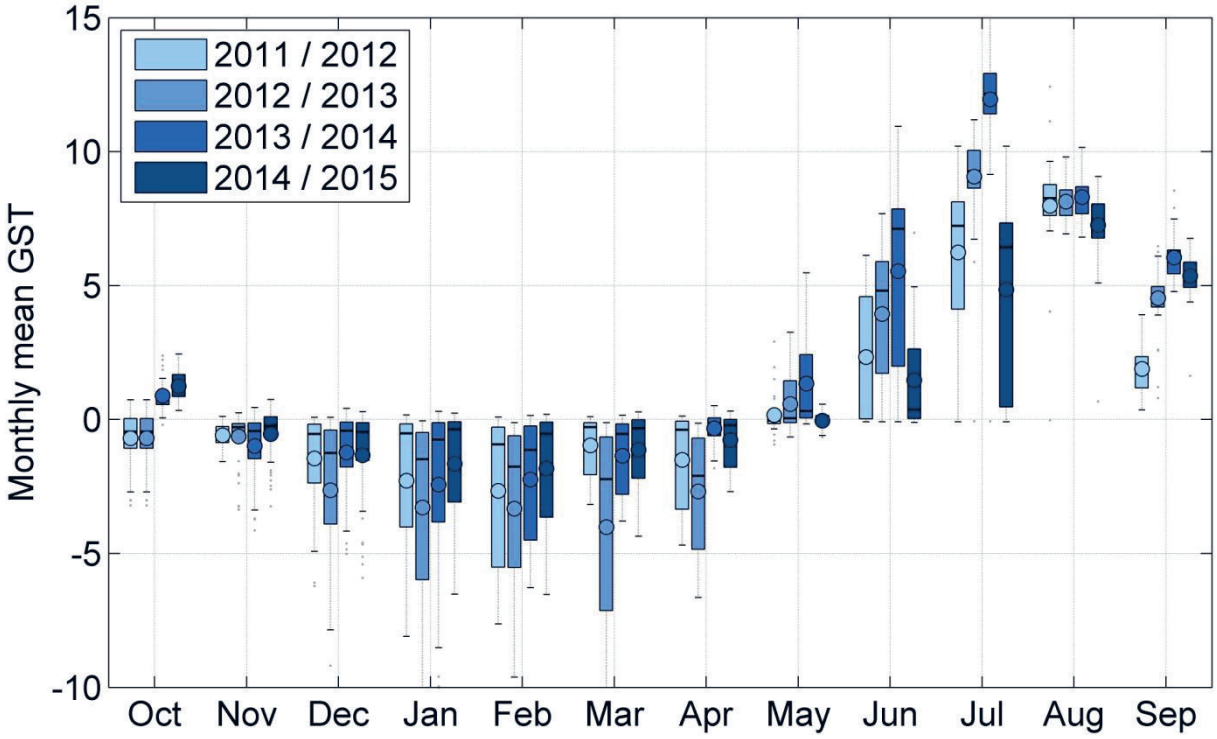

Figure 14: Inter-annual comparison of variation in monthly mean ground surface temperatures (GSTs) at Finse.

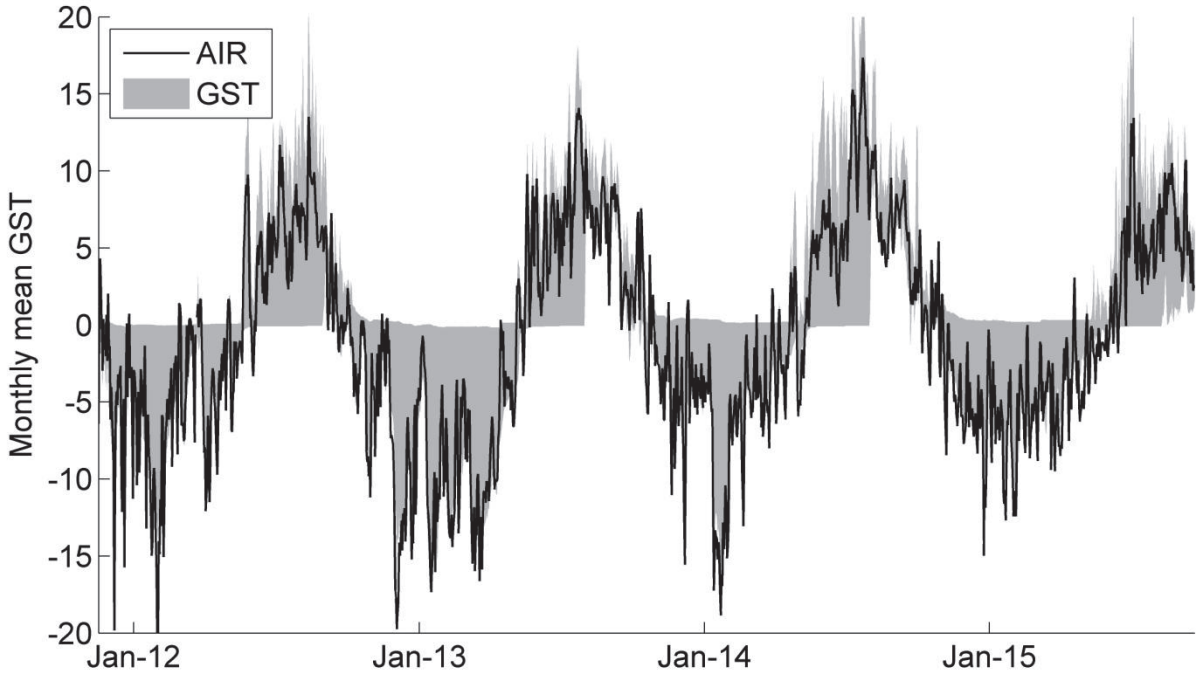

Figure 15: The spread of ground surface temperatures (GSTs) (grey shading) compared to air temperatures at Finse.

5.2.2 Controlling factors on the surface offset

Maximum snow depths and ground surface temperatures were measured at the GST-logger sites over two years at Juvvasshøe and in Ny-Ålesund, and over four years at Finse. *nT* and *nF* are calculated for each hydrological year, and the correlation to maximum snow depth and several surface parameters is evaluated. The surface parameters, described in Section 4.1.1, include surface type or material, relative wetness, incoming solar radiation, aspect, slope and curvature (Table 3). The distribution of data for each variable at Finse is shown in Figure 16.

Table 3: Surface parameters of the ground surface temperature (GST)-logger locations, accounted for in the multiple regression analysis.

Variable	Data type	Classification/range
Maximum snow depth (*SD*)	Continuous	0 m – 4 m
Potential Incoming Solar Radiation (*IR*)	Continuous	1.8e+03 - 5.5e+03
Surface material (Material)	Nominal	1 Organic, 2 Moraine, 3 Blocks, 4 Bedrock
Relative ground moisture (Wetness)	Ordinal	1 Dry, 2 Medium, 3 Wet
Slope	Continuous	0° – 45°
Aspect	Continuous	0° – 360°
Curvature	Continuous	-8 – 12 (upwardly convex > 0, concave < 0)

The contribution of each surface parameter to the spatial variation of *nT* and *nF* is evaluated by applying stepwise linear regression analysis. The MATLAB function stepwiselm.m is applied to add or remove predictors using both backward and forward stepwise regression, in order to obtain the best fit to a linear model. The steps in the regression are determined under the criteria of the *p*-value for an *F*-test of the change in the sum of squared error by adding or removing the term. An exponential correlation between maximum snow depth (*SD*) and *nF* is found, also shown in Paper I. The natural logarithm of *SD*, ln(*SD*), is therefore used as predictor in the regression analysis for *nF*, while *SD* is used for *nT*.

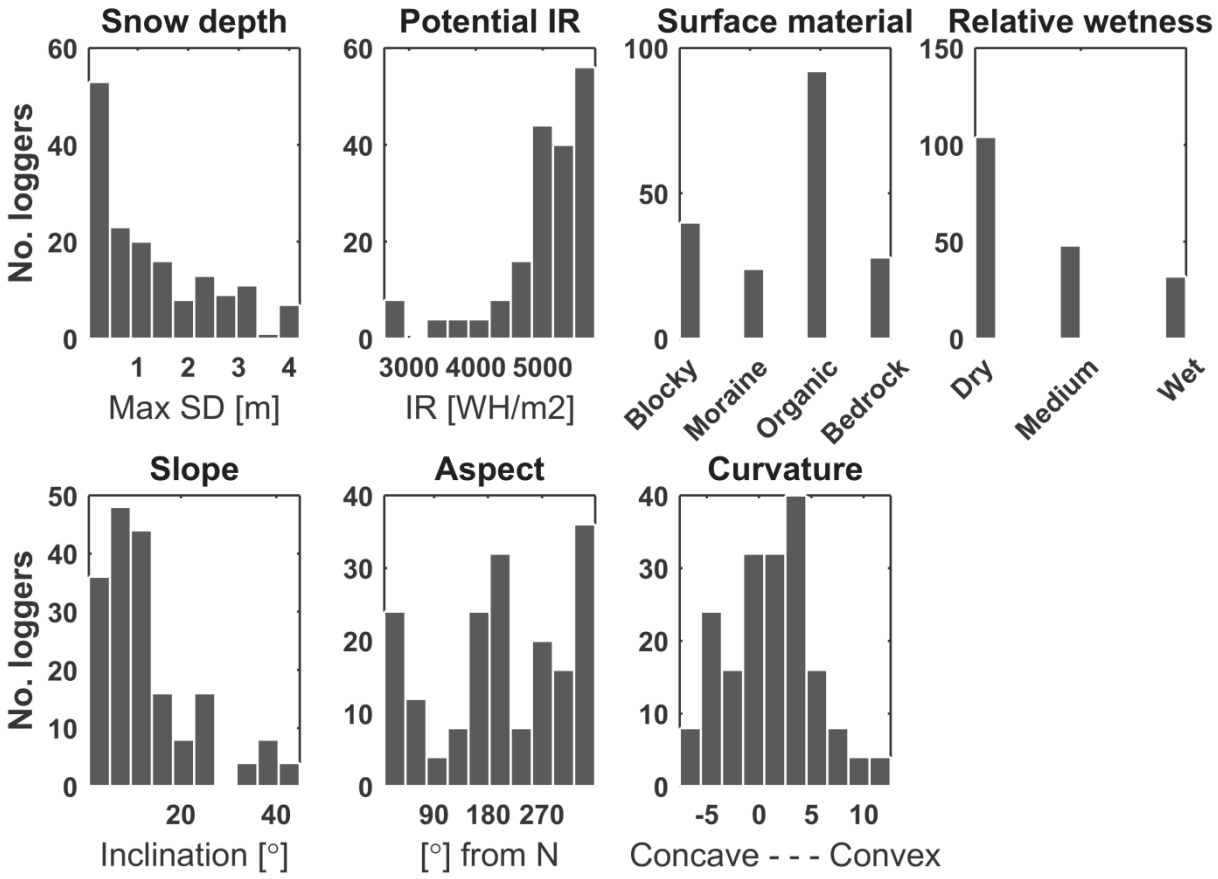

Figure 16: The distribution of the data for each of the surface variables at the Finse field site. The surface material are classified in to the classes 1. Blocky, 2. Moraine, 3. Organic, and 4. Bedrock.

The model statistics for each added predictor in the models for *nF* and *nT* at Finse are shown as graphs in Figure 17 a) and b). The coefficient of determination (R^2) is relatively high and the *RMSE* low at the first step for both *nF* and *nT*, when only *SD* is added. In both models the second and third variables to be included are incoming solar radiation and surface material. However, the model improvements with these steps are marginal, in particular for *nF*, with 16 % increase in R^2 and a reduction from 0.15 to 0.12 for *RMSE*. For *nT* the increase in R^2 is 20 %. This is also reflected in the *p-values*, indicating that snow has a much higher significance for the variation in surface offset than the other variables, both in summer and winter.

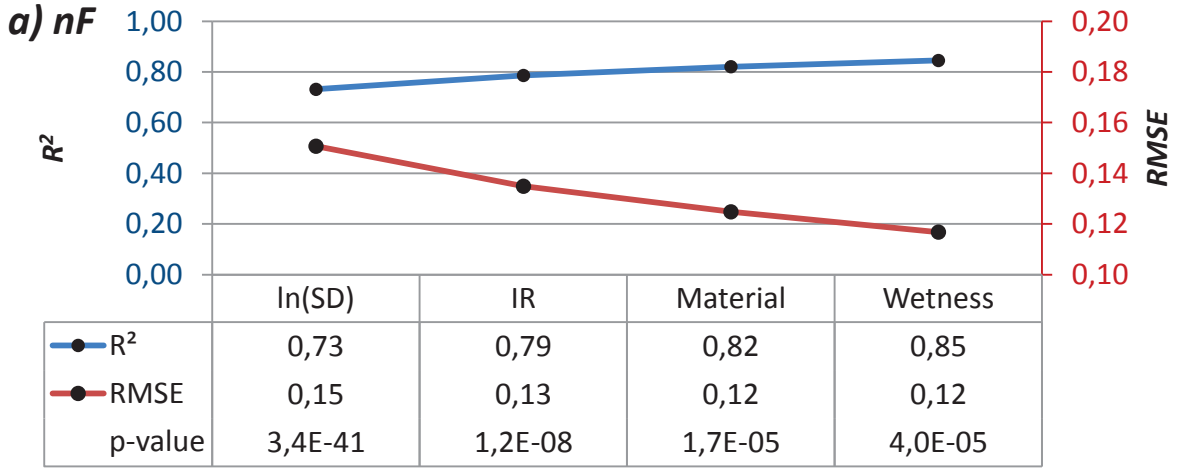

	ln(SD)	IR	Material	Wetness
R²	0,73	0,79	0,82	0,85
RMSE	0,15	0,13	0,12	0,12
p-value	3,4E-41	1,2E-08	1,7E-05	4,0E-05

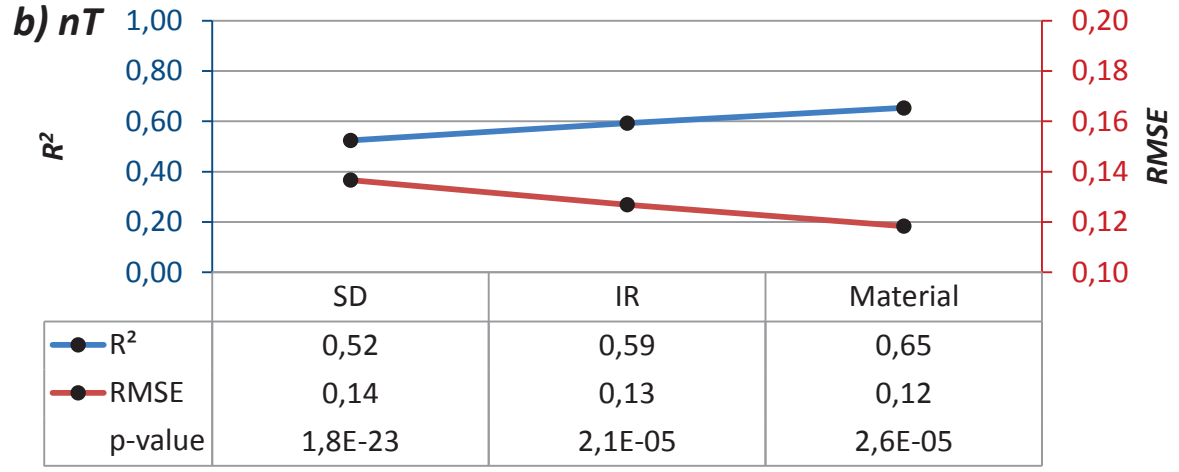

	SD	IR	Material
R²	0,52	0,59	0,65
RMSE	0,14	0,13	0,12
p-value	1,8E-23	2,1E-05	2,6E-05

Figure 17: The graph shows coefficient of determination (R^2) and root mean square error (*RMSE*) for each step in the linear regression models for *nF* (a) and *nT* (b) for the Finse field site. The *p-value* of each predictor added to the model is given below. The last two steps of the model for *nF* and the last step of the model for *nT* (Table 4) is excluded due to over-fitting of the model (relatively high *p-values* and marginal model improvements).

The results of the regression analysis for all three sites are presented in Table 4. Maximum snow depth is the first explaining variable in the regression models for both *nT* and *nF* at all three field sites, with *RMSE* of 0.15 or less in all models. The reductions in *RMSE* from this value to the final models are 0.04 or less. ln(*SD*) explains around 70 % ($R^2 > 0.68$) of the variation in the winter offset (represented as *nF)* at both Finse and in Ny-Ålesund. (*p-values* << 0.001). For the summer offset (represented as *nT) SD* explains between 50 % and 63 % of the spatial variation. The high correlation to *SD* shows that the effect of the variation in length of the summer season due to late snow melt overruns the variation in solar radiation during the snow free season. This indicates that the timing of melt-out is mainly controlled by the variation in maximum snow depths, and to lesser degree the variation in solar radiation. When comparing the timing of melt out to *SD* and *IR* at all the sites, we find much higher correlations with *SD* ($R^2 = 0.25$) and ln(*SD*) ($R^2 = 0.4$), than with *IR* ($R^2 < 0.1$).

The second predictor at Finse and Juvvasshøe is *IR* for both the summer and winter offsets. At the high-latitude site in Ny-Ålesund, slope and soil moisture are more significant. Here, the midnight sun results in nearly even amounts of incoming solar radiation from all directions during summer, while there is no effect of solar radiation during the polar night. Both in Finse and in Ny-Ålesund *SD* is the first variable and has high significance (*p-values* << 0.001) compared to the later variables, with minor model improvements after the first step. The generally higher *p-values* at Juvvasshøe results from the low number of observations, and here the difference is also less pronounced between the variables.

Table 4: Statistics for the stepwise multiple regression analysis to fit a linear model for *nT* and *nF* at the three field sites. Each column represents one step in the model, with the added predictor indicated at the header.

Finse	*nF*	Added	*ln(SD)*	*IR*	*Material*	*Moisture*	*Curvature*	*Slope*
		R^2	0,73	0,79	0,82	0,85	0,85	0,86
		RMSE	0,15	0,13	0,12	0,12	0,11	0,11
		p-value	3,4E-41	1,2E-08	1,7E-05	4,0E-05	1,2E-02	2,8E-02
	nT	Added	*SD*	*IR*	*Material*	*Slope*		
		R^2	0,52	0,59	0,65	0,67		
		RMSE	0,14	0,13	0,12	0,12		
		p-value	1,8E-23	2,1E-05	2,6E-05	1,4E-02		
Juvvasshøe	*nF*	Added	*ln(SD)*	*IR*	*Aspect*			
		R^2	0,46	0,61	0,66			
		RMSE	0,15	0,13	0,12			
		p-value	2,1E-07	1,2E-04	4,3E-02			
	nT	Added	*SD*	*IR*	*Moisture*	*Material*		
		R^2	0,57	0,67	0,73	0,78		
		RMSE	0,13	0,11	0,10	0,10		
		p-value	1,9E-09	7,6E-04	2,0E-02	3,3E-02		
Ny-Ålesund	*nF*	Added	*ln(SD)*	*Slope*	*Moisture*	*Aspect*		
		R^2	0,68	0,72	0,75	0,76		
		RMSE	0,15	0,14	0,13	0,13		
		p-value	1,1E-44	1,9E-06	4,9E-04	1,4E-02		
	nT	Added	*SD*	*Moisture*	*Slope*			
		R^2	0,63	0,67	0,68			
		RMSE	0,09	0,09	0,08			
		p-value	1,9E-40	1,4E-05	4,7E-03			

5.3 A statistical approach to represent small-scale variability of permafrost temperatures due to snow cover (Paper II).

In this paper we present observations and analysis from arrays of 35 to 100 GST-loggers distributed within footprints of 0.5 km^2 at the three field sites Finse, Juvvasshøe and Ny-Ålesund. Variations in *MAGST* over the hydrological year 2012/2013 of up to 5 °C were observed within the footprints, with the largest variation in the arctic field site, Ny-Ålesund. The variation stems mainly from the winter season, and most of the variation can be explained by variation in maximum snow depth. This highlights the important impact of snow distribution on the fine-scale variation of ground temperatures in these environments.

At each of the field sites the CryoGRID1 model is run with distributions of snow depth measured within a 1x1 km area around the logger sites. The resulting modelled distribution of *MAGST* manages to reproduce most of the observed variations. If the spatial distribution of snow depths is known, a statistical representation of the spatial variability of ground surface temperatures is feasible, even in a simple permafrost model. The study exemplifies the necessity of representing the sub-grid variability of ground temperatures in larger-scale model approaches.

5.4 Spatial and temporal variability of snow distribution in a high alpine catchment

The four years of manual snow depth measurements in the more than 200 snow survey points at Juvvasshøe and Finse show similar relative distributions of snow for all of the years (Figure 18). The main winter wind direction over the years of observation varies between to distinct patterns, particular at Juvvasshøe (). At Finse, where the wind direction is highly controlled by the direction of the valley, the main wind direction is most years from northwest, while in 2014 it was from southeast, the direct opposite direction. Still, the relative distribution between the survey points is nearly constant, with the largest inter-annual variations found in the outer parts of drift zones. Here, the snow depth is highly dependent on the size of the drift, as in point 125 – 150 at Juvvasshøe (Figure 18). This regular inter-annual pattern indicates that snow distributions within 1 km distances highly depend on the topography and the general degree of wind exposure at the location.

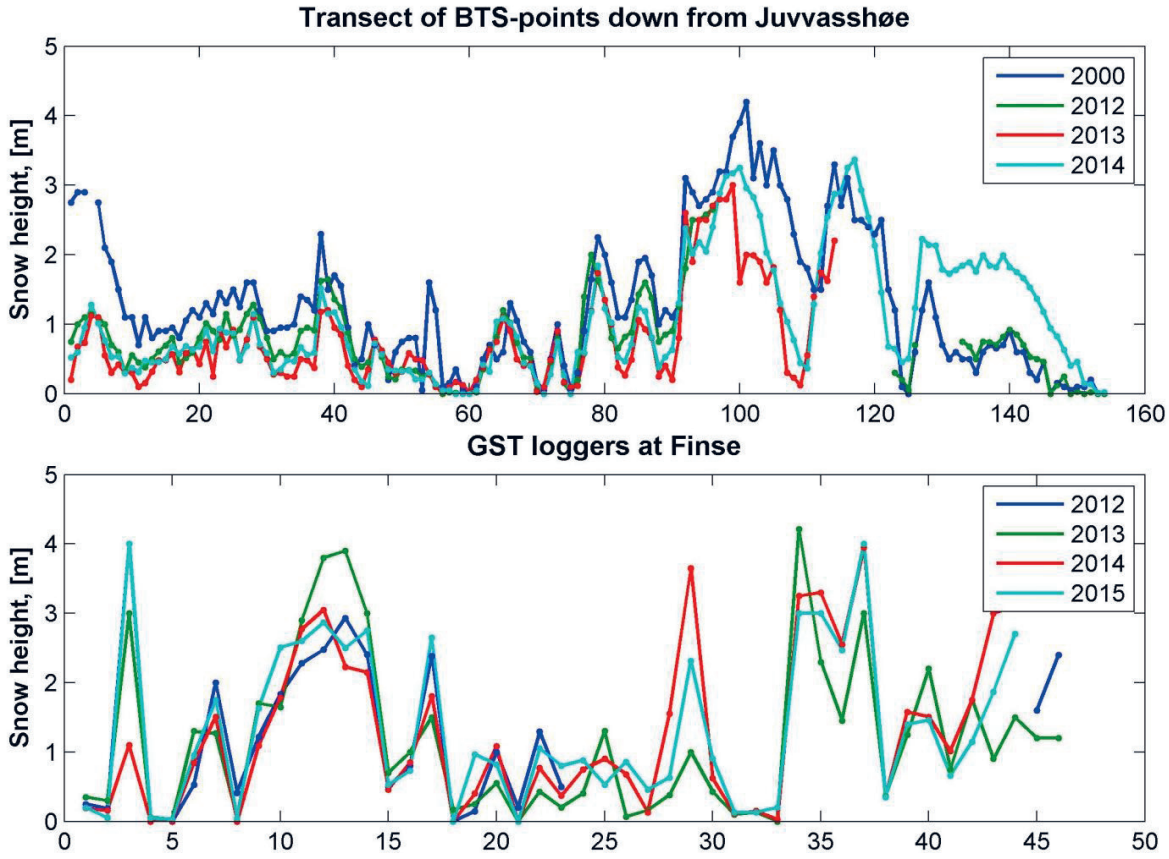

Figure 18: Snow depths at the logger sites (numbered on the x-axis) at Juvvasshøe (upper) and Finse (lower), measured manually with a probe at snow maximum over repeated years.

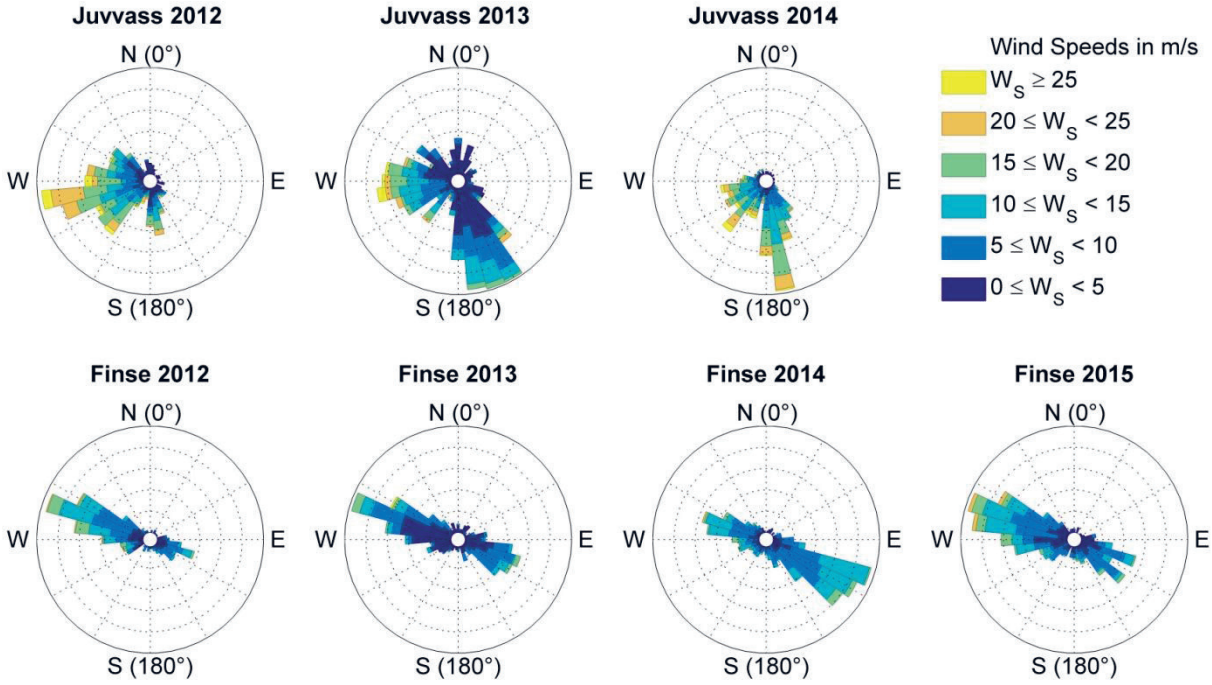

Figure 19: Distribution of wind directions in the snow accumulation season (here 1st December - 1st April). The observations are from the met-stations at Juvvasshøe and Finse.

The GPR-surveys of snow depths, conducted over four consecutive years at the 1 km^2 grid at Finse, show similar snow distributions for all years (Figure 20). The range of the distributions increases during the accumulation season from December to March, and there are gradually less snow free areas as the accumulation season progresses. In 2015 there is little change in the overall distribution from March to the end of May, even though substantial changes were observed at point locations. The *CV* is relatively similar with values from 0.68 to 0.78 for all snow surveys, except the February and March surveys in 2012 where it reaches a value of 1.0.

At Juvvasshøe snow depths in several 1 km^2 grid cells over a large terrain gradient have been measured with GPR, but with a coarser sampling than at Finse. Statistics for the GPR snow surveys in March 2012 and 2013 at Juvvasshøe are included in Appendix A1, together with the data from Finse and Ny-Ålesund. For both years the *CV* is highest at the highest elevations, while lower values of *CV* are found down towards the treeline. The correlation to elevation is explained by the higher wind exposure towards the top plateau. The inter-annual variation in *CV* is larger than at Finse, in particular for the higher elevations (*Area 1 to 4* at Juvvasshøe). Here, the inter-annual variation in *CV* is up to 0.3, found when comparing 2012 and 2013. These two years have significantly different wind directions, with main wind direction from the west in 2012, while a large amount of the wind is from south in 2013.

When comparing the sheltering index (*Sx*) calculated from the Winstral terrain parameter, the change in wind direction appears as a significant change in the sheltering of the area. Because of the field location at one side of a large massif, a major change in wind directions seems to affect the amount of redistribution significantly. These findings suggest that the main wind direction and general wind exposure should be accounted for in addition to the terrain.

At the Finse field site, two met-stations (*Thomas* and *Erika*) are located 500 m apart on opposing sides of a 30 meter high hill (Figure 4). The locations are chosen to be in direct lee or exposure of the two main wind directions from northwest and southeast. Wind observations at the two stations show differences in average hourly wind speeds of up to 15 m/s (Figure 21). Such large differences in the fine-scale wind speeds must be reproduced in order to model the correct snow redistribution with a physical model. This has shown to be a challenging task, and *Snowtran-3D* (Liston and Sturm, 1998) managed only to represent ¼ of the observed variation in wind speeds at Finse (Litherland, 2013).

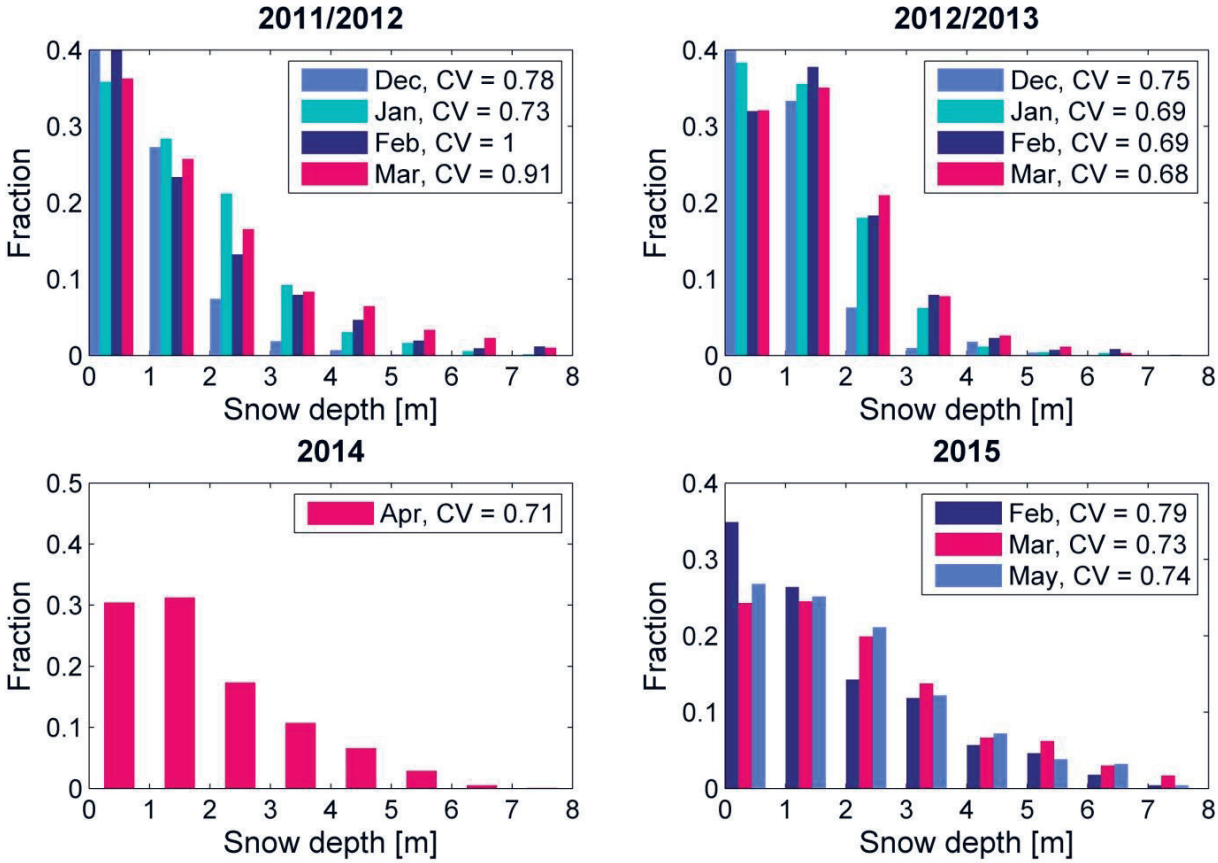

Figure 20: Measured distributions of snow depths at Finse. Coefficient of variation (*CV*) is given for all surveys. The snow depths are based on data from ground penetrating radar (GPR)-surveys, resampled to 1 meter resolution.

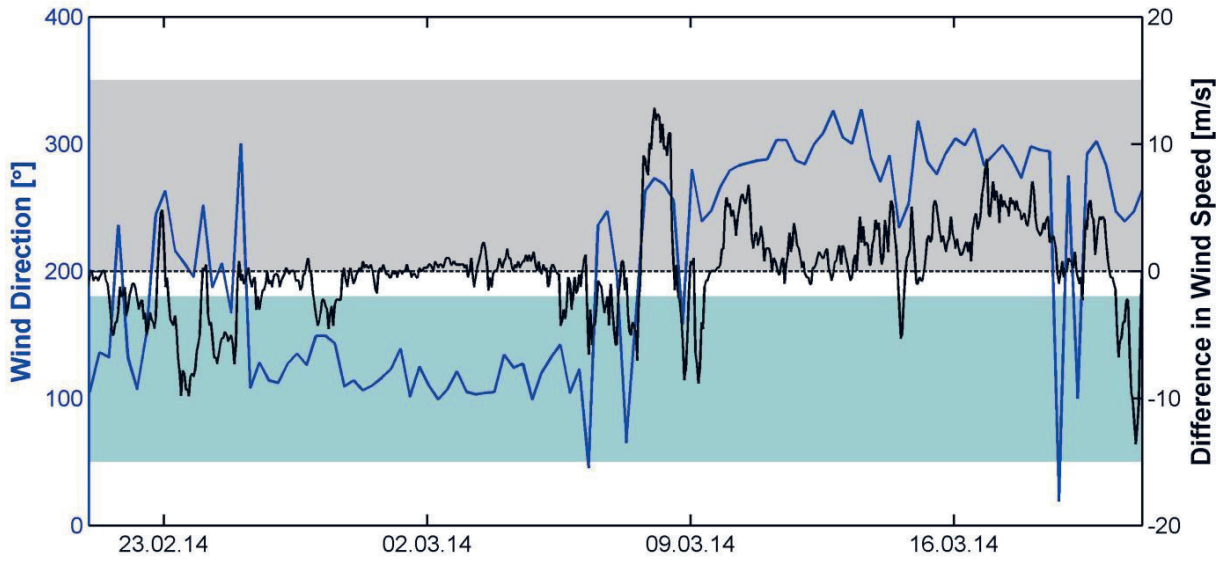

Figure 21: Differences in wind speed (black line) at the *Thomas* (exposed to westerly winds) and *Erika* (exposed to easterly winds) met-stations are related to wind directions (blue line). Positive values indicate stronger wind at the *Thomas* station, and negative more wind at the *Erika* station. The grey shading indicates the range of wind directions from west, and the green wind directions from east.

5.5 Sub-grid variation of snow in a regional permafrost model (Paper III)

In this paper we employ statistically derived snow distributions within 1 km² grid cells as input to a regional permafrost model in order to represent sub-grid variability of ground temperatures. Snow distributions are derived from a terrain-parameterization accounting for the winter wind directions. 100 model realizations with different snow depths for each grid cell enable a representation of the distribution of sub-grid ground temperatures. This allows for an estimate of the permafrost percentage, in addition to the average ground temperature within each grid cell. The model evaluation shows significant improvements of both the average and the total range of ground temperatures, compared to a model run without a sub-grid variability. Observed sub-grid ground temperature variations of up to 5 °C are reproduced, and 98% of the borehole observations are within the modelled temperature range.

Based on this more faithful representation of ground temperatures, we find the total permafrost area of mainland Norway to be nearly twice as large as what is modelled without a sub-grid approach. Here, we evaluate the model sensitivity to a climate forcing with increasing temperatures, with and without a sub-grid approach. Temperature anomalies are calculated as +100 TDD and +83 FDD for each 0.5 °C temperature increase, based on Lilleøren et al. (2012), and only open, non-vegetated areas are considered. The modelled permafrost area is six times as larger with the sub-grid approach, compared to the same model without a sub-grid representation. 1.5 % of the mainland will still be underlain by permafrost with a 1 °C temperature increase, while in the baseline model all permafrost areas will degrade with the same increase..

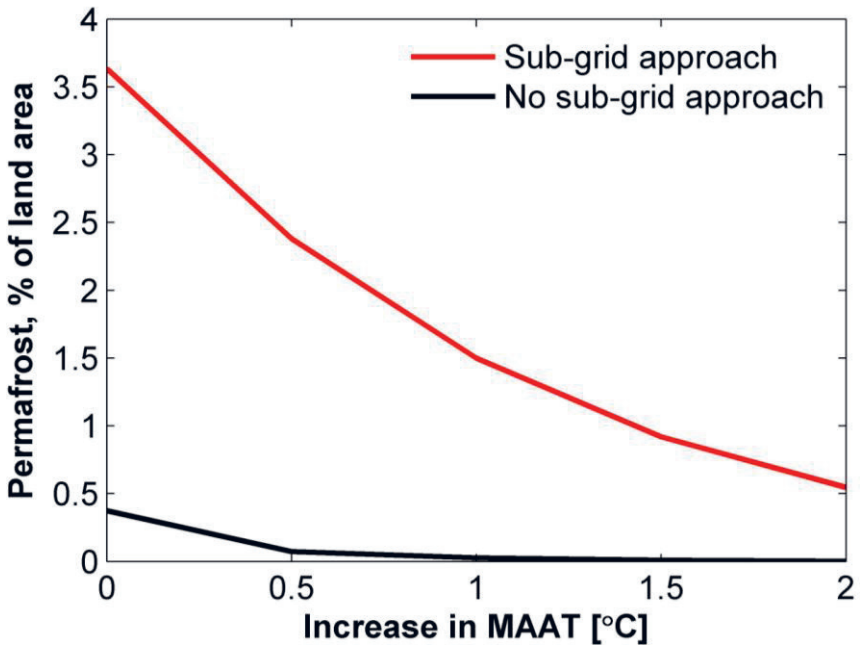

Figure 22: The figure shows the percentage of the Norwegian land area underlain by permafrost in equilibrium with warmer climates, modelled with (red line) and without (black line) a sub-grid representation of snow.

5.6 Snow covered fraction derived from repeated digital camera images and ground surface temperature loggers

Hourly images over the Bayelva area were taken by an automatic digital camera installed at Scheteligfjellet over the melt-seasons in 2012 - 2014. Images having good visibility to the ground are available for most days during the melt-season of 2012. As much as 400 images are orthorectified and classified. In 2013, the front of the camera box was covered by snow during parts of the season, in addition to several days with a low cloud cover. This resulted in only 93 images of good quality this year; however, most of the melt period is covered. In 2014 technical problems with the camera during the main part of the snow melt resulted in a large gap in the data series. The entire collection of good-quality images, both in raw format and orthorectified, are published in Westermann et al. (2015a).

The classification routine correctly separated snow covered from snow free ground for most images, also in shadowed areas (Figure 23). An ice surface happened to appear early in the melt season in areas where a thick ice layer was present below the snow layer, such as in the river Bayelva. These areas are classified as snow free. A heavy rain-on-snow event in the early winter of 2012 resulted in a thick ice layer of up to 30 cm on the ground in large parts of the field area. However, this did not significantly influence the melt-out pattern.

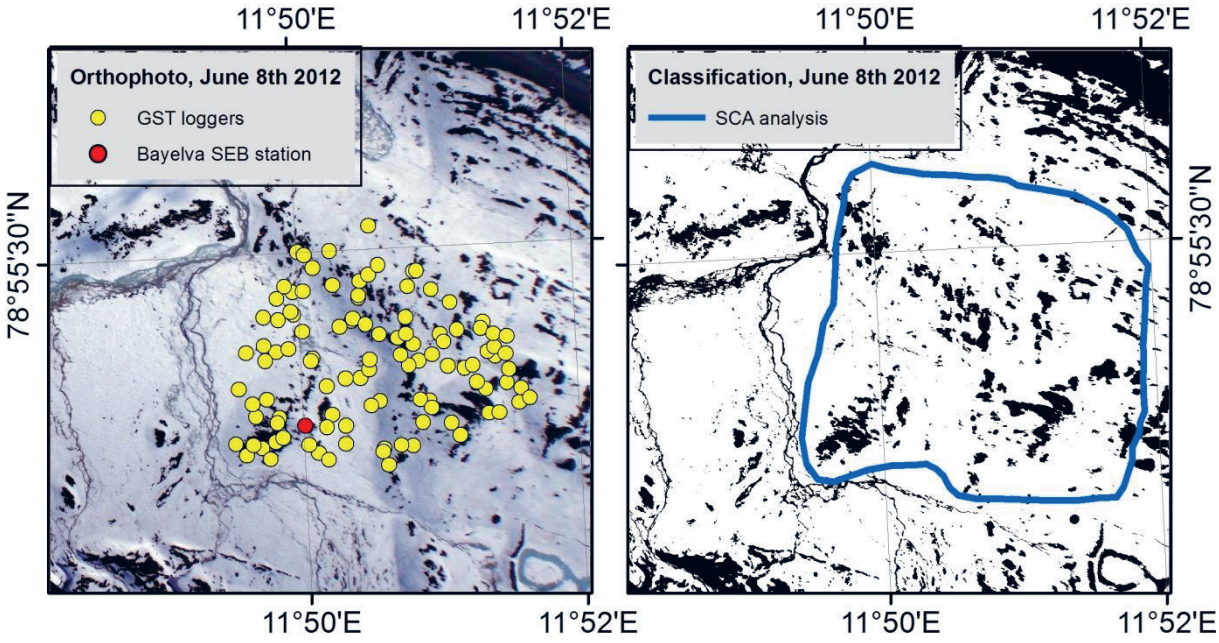

Figure 23: Left: Orthorectified images of the study area in June 2012, with the distribution of GST-loggers (yellow dots) and the Bayelva surface-energy balance station (red dot). Right: Classification of snow (white)/snow free (black) ground, with the area used for the snow covered fraction curves (blue line).

The snow covered fractions (SCF) from the analysed images (dots in Figure 24, upper) are compared to SCF-curves estimated from the GST-loggers (lines in Figure 24, upper). In 2013 representative data series from both methods are available through the entire melt-season. The correlations between logger- and camera- derived SCF-curves are good. At one occasion in 2013 the camera images show an increase in SCF of almost 0.2 in the middle of the melt-season, before again decreasing. This corresponds to a snow fall the 14th of June 2013, where the fresh snow was quickly melted by rain the next day. This event is not represented by the GST-loggers, because a short snow fall during summer will not insulate the ground, and also not release enough latent heat to significantly dampen the daily temperature variation and amplitude at the ground surface compared to the air temperatures.

The SCF-curves indicate a melt season duration of approximately one month for 2012 and 2013. The timing, corresponding to the entire month of June, is similar for these two years. In 2014 the melt season started approximately one month later, and lasted for only 2 to 3 weeks. The shorter melt season is a result of the later timing causing a more positive radiation balance due to the higher solar angle and 24-hours of sunlight.

Based on the good correlation between SCF-curves derived from camera observations and GST-loggers in Bayelva, the GST-logger method is also applied for the GST-data at Finse (Figure 24, lower). These SCF-curves serve as validation data for sub-grid snow distributions implemented in the WRF model (Paper IV). The GST-loggers at Finse are located in a 500 m x 500 m area at the hilltop east of Vetle Hansbunuten, an exposed area with high redistribution of snow and large bare blown areas. Several of the loggers are therefore snow free most of the winter season, and the SCF-curves start below 0.9. The melt seasons in 2012 to 2014 started in mid- to late May, while in 2015, a cold spring with fresh snow in the beginning of June resulted in a delayed melt-season. The melt seasons in 2013 and 2014 were similar, with durations of nearly two months and snow free ground during the first week of July. In 2012 and 2015 there was still snow in the end of August, and the melt seasons lasted for more than 2.5 months.

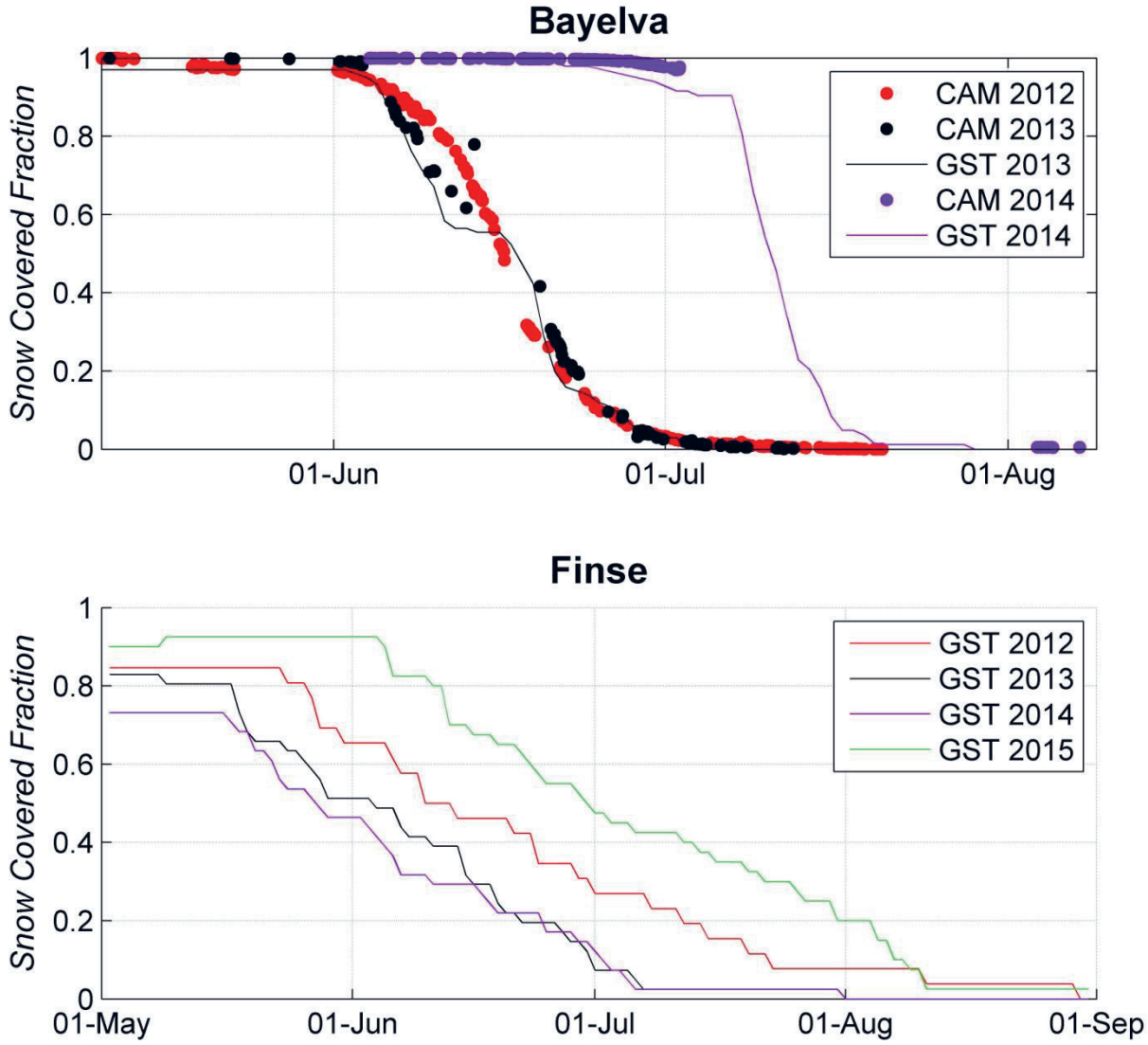

Figure 24: Snow covered fraction (SCF) over the melt seasons in 2012 - 2014 in Bayelva, and for 2012-2015 at the Finse field site. Snow covered fractions derived from digital camera images are shown as dots, while snow covered fractions derived from ground surface temperature (GST)-logger arrays are plotted as continuous lines of data.

5.7 A tiling approach to represent sub-grid snow variability in coupled land-surface – atmosphere models (Paper IV).

In this paper we implement and test the effect of a sub-grid representation of snow variation in a coupled atmosphere – land surface model (LSM). For this study we use the Weather Research and Forecasting (WRF) model with the Noah LSM, applied to the mountain regions of southern Norway, where the statistical snow distributions derived for Norway in Paper III are used to scale solid precipitation in ten sub-grid tiles. In this way we obtain a consistent, explicit representation of the variation in snow depths on sub-grid scales. By simulating individual soil properties for each tile, this approach also accounts for a number of secondary effects of an uneven snow distribution.

At the Finse field site, the transition time from full snow cover to snow-free ground increases from a few days with the default snow covered fraction (SCF) representation, to more than two months with the tiling approach. This agrees with the SCF derived from the surface temperature loggers (Figure 24, lower). The improved representation of sub-grid snow variation reduces the temperature bias at local noon by 4 °C during the first half of July, and improves the representation of the phase of the diurnal temperature cycle. On a regional scale, the mosaic snow approach removes the bimodal temperature bias observed in June, July and August, related to the binary SCF in the reference simulation. The lower albedo and higher skin temperatures during melt season increase the surface energy fluxes on local and regional scales. These changes in energy and moisture fluxes result in increased precipitation in the mosaic approach during the melting season. In the most affected sub-region the correlation between simulated and observed precipitation increases from 0.83 to 0.89.

Some of these improvements could have been achieved by implementation of a better SCF scheme combined with separate surface energy balance calculation for snow covered and snow free ground. There are, however, additional physical processes related to sub-grid snow variations that are naturally accounted for with sub-grid tiling. In addition, the current sub-grid tiling approach can account for the hysteresis effect while treating accumulation season and melting season in a consistent way. This approach can therefore be seen as the most flexible and physically consistent approach to account for sub-grid snow variations, although at the expense of increased computation time.

5.8 A new permafrost map for the Scandinavian Peninsula (Paper V).

The main goal of this paper is to provide a new accepted baseline for permafrost distribution in Scandinavia. We present a new permafrost map based on an implementation of the CryoGRID1 model at 1 km^2. The model is forced by a recently developed dataset of gridded daily air temperature and precipitation for Norway, Sweden and Finland. For non-vegetated areas the sub-grid scheme for snow, presented in Paper II and Paper III, is implemented, allowing for a more detailed representation of the permafrost boundaries. It is parameterized and evaluated with the use of all available field measurements, and thoroughly validated by a large collaborating permafrost research community in Scandinavia.

The new map provides a higher level of detail and stronger confidence in the model results than previous permafrost maps for this area. Compared to the more generalized "*International Permafrost Association Circum-Arctic Map of Permafrost and Ground Ice Conditions*" by (Brown et al., 1997), which has served as a reference map until now, it provides a similar, but more detailed picture of the distribution of mountain and lowland permafrost. Modelled average ground temperature in the grid cells is within ±2 °C of the observed ground temperatures in 25 boreholes, and all borehole temperatures are within the range of the modelled ground temperatures for the corresponding grid cell. The map is accepted by the local permafrost experts, and will serve as a validation for future global scale permafrost model attempts.

6 General discussion

Quantification of the sub-grid variability of ground temperatures is crucial in order to understand and improve the bias in permafrost models and land surface schemes. Based on detailed field observations, this thesis aims to quantify the spatial variation of the surface energy balance, here represented by ground surface temperatures, and the related surface variables, with main focus on snow distribution (Paper II). The measured spatial variation in mean annual ground surface temperatures (*MAGST*) over 1 km^2 areas, a typical size of a grid cell in regional permafrost and land surface models, is up to 5 °C in three different high-altitude to arctic environments in Norway. The findings presented here show that significant variation occurs also over much smaller scales and in more low relief environments than previously shown. The extensive amount of observation data over small areas collected in this study allows for a proper statistical analysis of the distribution of ground surface temperatures. Snow distribution is found to be the main explaining variable for the spatial variation in the surface offset, both in summer and winter, while it is to a lesser degree influenced by the variation in potential incoming solar radiation or ground materials. This holds for all field sites and over repeated seasons, and demonstrates that even in the low relief arctic site in Ny-Ålesund, featuring less variation in snow depths, the impact from the snow on ground temperatures is as large as or larger than at the high mountain sites.

The large variation in ground temperatures in high mountain areas is previously emphasized by several studies (e.g. Gruber and Hoelzle, 2001; Isaksen et al., 2002; Etzelmüller et al., 2007; Gubler et al., 2011), reporting of variations in *MAGST* of up to 6 °C within elevation bands of 200 m – 300 m. There is only a small correlation with elevation, and surface

material, vegetation, terrain parameters and snow cover are addressed as the explaining variables. Based on systematic observations of ground temperatures over a 16 km^2 are in the Swiss Alps, Gubler et al. (2011) concluded that the variation in *MAGST* can be explained by the topographic variables elevation, slope, aspect and ground cover type. In this work we aim to quantify the variation over areas of a typical grid-cell in the regional models. The field areas have relatively small internal elevation differences (< 100 m), and the entire variation in *MAGST* is related to other topographic variables than elevation. The findings suggest that most of the fine-scale variation in *MAGST,* in environments similar to the alpine sites in southern Norway and the arctic site in Svalbard, can be explained by variation in maximum snow depths alone.

Furthermore, the field data supports the established knowledge that the insulating effect of the snow cover is non-linear and highly sensitive to variations in snow depths below 1 meter. The observed distributions of snow in mountain environments are highly asymmetric, and follow a lognormal to a gamma distribution (Paper II and III). Consequently, the measured average *MAGST* within a 1x1 km area differs significantly from the *MAGST* expected at a site with the average snow depth. Additionally, we find the timing of melt-out at our field sites to be controlled mainly by the variation of maximum snow depth, and less by the variation in incoming solar radiation. While variation in snow depths exceeding 1 to 2 meters does not introduce large variation in the surface offset during winter, it highly influences the length of the thawing season at the ground surface. At very snow rich sites the cooling effect of a shorter summer season may exceed the insulating effect of the snow cover. It is therefore important to represent the full range of snow depths in order to precisely model the gradual depletion of the snow cover and thus the correct variation in the surface energy balance. In Paper II we demonstrate that the fine-scale variation in *MAGST* can be reproduced in a simple permafrost model by only accounting for the variation in maximum snow depths.

6.1 Statistical representation of fine-scale snow variation

The highly variable pattern of snow depths at the high-mountain field sites was found to repeat each winter season. The inter-annual variation in relative snow distribution at the logger sites was minor, even though the variation in total amount of snow was significant. The coefficient of variation for snow depths within 1 km^2 areas exhibited relatively low inter-annual variation, except for in some areas sheltered by larger mountains (Paper III). Here,

changes in the prevailing winter wind direction may shelter the entire area, and influence the snow distribution.

A range of different model approaches attempting to represent local snow drift patterns have previously been developed, lately at a high level of physical complexity. In order to model redistribution of snow using a physical representation, the wind pattern must be reproduced at sufficiently high resolution. We find that the observed variations in wind speed and resulting snow depths at Finse are difficult to reproduce using the available physical snow drift models, even with extensive site specific calibration. The required amount of input parameters, the computational cost, as well as the need for site specific calibration, cause distributed physical snow models to be unsuitable for representing sub-grid variation in regional models.

We show that statistical representations of snow distributions are able to reproduce the observed snow distribution over regional scales. Based on a fine-resolution terrain parameterization together with main wind directions, maximum snow depth and elevation, we derive snow distributions at 1 km^2 for all of the non-forested parts of mainland Norway. A statistical scheme has the disadvantage of not representing the physical properties of the snow pack, and it might therefore not reproduce the changes in snow pattern with a changing climate. However, when calibrated with spatially large, but detailed, datasets of the critical parameters this type of approach might reproduce the current situation just as well, or even better, than a physical model without appropriate quality or resolution of the required input parameters. We find that our statistical representation of snow distributions is able to reproduce observed coefficients of variation with a precision of c. ±0.1. Because of few input parameters and the low computational cost, statistical representations of snow are suitable for implementation in land surface schemes and large-scale permafrost models.

6.2 The effect of a sub-grid representation of snow in regional permafrost models and land-surface schemes

The implementation of a statistical representation of snow distribution in a regional permafrost model shows large improvements in correlation of modelled and observed ground temperatures (Paper III). The improved representation shows a doubling of the permafrost area compared to the same model without a sub-grid representation of snow. The total modelled permafrost area classified as sporadic, discontinuous or continuous is significantly

larger than what is modelled as permafrost in the binary representation of permafrost in the model without a snow distribution. However, the area of continuous permafrost is significantly smaller, and the lowest sub-grid mean annual ground temperatures are several degrees colder than what is modelled without a sub-grid approach. Consequently, the latter will respond with a more rapid decrease in permafrost area compared to the sub-grid approach, which still indicates sporadic permafrost in the high mountain areas of Norway in equilibrium with a climate 2 °C warmer than the current climate.

We also show that a coupled atmosphere – land surface model benefits from the addition of a sub-grid representation of snow (Paper IV). The implementation of statistical snow distributions as sub-grid tiles significantly prolongs the duration of the melt-season, in accordance with observations. This influences the albedo, the net flux of long-wave radiation and the evapotranspiration. As a result, the modelled near surface temperatures in mountain areas during the melt season are significantly improved. Because of the changes in evapotranspiration, feedbacks are also seen on the larger scale precipitation pattern.

6.3 A new baseline map for permafrost in Scandinavia

The implementation of a sub-grid snow distribution in the CryoGRID 1 model for Scandinavia results in a model capable of representing the regional patterns of permafrost (Paper V). It manages to reproduce both observed ground temperatures and lower limits of permafrost at a local scale. This demonstrates that simple equilibrium model approaches can be accurate if the quality of the input data is good and the parameterization is based on a large ensemble of field investigations collected from large parts of the modelling domain. However, such model approaches can only reproduce the ground temperatures in equilibrium with the climate forcing. With a parameterization derived from field observations in the current climate, only the current climate can be modelled sufficiently. In order to make climate change analysis, a transient representation of the climate system and the ground thermal regime is required. The new permafrost map for Scandinavia will serve as a validation dataset for such model approaches, as it is thoroughly validated and accepted as the baseline map by the permafrost community in Scandinavia.

6.4 Bridging terrestrial and atmosphere models

The field observations and modelling efforts presented in this thesis demonstrate that land surface models and permafrost models with grid resolutions of 1 km^2 or coarser will introduce biases in the surface energy balance if they do not adequately represent the sub-grid variation of snow. For permafrost models, not only the total distribution of permafrost will be biased, but also the response to changes in the climate forcing will be incorrect if the full range of sub-grid ground temperatures is not represented. In land surface schemes not including the effects of the fine-scale variation of snow explicitly, the averages of the net surface fluxes will be biased. In a coupled model this will propagate back into the atmosphere model, and as shown in Paper IV this may introduce significant biases in the entire system.

The future climate changes projected by the General Circulation Models have resulted in a high interest in land surface models that are able to model the effect of the projected future climate on the surface energy budget. The projected future, but also the already observed, increase in temperatures, is highest in arctic and high-altitude areas. In these areas, changes in the surface energy budget, which is highly controlled by the seasonal or perennial snow cover, will have a large impact on the terrestrial cryosphere. Permafrost, being a key element in the terrestrial cryosphere, is projected by the *IPCC* to become a net emitter of carbon over the next century as a response to the warming of the climate and thus changes in the surface energy balance. Permafrost areas will therefore act as a positive feedback mechanism on the climate system.

Together with estimates of potential release of carbon from the ground, these projections rely on estimated permafrost degradation in response to the climate change. The estimates are derived from ESMs, run at ground resolutions normally much coarser than 1 km^2, or from permafrost models forced with output from the GCMs. As a result of the increased focus on model representations of the surface energy balance, much attention has lately been drawn towards the mismatch between the scales at which atmospheric and surface variables operate. There is an urgent need for increased knowledge of how the fine-scale processes can be sufficiently represented in regional models, and their effect on the larger scale climate. Techniques for up and downscaling of processes between the atmosphere and the land surface, as presented in this thesis, are therefore highly relevant in the context of the current major research questions.

6.5 Outlook

The work presented in this thesis shows that the inclusion of sub-grid snow distributions clearly improves the model representation of the surface energy balance in arctic and high-latitude environments similar to those in Scandinavia and Svalbard. Furthermore, we have presented a computationally cost effective statistical approach combining a simple terrain parameterization with a few key input parameters, all which are normally available over larger regions. This approach, shown to significantly improve the model results, is simple enough to be implemented in regional models. Based on the findings in this work, it is suggested that the sub-grid variability of snow should be explicitly represented in future land surface and permafrost models.

The field investigations show that the inter-annual variations in snow distribution are relatively low, even with different wind patterns over the winter. The main controlling factor is the variation in exposures over the terrain, and in high mountain areas the extensive wind drift allows for a significant smoothing of the snow surface filling up depressions in the terrain every winter. However, the degree of redistribution varies between winters with the amount of strong wind events, and the terrain depressions might not be filled up in all areas. Further development of the snow distribution routine should therefore include high resolution gridded wind data if available.

There is an ongoing development of remote sensing techniques to record snow properties from space. One example of such a product is the fractional snow cover at 500 m resolutions from MODIS. When compared to field observations at Finse and Svalbard the data quality was found to be too poor with many outliers during the melt-season. However, the beginning and end of the snow season could be extracted. Future work should aim to derive sub-grid snow distributions from similar satellite data.

The field investigations in this thesis are focused on high-mountain and arctic environments. However, similar investigations in other environments, i.e. tundra and mire areas, are crucial to improve representation of permafrost distribution and response to climate changes for these areas. In permafrost areas at more southerly latitudes the solar radiation and other surface variables might be more important for the surface energy balance. Here, a similar statistical downscaling approach could additionally include these variables.

7 Conclusions

The main achievements and conclusions of the research and discussions in this thesis are summarized in the following:

- Measured spatial variation in mean annual ground surface temperatures within 0.5 km^2 footprints ranges from 2.5 °C to 5 °C at three field sites in high-mountain and arctic environments in Norway and Svalbard. The fine-scale variability is introduced during the snow covered season and the melt-out in spring, and is highly correlated to maximum snow depths. The variation in incoming solar radiation and surface materials has minor influence.
- Observed snow distribution at distances below 1 km in exposed mountain areas is highly related to topography. The coefficient of variation (*CV*) of maximum snow depths could be represented with a precision of ±0.1 using a terrain parameterization accounting for winter wind directions and average maximum snow depth.
- The implementation of statistical snow distributions at a sub-grid level in a regional permafrost model with 1 km^2 resolution doubles the modelled permafrost area, compared to a baseline run of the same model. In the sub-grid approach the entire range of ground temperatures within each grid cell is represented, allowing for a gradual transition from permafrost areas to no-permafrost areas. The full range of sub-grid temperatures must be represented in order to model the correct response of ground temperature and potential permafrost degradation to a changing climate.
- Using sub-grid snow distributions to break grid cells into tiles of varying snow depth in a coupled atmosphere – land-surface scheme yields significant improvements to the representation of the transition time from full snow cover to snow-free ground. The

improved representation of sub-grid snow variation reduces a cold bias found in the reference simulation, increases the surface energy fluxes on local and regional scales, and has an appreciable effect on simulated regional precipitation.

- The work presented in this thesis demonstrates that a representation of sub-grid snow distributions is crucial to obtain a precise representation of the surface energy balance. The use of statistical snow distributions has shown to be a robust and cost effective way to include the non-linear effects of the snow cover, both in regional permafrost models and in coupled atmosphere – land-surface schemes.

8 References

Anders, A. M., Roe, G. H., Durran, D. R., and Minder, J. R.: Small-Scale Spatial Gradients in Climatological Precipitation on the Olympic Peninsula, Journal of Hydrometeorology, 8, 1068-1081, 10.1175/JHM610.1, 2007.

Andreassen, L. M., and Winsvold, S. H.: Inventory of Norwegian glaciers, Direktoratet, Oslo, 236 s. : ill. pp., 2012.

Aune-Lundberg, L., and Strand, G.-H.: CORINE Land Cover 2006. The Norwegian CLC2006 project, Report from the Norwegian Forest and Landscape Institute: 11/10, 14p, 2010.

Bartelt, P., and Lehning, M.: A physical SNOWPACK model for the Swiss avalanche warning:: Part I: numerical model, Cold Regions Science and Technology, 35, 123-145, 2002.

Bernhardt, M., Zängl, G., Liston, G., Strasser, U., and Mauser, W.: Using wind fields from a high resolution atmospheric model for simulating snow dynamics in mountainous terrain, Hydrological Processes, 23, 1064-1075, 2009.

Bernhardt, M., Schulz, K., Liston, G. E., and Zängl, G.: The influence of lateral snow redistribution processes on snow melt and sublimation in alpine regions, Journal of Hydrology, 424–425, 196-206, http://dx.doi.org/10.1016/j.jhydrol.2012.01.001, 2012.

Camera Calibration Toolbox for Matlab: http://www.vision.caltech.edu/bouguetj/calib_doc/index.html#ref, accessed: 14th Oct, 2015. Last Updated: 2nd Dec, 2013.

Brown, J., Ferrians, O. J. J., Heginbottom, J. A., and Melnikov, E. S.: International Permafrost Association Circum-Arctic Map of Permafrost and Ground Ice Conditions., U.S. Geological Survey., 1997.

Bruland, O., Sand, K., and Killingtveit, A.: Snow distribution at a high arctic site at Svalbard, Nordic hydrology, 32, 1-12, 10.2166/nh.2000.001, 2001.

Bruland, O., Liston, G. E., Vonk, J., Sand, K., and Killingtveit, A.: Modelling the snow distribution at two high arctic sites at Svalbard, Norway, and at an alpine site in central Norway, Nordic hydrology, 35, 191-208, 2004.

Burgess, M. M., Smith, S. L., Brown, J., Romanovsky, V. E., and Hinkel, K.: Global Terrestrial Network for Permafrost (GTNet-P): permafrost monitoring contributing to global climate observations, Geological Survey of Canada, Current Reseach 2000-E14, 8, 2000.

Burn, C., and Smith, C.: Observations of the "thermal offset" in near-surface mean annual ground temperatures at several sites near Mayo, Yukon Territory, Canada., Arctic, 41, 99-104, 1988.

Carlson, H.: Calculation of depth of thaw in frozen ground, in: Frost action in soils. Highway Research Board Special Report Number 2., 192–223, 1952.

Christiansen, H. H., Etzelmüller, B., Isaksen, K., Juliussen, H., Farbrot, H., Humlum, O., Johansson, M., Ingeman-Nielsen, T., Kristensen, L., Hjort, J., Holmlund, P., Sannel, A. B. K., Sigsgaard, C., Åkerman, H. J., Foged, N., Blikra, L. H., Pernosky, M. A., and Ødegård, R. S.: The thermal state of permafrost in the nordic area during the international polar year 2007–2009, Permafrost and Periglacial Processes, 21, 156-181, 10.1002/ppp.687, 2010.

Dingman, S. L., and Koutz, F. R.: Relations among Vegetation, Permafrost, and Potential Insolation in Central Alaska, Arctic and Alpine Research, 6, 37-47, 1974.

Dingman, S. L.: Physical hydrology, Prentice Hall, Upper Saddle River, N.J., X, 646 s. pp., 2002.

Durand, Y., Guyomarc'h, G., Mérindol, L., and Corripio, J. G.: Improvement of a numerical snow drift model and field validation, Cold Regions Science and Technology, 43, 93-103, 2005.

Egli, L., Jonas, T., Grünewald, T., Schirmer, M., and Burlando, P.: Dynamics of snow ablation in a small Alpine catchment observed by repeated terrestrial laser scans, Hydrological Processes, 26, 1574-1585, 2012.

Ekman, S.: Die Gewæsser des Abisko-Gebietes und ihre Bedingungen (In German), Handlingar, 4. serien, Almqvist & Wiksell, Stockholm, 172 s. pp., 1957.

Elberling, B., Christiansen, H. H., and Hansen, B. U.: High nitrous oxide production from thawing permafrost, Nature geoscience, 3, 332-335, 2010.

Erlandsen, A. H., Faugli, P. E., and Grimstad, C.-E.: Vannets kraft: samfunnsbygger og miljøpåvirker, Publikasjon, Organisasjonen, Oslo, 80 s., [81] fold. pl. pp., 1997.

Essery, R., Li, L., and Pomeroy, J.: A distributed model of blowing snow over complex terrain, Hydrological Processes, 13, 2423-2438, 1999.

Etzelmüller, B., Berthling, I., and Sollid, J. L.: The distribution of permafrost in Southern Norway; a GIS approach, Seventh International Conference on Permafrost, Proceedings, Université Lavall, Québec, PQ, Canada, 1998, 251–257,

Etzelmüller, B., Hoelzle, M., Heggem, E. S. F., Isaksen, K., Mittaz, C., Mühll, D. V., Ødegård, R. S., Haeberli, W., and Sollid, J. L.: Mapping and modelling the occurrence and distribution of mountain permafrost, Norsk Geografisk Tidsskrift-Norwegian Journal of Geography, 55, 186-194, 2001.

Etzelmüller, B., Berthling, I., and Sollid, J. L.: Aspects and concepts on the geomorphological significance of Holocene permafrost in southern Norway, Geomorphology, 52, 87-104, 10.1016/s0169-555x(02)00250-7, 2003.

Etzelmüller, B., Farbrot, H., Guðmundsson, Á., Humlum, O., Tveito, O. E., and Björnsson, H.: The regional distribution of mountain permafrost in Iceland, Permafrost and Periglacial Processes, 18, 185-199, 10.1002/ppp.583, 2007.

Etzelmüller, B., Christiansen, H., Humlum, O., Farbrot, H., Juliussen, H., Isaksen, K., Schuler Thomas, V., and Ødegaard Rune, S.: Mapping and modelling the distribution of permafrost in the Nordic countries, 33rd international geological congress. Oslo NOR Norway. Aug, 2008, 2009-049439,

Farbrot, H., Isaksen, K., and Etzelmüller, B.: Present and past distribution of mountain permafrost in Gaissane Mountains, Northern Norway, In: Proceeding of the Ninth International Conference on Permafrost, Fairbanks, Alaska, 2008, 427–432,

Farbrot, H., Hipp, T. F., Etzelmüller, B., Isaksen, K., Ødegård, R. S., Schuler, T. V., and Humlum, O.: Air and Ground Temperature Variations Observed along Elevation and Continentality Gradients in Southern Norway, Permafrost and Periglacial Processes, 22, 343-360, 10.1002/ppp.733, 2011.

Farbrot, H., Isaksen, K., Etzelmüller, B., and Gisnås, K.: Ground Thermal Regime and Permafrost Distribution under a Changing Climate in Northern Norway, Permafrost and Periglacial Processes, 24, 20-38, 10.1002/ppp.1763, 2013.

French, H.: The Periglacial Environment, 3. ed., John Wiley and Sons Ltd, Chichester, UK, 458 pp., 2007.

Fu, P., and Rich, P. M.: A geometric solar radiation model with applications in agriculture and forestry, Computers and Electronics in Agriculture, 37, 25-35, http://dx.doi.org/10.1016/S0168-1699(02)00115-1, 2002.

Førland, E. J., Hanssen-Bauer, I., and Nordli, P.: Orographic precipitation at the glacier Austre Brøggerbreen, Svalbard, Norwegian Meteorological Institute, Oslo, 1997.

Gabrielsen, R. H., Faleide, J. I., Pascal, C., Braathen, A., Nystuen, J. P., Etzelmuller, B., and O'Donnell, S.: Latest Caledonian to Present tectonomorphological development of southern Norway, Marine and Petroleum Geology, 27, 709-723, http://dx.doi.org/10.1016/j.marpetgeo.2009.06.004, 2010.

Gauer, P.: Numerical modeling of blowing and drifting snow in Alpine terrain, Journal of Glaciology, 47, 97-110, 10.3189/172756501781832476, 2001.

Gisnås, K.: Permafrost distribution in Norway - Implementation of two equilibrium models on regional scale, Master, Department of Geosciences, University of Oslo, DUO: http://urn.nb.no/URN:NBN:no-29034, 2011.

Gisnås, K., Etzelmuller, B., Farbrot, H., Schuler, T. V., and Westermann, S.: CryoGRID 1.0: Permafrost Distribution in Norway estimated by a Spatial Numerical Model, Permafrost and Periglacial Processes, 24, 2-19, 10.1002/ppp.1765, 2013.

Goodrich, L. E.: Some results of a numerical study of ground thermal regimes, Third International Conference on Permafrost, Edmonton, Canada., 1978, 29-34,

Goodrich, L. E.: The influence of snow cover on the ground thermal regime, Can. Geotech. J., 19, 421-432, 1982.

Groot Zwaaftink, C. D., Löwe, H., Mott, R., Bavay, M., and Lehning, M.: Drifting snow sublimation: A high-resolution 3-D model with temperature and moisture feedbacks, Journal of Geophysical Research: Atmospheres, 116, n/a-n/a, 10.1029/2011JD015754, 2011.

Gruber, S., and Hoelzle, M.: Statistical modelling of mountain permafrost distribution: local calibration and incorporation of remotely sensed data, Permafrost and Periglacial Processes, 12, 69-77, 10.1002/ppp.374, 2001.

Gruber, S., Hoelzle, M., and Haeberli, W.: Permafrost thaw and destabilization of Alpine rock walls in the hot summer of 2003, Geophysical Research Letters, 31, L13504, 2004a.

Gruber, S., King, L., Kohl, T., Herz, T., Haeberli, W., and Hoelzle, M.: Interpretation of geothermal profiles perturbed by topography: the alpine permafrost boreholes at Stockhorn Plateau, Switzerland, Permafrost and Periglacial Processes, 15, 349-357, 10.1002/ppp.503, 2004b.

Gruber, S., and Haeberli, W.: Permafrost in steep bedrock slopes and its temperature-related destabilization following climate change, Journal of Geophysical Research, 112, F02S18, 10.1029/2006JF000547, 2007.

Gubler, H., Fiddes, J., Gruber, S., and Keller, M.: Scale-dependent measurement and analysis of ground surface temperature variability in alpine terrain, The Cryosphere, 5, 307-338, 10.5194/tcd-5-307-2011, 2011.

Haeberli, W.: Die Basis-Temperatur der winterlichen Schneedecke als möglicher Indikator für die Verbreitung von Permafrost in den Alpen, Zeitschrift für Gletscherkunde und Glazialgeologie, 9, 221-227, 1973.

Harris, C., Davies, M., and Etzelmüller, B.: The assessment of potential geotechnical hazards associated with mountain permafrost in a warming global climate, Permafrost and Periglacial Processes, 12, 145-156, 2001a.

Harris, C., Haeberli, W., Mühll, D., and King, L.: Permafrost monitoring in the high mountains of Europe: the PACE project in its global context, Permafrost and Periglacial Processes, 12, 3-11, 2001b.

Harris, C., Vonder Mühll, D., Isaksen, K., Haeberli, W., Sollid, J. L., King, L., Holmlund, P., Dramis, F., Guglielmin, M., and Palacios, D.: Warming permafrost in European mountains, Global and Planetary Change, 39, 215-225, DOI: 10.1016/j.gloplacha.2003.04.001, 2003.

Harris, C., Arenson, L. U., Christiansen, H. H., Etzelmüller, B., Frauenfelder, R., Gruber, S., Haeberli, W., Hauck, C., Hölzle, M., Humlum, O., Isaksen, K., Kääb, A., Lehning, M., Lütschg, M. A., Matsuoka, N., Murton, J., Nötzli, J., Phillips, M., Ross, N., Seppälä, M., Springman, S., and Vonder Muhll, D.: Permafrost and climate in Europe: Monitoring and modelling thermal, geomorphological and geotechnical responses, Earth Science Reviews, 92, 117-171, 2009.

Hartman, D. L.: Global Physical Climatology, International Geophysics Series, 56, edited by: Dmowska, R., and Holton, J. R., Academic Press, San Diego, California, USA 411 pp., 1994.

Hauck, C., Isaksen, K., Mühll, D. V., and Sollid, J. L.: Geophysical surveys designed to delineate the altitudinal limit of mountain permafrost: an example from Jotunheimen, Norway, Permafrost and Periglacial Processes, 15, 191-205, DOI: 10.1002/ppp.493, 2004.

Heggem, E. S. F., Juliussen, H., and Etzelmuller, B.: Mountain permafrost in the Solen massif, Central-Eastern Norway - First results, 8th International Conference on Permafrost, July 21-25 2003, Zürich, Switzerland, 2003, ISI:000185049300066, 367-371,

Heggem, E. S. F., Juliussen, H., and Etzelmüller, B.: Mountain permafrost in central-eastern Norway, Norsk Geografisk Tidsskrift-Norwegian Journal of Geography, 59, 94-108, 2005.

Heggem, E. S. F., Etzenmuller, B., Anarmaa, S., Sharkhuu, N., Goulden, C. E., and Nandinsetseg, B.: Spatial distribution of ground surface temperatures and active layer depths in the Hovsgol area, northern Mongolia, Permafrost and Periglacial Processes, 17, 357-369, 10.1002/ppp.568, 2006.

Heggem, E. S. F., and Strand, G.-H.: CORINE Land Cover 2000. The Norwegian CLC2000 project., Rapport fra Skog og Landskap.10/10, 23, 2010.

Hipp, T.: Mountain Permafrost in Southern Norway. Distribution, Spatial Variability and Impacts of Climate Change., PhD, Faculty of Mathematics and Natural Sciences, Department of Geosciences, University of Oslo, 166 pp., 2012.

Hoelzle, M.: Mapping and modelling of mountain permafrost distribution in the Alps, Norsk Geografisk Tidsskrift-Norwegian Journal of Geography, 50, 11-15, 1996.

Hofgaard, A., and Wilmann, B.: Monitoring of palsa peatlands. First 5-year reanalysis in Haukskardmyrin and Haugtjørnin, Dovre, NINA-Report: Norsk institutt for naturforskning, Trondheim, 42, 2011.

Houze, R. A.: Orographic effects on precipitating clouds, Reviews of Geophysics, 50, n/a-n/a, 10.1029/2011RG000365, 2012.

IPCC: Summary for Plicymakers, Climate Change 2013: The Physical Science Basis. Contribution of Working Group I to the Fifth Assessment Report of the Intergovernmental Panel on Climate Change, edited by: Stocker, T. F., Qin, D., Plattner, G.-K., Tignor, M., Allen, S. K., Boschung, J., Nauels, A., Xia, Y., Bex, V., and Midgley, P. M., Cambridge University Press, Cambridge, United Kingdom and New York, NY, USA, 2013.

IPCC: Climate Change 2014: Synthesis Report. Contribution of Working Groups I, II and III to the Fifth Assessment Report of the Intergovernmental Panel on Climate Change, edited by: Core Writing Team, Pachauri, R. K., and Meyer, L. A., IPCC, Geneva, Switzerland, 151 pp., 2014.

Isaksen, K., Holmlund, P., Sollid, J., and Harris, C.: Three deep alpine-permafrost boreholes in Svalbard and Scandinavia, Permafrost and Periglacial Processes, 12, 13-25, 10.1002/ppp.380 2001.

Isaksen, K., Hauck, C., Gudevang, E., Ødegård, R. S., and Sollid, J. L.: Mountain permafrost distribution in Dovrefjell and Jotunheimen, southern Norway, based on BTS and DC resistivity tomography data, Norsk Geografisk Tidsskrift-Norwegian Journal of Geography, 56, 122-136, 10.1080/00291950276005645 9, 2002.

Isaksen, K., Farbrot, H., Blikra, L., Johansen, B., Sollid, J., and Eiken, T.: Five year ground surface temperature measurements in Finnmark, Northern Norway., Ninth International Conference on Permafrost, Fairbanks, Alaska, 2008a, 789–794,

Isaksen, K., Farbrot, H., Etzelmuller, B., Christiansen Hanne, H., Blikra Lars, H., Midttomme, K., and Ronning Jan, S.: TSP NORWAY; thermal monitoring of mountain permafrost in Northern Norway, Ninth international conference on Permafrost., Fairbanks, United States, 2008b, 108113,

Isaksen, K., Ødegård, R. S., Etzelmüller, B., Hilbich, C., Hauck, C., Farbrot, H., Eiken, T., Hygen, H. O., and Hipp, T. F.: Degrading Mountain Permafrost in Southern Norway: Spatial and Temporal Variability of Mean Ground Temperatures, 1999–2009, Permafrost and Periglacial Processes, 22, 361-377, 10.1002/ppp.728, 2011.

Ishikawa, M.: Thermal regimes at the snow–ground interface and their implications for permafrost investigation, Geomorphology, 52, 105-120, 10.1016/S0169-555X(02)00251-9, 2003.

Jaedicke, C., Thiis, T., Sandvik, A. D., and Gjessing, Y.: Drifting snow in complex terrain - Comparison of measured snow distribution and simulated wind field, Snow Engineering: Recent Advances and Developments, edited by: HjorthHansen, E., Holand, I., Loset, S., and Norem, H., 65-73 pp., 2000.

Jarosch, A., Anslow, F., and Clarke, G. C.: High-resolution precipitation and temperature downscaling for glacier models, Climate Dynamics, 38, 391-409, 10.1007/s00382-010-0949-1, 2012.

Jeckel, P.: Permafrost and its altitudinal zonation in N. Lapland, Proceedings of the Fifth International Conference on Permafrost, Trondheim, Norway, 1988, 170-175,

Johansen, O.: Thermal conductivity of soils, PhD Thesis, Institute for Kjoleteknikk, Norges Tekniske Høyskole, NTH, Trondheim, Norway, 1975.

Jorgenson, M., and Kreig, R.: A model for mapping permafrost distribution based on landscape component maps and climatic variables., Proceedings, Fifth International Conference on Permafrost, Trondheim, Norway, 1988, 176-182,

Juliussen, H., and Humlum, O.: Towards a TTOP ground temperature model for mountainous terrain in central-eastern Norway, Permafrost and Periglacial Processes, 18, 161-184, 2007.

Juliussen, H., and Humlum, O.: Thermal regime of openwork block fields on the mountains Elgåhogna and Sølen, central-eastern Norway, Permafrost and Periglacial Processes, 19, 1-18, 2008.

Karunaratne, K., and Burn, C.: Relations between air and surface temperature in discontinuous permafrost terrain near Mayo, Yukon Territory, Canadian Journal of Earth Sciences, 41, 1437-1451, 2004.

King, L.: Qualitative und quantitative Erfassung von Permafrost in Tarfala (Schwedisch Lappland) und Jotunheimen (Norwegen) mit Hilfe geoelektrischer Sondierungen, Zeitschrift für Geomorphologie, Supplement-Band 43, 139-160, 1982.

King, L.: High mountain permafrost in Scandinavia, Fourth International Conference on Permafrost, 1983, 612-617,

King, L., and Seppälä, M.: Permafrost Thickness and Distribution in Finnish Lapland - Results of Geoelectrical Soundings, Polarforschung, 57, 127-147, 1987.

King, L., and Åkerman, H. J.: Mountain permafrost in Europe, the Sixth International Conference on Permafrost, Beijing, China, 1993, 1022–1027,

Klene, A., Nelson, F., Shiklomanov, N., and Hinkel, K.: The N-factor in natural landscapes: variability of air and soil-surface temperatures, Kuparuk River basin, Alaska, USA, Arctic, Antarctic, and Alpine Research, 33, 140-148, 2001.

Kovacs, A., Gow, A. J., and Morey, R. M.: The in-situ dielectric constant of polar firn revisited, Cold Regions Science and Technology, 23, 245-256, 10.1016/0165-232X(94)00016-Q, 1995.

Koven, C. D., Ringeval, B., Friedlingstein, P., Ciais, P., Cadule, P., Khvorostyanov, D., Krinner, G., and Tarnocai, C.: Permafrost carbon-climate feedbacks accelerate global warming, Proceedings of the National Academy of Sciences, 108, 14769-14774, 10.1073/pnas.1103910108, 2011.

Koven, C. D., Riley, W. J., and Stern, A.: Analysis of Permafrost Thermal Dynamics and Response to Climate Change in the CMIP5 Earth System Models, Journal of Climate, 26, 1877-1900, 10.1175/JCLI-D-12-00228.1, 2012.

Krautblatter, M., Funk, D., and Günzel, F. K.: Why permafrost rocks become unstable: a rock–ice-mechanical model in time and space, Earth Surf. Process. Landf., 38, 876-887, 2013.

Kronholm, K., Jaedicke, C., and Sandersen, F.: Varsling av regional snøskredfare. Metoder og data til vurdering av faregrad., Norwegian Geotechnical Institute (NGI), 2010.

Kudryavtsev , V. A.: Permafrost (short edition), in Russian, MSU Press, 1981.

Lawrence, D. M., and Slater, A. G.: A projection of severe near-surface permafrost degradation during the 21st century, Geophysical Research Letters, 32, 10.1029/2005gl025080, 2005.

Lawrence, D. M., Slater, A. G., and Swenson, S. C.: Simulation of Present-Day and Future Permafrost and Seasonally Frozen Ground Conditions in CCSM4, Journal of Climate, 25, 2207-2225, 10.1175/JCLI-D-11-00334.1, 2011.

Lehning, M., and Fierz, C.: Assessment of snow transport in avalanche terrain, Cold Regions Science and Technology, 51, 240-252, 10.1016/j.coldregions.2007.05.012, 2008.

Lewkowicz, A. G.: Evaluation of miniature temperature-loggers to monitor snowpack evolution at mountain permafrost sites, northwestern Canada, Permafrost and Periglacial Processes, 19, 323-331, 2008.

Lewkowicz, A. G., Bonnaventure, P. P., Smith, S. L., and Kuntz, Z.: Spatial and thermal characteristics of mountain permafrost, northwest Canada., Geografiska Annaler: Series A, Physical Geography, 94, 195-213, 10.1111/j.1468-0459.2012.00462.x, 2012.

Li, L., and Pomeroy, J. W.: Estimates of Threshold Wind Speeds for Snow Transport Using Meteorological Data, Journal of Applied Meteorology, 36, 205-213, 10.1175/1520-0450(1997)036<0205:EOTWSF>2.0.CO;2, 1997.

Lilleøren, K. S., and Etzelmüller, B.: A regional inventory of rock glaciers and ice-cored moraines in Norway., Geografiska Annaler: Series A, Physical Geography, 93, 175-191, 10.1111/j.1468-0459.2011.00430.x, 2011.

Lilleøren, K. S., Etzelmüller, B., Schuler, T. V., Gisnås, K., and Humlum, O.: The relative age of mountain permafrost — estimation of Holocene permafrost limits in Norway, Global and Planetary Change, 92–93, 209-223, 10.1016/j.gloplacha.2012.05.016, 2012.

Lilleøren, K. S., Humlum, O., Nesje, A., and Etzelmüller, B.: Holocene development and geomorphic processes at Omnsbreen, southern Norway: Evidence for glacier–permafrost interactions, The Holocene, 23, 796-809, 10.1177/0959683612471984, 2013.

Liston, G., and Sturm, M.: The role of winter sublimation in the Arctic moisture budget, Nordic hydrology, 35, 325-334, 2004.

Liston, G. E.: Local advection of momentum, heat, and moisture during the melt of patchy snow covers, Journal of Applied Meteorology, 34, 1705-1715, 1995.

Liston, G. E., and Sturm, M.: A snow-transport model for complex terrain, Journal of Glaciology, 44, 498-516, 1998.

Liston, G. E.: Interrelationships among Snow Distribution, Snowmelt, and Snow Cover Depletion: Implications for Atmospheric, Hydrologic, and Ecologic Modeling, Journal of Applied Meteorology, 38, 1474-1487, 10.1175/1520-0450(1999)038<1474:IASDSA>2.0.CO;2, 1999.

Liston, G. E.: Representing Subgrid Snow Cover Heterogeneities in Regional and Global Models, Journal of Climate, 17, 1381-1397, 10.1175/1520-0442(2004)017<1381:RSSCHI>2.0.CO;2, 2004.

Liston, G. E., Haehnel, R. B., Sturm, M., Hiemstra, C. A., Berezovskaya, S., and Tabler, R. D.: Instruments and methods simulating complex snow distributions in windy environments using SnowTran-3D, Journal of Glaciology, 53, 241-256, 2007.

Liston, G. E., and Hiemstra, C. A.: A simple data assimilation system for complex snow distributions (SnowAssim), Journal of Hydrometeorology, 9, 989-1004, 2008.

Litherland, T.: Snow Redistribution Modelling in Alpine Norway : Validation of SnowModel for a wet, high mountain climate, Master degree, Department of Geosciences, Faculty of Mathematics and Natural Sciences, University of Oslo, DUO, Digital publications at UiO, 101 pp., 2013.

Luetschg, M., Stoeckli, V., Lehning, M., Haeberli, W., and Ammann, W.: Temperatures in two boreholes at Flüela Pass, Eastern Swiss Alps: the effect of snow redistribution on permafrost distribution patterns in high mountain areas, Permafrost and Periglacial Processes, 15, 283-297, 10.1002/ppp.500, 2004.

Luetschg, M., Lehning, M., and Haeberli, W.: A sensitivity study of factors influencing warm/thin permafrost in the Swiss Alps, Journal of Glaciology, 54, 696-704, 10.3189/002214308786570881, 2008.

Lunardini, V.: Heat transfer in cold climates, Van Nostrand Reinhold, New York, 731 pp., 1981.

Lunardini, V. J.: Theory of n-factors and correlation of data, Proceedings of the Third International Conference on Permafrost, Edmonton Plaza Hotel, Edmonton, Canada, 1978, 40–46,

Marchand, W.-D., and Killingtveit, Å.: Statistical probability distribution of snow depth at the model sub-grid cell spatial scale, Hydrological Processes, 19, 355-369, 10.1002/hyp.5543, 2005.

Moeser, D., Morsdorf, F., and Jonas, T.: Novel forest structure metrics from airborne LiDAR data for improved snow interception estimation, Agricultural and Forest Meteorology, 208, 40-49, http://dx.doi.org/10.1016/j.agrformet.2015.04.013, 2015.

Mohr, M., and Tveito, O.: Daily temperature and precipitation maps with 1 km resolution derived from Norwegian weather observations, 13th Conference on Mountain Meteorology/17th Conference on Applied Climatology, Whistler, BC, Canada, 2008,

Morse, P. D., Burn, C. R., and Kokelj, S. V.: Influence of snow on near-surface ground temperatures in upland and alluvial environments of the outer Mackenzie Delta, Northwest Territories1This article is one of a series of papers published in this CJES Special Issue on the theme of Fundamental and applied research on permafrost in Canada, Canadian Journal of Earth Sciences, 49, 895-913, 10.1139/e2012-012, 2012.

Mott, R., and Lehning, M.: Meteorological Modeling of Very High-Resolution Wind Fields and Snow Deposition for Mountains, Journal of Hydrometeorology, 11, 934-949, 2010.

Mott, R., Egli, L., Grünewald, T., Dawes, N., Manes, C., Bavay, M., and Lehning, M.: Micrometeorological processes driving snow ablation in an Alpine catchment, The Cryosphere, 5, 1083-1098, 10.5194/tc-5-1083-2011, 2011.

Mott, R., Scipión, D., Schneebeli, M., Dawes, N., Berne, A., and Lehning, M.: Orographic effects on snow deposition patterns in mountainous terrain, Journal of Geophysical Research: Atmospheres, 119, 1419-1439, 10.1002/2013JD019880, 2014.

Nelson, F., Anisimov, O., and Shiklomanov, N. I.: Climate change and hazard zonation in the circum-Arctic permafrost regions, Natural Hazards, 26, 203-225, 2002.

Nelson, F. E., Shiklomanov, N. I., Mueller, G. R., Hinkel, K. M., Walker, D. A., and Bockheim, J. G.: Estimating active-layer thickness over a large region: Kuparuk River Basin, Alaska, USA, Arctic and Alpine Research, 29, 367-378, 1997.

Nelson, F. E., Shiklomanov, N. I., Hinkel, K. M., and Christiansen, H. H.: The Circumpolar Active Layer Monitoring (CALM) Workshop and THE CALM II Program, Polar Geography, 28, 253-266, 10.1080/789610205, 2004.

Nicolsky, D. J., Romanovsky, V. E., Alexeev, V. A., and Lawrence, D. M.: Improved modeling of permafrost dynamics in a GCM land-surface scheme, Geophysical Research Letters, 34, 10.1029/2007gl029525, 2007.

Noetzli, J., Huggel, C., Hoelzle, M., and Haeberli, W.: GIS-based modelling of rock-ice avalanches from Alpine permafrost areas, Comput Geosci, 10, 161-178, 10.1007/s10596-005-9017-z, 2006.

Noetzli, J., Gruber, S., Kohl, T., Salzmann, N., and Haeberli, W.: Three-dimensional distribution and evolution of permafrost temperatures in idealized high-mountain topography, Journal of Geophysical Research, 112, F02S13, 10.1029/2006JF000545, 2007.

Olesen, O., Brönner, J., Ebbing, J., Gellein, J., Gernigon, L., Koziel, J., Lauritsen, T., Myklebust, R., Pascal, C., Sand, M., Solheim, D., and Usov, S.: New aeromagnetic and gravity compilations from Norway and adjacent areas: methods and applications., in: Petroleum Geology: From Mature Basins to New Frontiers—Proceedings of the 7th Petroleum Geology Conference, edited by: Vining, B. A., and Pickering, S. C., 2010, Geological Society, London, 559-586, 2010.

Pomeroy, J., and Gray, D.: Snow Accumulation, Relocation and Management, National Hydrology Research Institute, Supply and Services Canada., Saskatoon, Saskatchewan., 144 pp., 1995.

Pomeroy, J., Gray, D., Shook, K., Toth, B., Essery, R., Pietroniro, A., and Hedstrom, N.: An evaluation of snow accumulation and ablation processes for land surface modelling, Hydrological Processes, 12, 2339-2367, 1998.

Pomeroy, J. W., Marsh, P., and Gray, D. M.: Application of a distributed blowing snow model to the Arctic, Hydrological Processes, 11, 1451-1464, 10.1002/(sici)1099-1085(199709)11:11<1451::aid-hyp449>3.0.co;2-q, 1997.

Pomeroy, J. W., Toth, B., Granger, R. J., Hedstrom, N. R., and Essery, R. L. H.: Variation in Surface Energetics during Snowmelt in a Subarctic Mountain Catchment, Journal of Hydrometeorology, 4, 702-719, 10.1175/1525-7541(2003)004<0702:VISEDS>2.0.CO;2, 2003.

Pomeroy, J. W., Marks, D., Link, T., Ellis, C., Hardy, J., Rowlands, A., and Granger, R.: The impact of coniferous forest temperature on incoming longwave radiation to melting snow, Hydrological processes, 23, 2513-2525, 10.1002/hyp.7325, 2009.

Raderschall, N., Lehning, M., and Schär, C.: Fine-scale modeling of the boundary layer wind field over steep topography, Water Resources Research, 44, 2008.

Rapp, A., and Annersten, L.: Permafrost and Tundra poly- gons in Northern Sweden in: The Periglacial Environment. Past and Present., Symposium on Cold Climate Environments and Processes, seventh congress of the International Association for Quaternary Research, Fairbanks, Alaska, 1970, 65-91,

Rapp, A., and Clark, G. M.: Large Nonsorted Polygons in Padjelanta National Park, Swedish Lappland, Geografiska Annaler. Series A, Physical Geography, 53, 71-85, 10.2307/520666, 1971.

Rapp, A.: Zonation of permafrost indicators in Swedish Lappland, Geografisk Tidsskrift-Danish Journal of Geography, 82, 37-38, 10.1080/00167223.1982.10649147, 1982.

Reusch, H.: Vore dale og fjelde: hvorledes formen af Norges overflade er dannet (In Norwegian), John Griegs Bogtrykkeri, Bergen, 51 s. pp., 1902.

Rich, P., Dubayah, R., Hetrick, W., and Saving, S.: Using viewshed models to calculate intercepted solar radiation: applications in ecology. American Society for Photogrammetry and Remote Sensing Technical Papers, 1994.

Ridefelt, H., Etzelmuller, B., Boelhouwers, J., and Jonasson, C.: Statistic-empirical modelling of mountain permafrost distribution in the Abisko region, sub-Arctic northern Sweden, Norsk Geografisk Tidsskrift-Norwegian Journal of Geography, 62, 278-289, 10.1080/00291950802517890, 2008.

Riseborough, D.: Exploring the parameters of a simple model of the permafrost–climate relationship., PhD Dissertation, Department of Geography and Environmental Studies, Carleton University, Ottawa, 330 pp., 2004.

Riseborough, D.: The effect of transient conditions on an equilibrium permafrost-climate model, Permafrost and Periglacial Processes, 18, 21-32, 10.1002/ppp.579, 2007.

Riseborough, D., Shiklomanov, N., Etzelmüller, B., Gruber, S., and Marchenko, S.: Recent advances in permafrost modelling, Permafrost and Periglacial Processes, 19, 137-156, 2008.

Romanovsky, V., Drozdov, D., Oberman, N., Malkova, G., Kholodov, A., Marchenko, S., Moskalenko, N., Sergeev, D., Ukraintseva, N., and Abramov, A.: Thermal state of permafrost in Russia, Permafrost and Periglacial Processes, 21, 136-155, 2010a.

Romanovsky, V., Smith, S., and Christiansen, H.: Permafrost thermal state in the polar Northern Hemisphere during the international polar year 2007–2009: a synthesis, Permafrost and Periglacial Processes, 21, 106-116, 2010b.

Romanovsky, V. E., and Osterkamp, T. E.: Interannual variations of the thermal regime of the active layer and near-surface permafrost in Northern Alaska, Permafrost and Periglacial Processes, 6, 313-335, 1995.

Saloranta, T. M.: Simulating snow maps for Norway: description and statistical evaluation of the seNorge snow model, The Cryosphere, 6, 1323-1337, 10.5194/tc-6-1323-2012, 2012.

Sannel, A. B. K., Hugelius, G., Jansson, P., and Kuhry, P.: Permafrost Warming in a Subarctic Peatland – Which Meteorological Controls are Most Important?, Permafrost and Periglacial Processes, n/a-n/a, 10.1002/ppp.1862, 2015.

Sazonova, T., and Romanovsky, V.: A model for regional scale estimation of temporal and spatial variability of active layer thickness and mean annual ground temperatures, Permafrost and Periglacial Processes, 14, 125-139, 2003.

Schuler, T. V., Crochet, P., Hock, R., Jackson, M., Barstad, I., and Jóhannesson, T.: Distribution of snow accumulation on the Svartisen ice cap, Norway, assessed by a model of orographic precipitation, Hydrological Processes, 22, 3998-4008, 10.1002/hyp.7073, 2008.

Schuur, E. A. G., Bockheim, J., Canadell, J. G., Euskirchen, E., Field, C. B., Goryachkin, S. V., Hagemann, S., Kuhry, P., Lafleur, P. M., Lee, H., Mazhitova, G., Nelson, F. E., Rinke, A., Romanovsky, V. E., Shiklomanov, N., Tarnocai, C., Venevsky, S., Vogel, J. G., and Zimov, S. A.: Vulnerability of Permafrost Carbon to Climate Change: Implications for the Global Carbon Cycle, BioScience, 58, 701-714, 10.1641/b580807, 2008.

Seppälä, M.: The Origin of Palsas, Geografiska Annaler. Series A, Physical Geography, 68, 141-147, 1986.

Seppälä, M.: Distribution of permafrost in Finland, Bulletin of the geological Society of Finland, 69, 87-96, 1997.

Shiklomanov, N., and Nelson, F.: Statistical representation of landscape-specific active-layer variability, 2003, 1039–1044,

Smith, M. W.: Microclimatic Influences on Ground Temperatures and Permafrost Distribution, Mackenzie Delta, Northwest Territories, Canadian Journal of Earth Sciences, 12, 1421-1438, 10.1139/e75-129, 1975.

Smith, M. W., and Riseborough, D. W.: Permafrost monitoring and detection of climate change, Permafrost and Periglacial Processes, 7, 301-309, 10.1002/(SICI)1099-1530(199610)7:4<301::AID-PPP231>3.0.CO;2-R, 1996.

Smith, M. W., and Riseborough, D. W.: Climate and the limits of permafrost: a zonal analysis, Permafrost and Periglacial Processes, 13, 1-15, 10.1002/ppp.410, 2002.

Smith, S. L., Romanovsky, V. E., Lewkowicz, A. G., Burn, C. R., Allard, M., Clow, G. D., Yoshikawa, K., and Throop, J.: Thermal state of permafrost in North America: a contribution to the international polar year, Permafrost and Periglacial Processes, 21, 117-135, 10.1002/ppp.690, 2010.

Sollid, J. L., and Sørbel, L.: Palsa bogs at Haugtjørnin, Dovrefjell, South Norway, Norsk Geografisk Tidsskrift-Norwegian Journal of Geography, 28, 53-60, 1974.

Sollid, J. L., and Sørbel, L.: Palsa Bogs as a Climate Indicator: Examples from Dovrefjell, Southern Norway, Ambio, 27, 287-291, 10.2307/4314737, 1998.

Sollid, J. L., Isaksen, K., Eiken, T., and Ødegård, R. S.: The transition zone of mountain permafrost on Dovrefjell, southern Norway, Eight International Conference on Permafrost, Zürich, Switzerland, 2003, 1085-1090,

Stendel, M., Romanovsky, V. E., Christensen, J. H., and Sazonova, T.: Using dynamical downscaling to close the gap between global change scenarios and local permafrost dynamics, Global and Planetary Change, 56, 203-214, 2007.

Sturm, M.: Snow Distribution and Heat Flow in the Taiga, Arctic and Alpine Research, 24, 145-152, 10.2307/1551534, 1992.

Sturm, M., Holmgren, J., and Liston, G. E.: A seasonal snow cover classification system for local to global applications, Journal of Climate, 8, 1261-1283, 1995.

Sturm, M., Holmgren, J., Konig, M., and Morris, K.: The thermal conductivity of seasonal snow, Journal of Glaciology, 43, 26-41, 1997.

Sushama, L., Laprise, R., and Allard, M.: Modeled current and future soil thermal regime for northeast Canada, Journal of Geophysical Research-Atmospheres, 111, D18111, 10.1029/2005jd007027, 2006.

Taylor, A.: Field measurements of n-factors for natural forest areas, Mackenzie Valley, Northwest Territories., in Current Research 1995-B, Geological Survey of Canada, 89-98, 1995.

Taylor, K. E., Stouffer, R. J., and Meehl, G. A.: An Overview of CMIP5 and the Experiment Design, Bulletin of the American Meteorological Society, 93, 485-498, 10.1175/BAMS-D-11-00094.1, 2011.

Thoresen, M. K.: Kvartærgeologisk kart over Norge, tema jordarter., Norges geologiske undersøkelse., 1991.

Tveito, O. E., and Førland, E. J.: Mapping temperatures in Norway applying terrain information, geostatistics and GIS., Norsk Geografisk Tidsskrift, 53, 202-212, 1999.

Vieira, G., Bockheim, J., Guglielmin, M., Balks, M., Abramov, A. A., Boelhouwers, J., Cannone, N., Ganzert, L., Gilichinsky, D. A., and Goryachkin, S.: Thermal state of permafrost and active-layer monitoring in the antarctic: Advances during the international polar year 2007–2009, Permafrost and Periglacial Processes, 21, 182-197, 2010.

Westermann, S., Gisnås, K., and Etzelmuller, B.: Snow melt monitoring at Scheteligfjellet, near Ny-Ålesund, Svalbard, in 2014, links to images, PANGAEA® Data Publisher for Earth & Environmental Science, http://doi.pangaea.de/10.1594/PANGAEA.846616, 2015a.

Westermann, S., Østby, T., Gisnås, K., Schuler, T. V., and Etzelmüller, B.: A ground temperature map of the North Atlantic permafrost region based on remote sensing and reanalysis data, The Cryosphere Discuss., 9, 753-790, 10.5194/tcd-9-753-2015, 2015b.

Williams, P. J., and Smith, M. W.: The frozen earth: fundamentals of geocryology, Cambridge University Press, Cambridge, xvi, 306 pp., 1989.

Winstral, A., Elder, K., and Davis, R. E.: Spatial snow modeling of wind-redistributed snow using terrain-based parameters, Journal of Hydrometeorology, 3, 524-538, http://dx.doi.org/10.1175/1525-7541(2002)003<0524:SSMOWR>2.0.CO;2, 2002.

Winstral, A., and Marks, D.: Simulating wind fields and snow redistribution using terrain-based parameters to model snow accumulation and melt over a semi-arid mountain catchment, Hydrological Processes, 16, 3585-3603, 10.1002/hyp.1238, 2002.

Winther, J.-G., Godtliebsen, F., Gerland, S., and Isachsen, P. E.: Surface albedo in Ny-Ålesund, Svalbard: variability and trends during 1981–1997, Global and Planetary Change, 32, 127-139, 10.1016/S0921-8181(01)00103-5, 2002.

Winther, J., Bruland, O., Sand, K., Killingtveit, A., and Marechal, D.: Snow accumulation distribution on Spitsbergen, Svalbard, in 1997, Polar Research, 17, 155-164, 1998.

Wright, J., Duchesne, C., and Côté, M.: Regional-scale permafrost mapping using the TTOP ground temperature model, in: Proceedings of the Eighth International Conference on Permafrost., In: Permafrost: proceedings of the eighth International Conference on Permafrost, 21-25 July 2003, Zurich, Switzerland, Lisse, 2003, 1241–1246,

Zhang, T., Heginbottom, J. A., Barry, R. G., and Brown, J.: Further statistics on the distribution of permafrost and ground ice in the Northern Hemisphere, Polar Geography, 24, 126 - 131, 2000.

Zhang, T., Barry, R. G., and Haeberli, W.: Numerical simulations of the influence of the seasonal snow cover on the occurrence of permafrost at high latitudes, Norsk Geografisk Tidsskrift - Norwegian Journal of Geography, 55, 261-266, 10.1080/00291950152746621, 2001.

Zhang, T.: Influence of the seasonal snow cover on the ground thermal regime: An overview, Reviews of Geophysics, 43, 1944-9208, 10.1029/2004rg000157, 2005.

Zhang, Y., Chen, W. J., and Riseborough, D. W.: Transient projections of permafrost distribution in Canada during the 21st century under scenarios of climate change, Global and Planetary Change, 60, 443-456, 10.1016/j.gloplacha.2007.05.003, 2008.

Zhao, L., Wu, Q., Marchenko, S., and Sharkhuu, N.: Thermal state of permafrost and active layer in Central Asia during the International Polar Year, Permafrost and Periglacial Processes, 21, 198-207, 2010.

Ødegaard, R. S., Isaksen, K., Eiken, T., and Sollid, J. L.: MAGST in Mountain Permafrost, Dovrefjell, Southern Nroway, 2001-2006, Ninth International Conference on Permafrost (NICOP) 2008, Fairbanks, Alaska, June 29 - July 3, 2008.

Ødegård, R., Hoelzle, M., Vedel Johansen, K., and Sollid, J.: Permafrost mapping and prospecting in southern Norway, Norsk Geografisk Tidsskrift, 50, 41-54, 1996.

Ødegård, R. S., Sollid, J. L., and Liestøl, O.: Ground temperature measurements in mountain permafrost, Jotunheimen, southern Norway, Permafrost and Periglacial Processes, 3, 231-234, 10.1002/ppp.3430030310, 1992.

Østrem, G.: Ice-Cored Moraines in Scandinavia, Geografiska Annaler, 46, 282-337, 10.2307/520383, 1964.

Åhman, R.: Palsar I Nordnorge, Lund Univeristy, Meddelanden från Lund Universitetets Geografiska Institution. Avhandlingar 78, 1-165 pp., 1977.

9 Other publications during the PhD period

9.1 Scientific publications

Westermann S., T. Østby, K. Gisnås, T.V. Schuler & B. Etzelmüller (2015). A ground temperature map of the North Atlantic permafrost region based on remote sensing and reanalysis data. *The Cryosphere Discussion*, **9**, 753-790.

Westermann S., T. V. Schuler, K. Gisnås, and B. Etzelmüller (2013). Transient thermal modeling of permafrost conditions in Southern Norway, *The Cryosphere*, **7**: 719-739.

Farbrot H., B. Etzelmüller, K. Isaksen & K. Gisnås (2013). Ground thermal regime and permafrost distribution under a changing climate in northern Norway. *Permafrost and Periglacial Processes*, **24**: 20-38.

Lilleøren K.S., B. Etzelmüller, K. Gisnås, T.V. Schuler & O. Humlum (2012). The relative age of mountain permafrost — estimation of Holocene permafrost limits in Norway. *Global and Planetary Change* 92–93, 209-223.

9.2 Conference publications

Gisnås K., S. Westermann, T.V. Schuler & B. Etzelmuller (2014). Towards Inclusion of Sub-grid Variability of Snow in Distributed Permafrost Models. AGU Fall meeting 2014, 15th -19th December 2014. San Francisco, California, USA. **Oral presentation, Presenting author K. Gisnås.**

Gisnås K., S. Westermann, B. Etzelmuller, T.V. Schuler, K. Isaksen, T. Litherland & J. Boike (2014). *A probabilistic approach to represent small-scale variability of permafrost temperatures due to snow cover.* 4th European Conference on Permafrost, 18th -21st June 2014, Évora, Portugal. **Oral presentation, Presenting author K. Gisnås.**

Gisnås K., S. Westermann, B. Etzelmüller & T.V. Schuler. *From Snow Depth Distribution to Small-Scale Variability of Soil Temperatures*. European Geoscience Union. General Assembly 2013, 7th-12th April 2013. Vienna, Austria. **Oral presentation, Presenting author K. Gisnås.**

Gisnås K., S. Westermann, T. Hipp, B. Etzelmüller & T.V. Schuler (2012). *From Snow Depth Distribution to Small-Scale Variability of Soil Temperatures – a Probabilistic View on Permafrost in Norway.* Tenth International Conference on Permafrost, 25th – 29th June 2012. Salekhard, Yamal-Nenets Autonomous District, Russia. **Oral presentation, presenting author K. Gisnås.**

Gisnås K., H. Farbrot, B. Etzelmüller & T.V. Schuler. *Regional scale distribution of permafrost in Norway based on two equilibrium models*. European Geoscience Union. General Assembly 2011, 3rd-8th April 2011. Vienna, Austria. **Oral presentation. Presenting author K. Gisnås.**

A Appendix

A1 Snow distribution observations

	Location (utm33)		Elevation		1 meter average				10 meter average			
Date	*East*	*North*	*Mean*	*Range*	*N*	*SD*	*CS*	*CV*	*N*	*SD*	*CS*	*CV*
Finse												
17.12.2011	92000	6739000	1283	115	14542	1.00	1.67	0.80	830	1.02	1.64	0.75
30.01.2012	92000	6739000	1272	123	25601	0.70	1.17	0.73	1686	1.76	1.25	0.73
27.02.2012	92000	6739000	1267	122	16341	1.69	1.88	1.04	932	1.74	1.76	0.99
22.03.2012	92000	6739000	1276	125	36201	2.00	1.52	0.91	1968	2.05	1.47	0.88
12.12.2013	92000	6739000	1257	111	4220	1.11	2.25	0.80	408	1.09	2.33	0.71
22.01.2013	92000	6739000	1278	124	17200	1.42	1.26	0.72	1400	1.52	1.35	0.67
25.02.2013	92000	6739000	1273	122	20856	1.60	1.60	0.72	1766	1.72	1.33	0.66
20.03.2013	92000	6739000	1272	126	16844	1.63	1.16	0.70	1616	1.71	1.05	0.71
23.04.2014	92000	6739000	1257	127	4080	1.94	1.02	0.71	563	1.72	0.89	0.72
21.02.2015	92000	6739000	1282	120	11522	2.00	1.10	0.79	765	2.05	1.11	0.76
25.03.2015	92000	6739000	1283	129	15352	2.10	1.10	0.77	1046	2.07	1.04	0.76
05.05.2015	92000	6739000	1293	117	23606	2.19	1.05	0.73	1443	2.32	0.98	0.74
Juvvasshøe												
03.05.2009												
Area 1	150000	6856000	1568	186	1126	0.87	1.75	0.73	193	0.87	1.77	0.74
Area 3	151000	6857000	1742	176	883	0.45	3.65	0.92	147	0.45	3.29	0.86
Area 5	151000	6858000	1711	135	820	1.47	1.22	0.69	134	1.36	1.43	0.69
Area 6	151000	6859000	1377	718	1533	0.73	1.26	0.61	252	0.69	1.60	0.56
29.03.2012												
Area 1	150000	6856000	1731	164	2565	1.16	1.12	0.70	282	1.17	0.97	0.68
Area 2	150000	6857000	1620	172	926	1.71	0.80	0.61	138	1.76	0.88	0.60
Area 3	151000	6857000	1500	188	361	1.68	0.85	0.67	123	1.65	0.88	0.66
Area 4	150000	6858000	1552	116	2870	1.43	0.94	0.68	162	1.42	0.95	0.66
Area 5	151000	6858000	1379	207	4722	1.18	1.56	0.71	420	1.31	1.84	0.78
Area 6	151000	6859000	1317	216	1685	0.75	0.64	0.55	157	0.83	0.64	0.54
15.03.2013												
Area 1	150000	6856000	1724	145	1151	1.31	1.66	0.88	173	1.32	1.70	0.89
Area 2	150000	6857000	1589	101	1074	1.05	1.35	0.91	153	0.96	1.48	0.90
Area 3	151000	6857000	1502	152	803	1.19	0.53	0.61	129	1.14	0.69	0.64
Area 4	150000	6858000	1522	114	1091	1.28	1.77	0.82	217	1.28	1.73	0.85
Area 5	151000	6858000	1412	166	2779	0.78	1.16	0.66	440	0.73	1.30	0.66
Area 6	151000	6859000	1310	60	595	0.87	0.99	0.57	73	0.93	0.87	0.54
Ny-Ålesund: Bayelva												
23.04.2013	432000	8763000	23	32	23329	0.53	2.30	0.63	3291	0.53	2.29	0.60
Ny-Ålesund: Kvadehuksletta												
24.04.2013	424000	8766000	34	47	14666	0.32	2.46	0.91	2493	0.32	2.49	0.89